

AD-A100 461

VARIAN ASSOCIATES INC PALO ALTO CA  
INTERACTION STRUCTURES FOR NARROW-BAND MILLIMETER-WAVE COMMUNIC--ETC(U)  
APR 81 A KARP

F/6 9/1

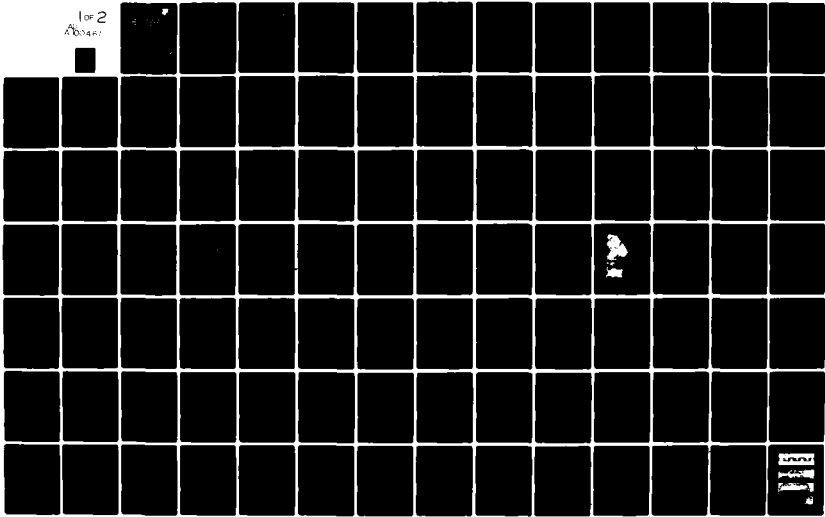
F30602-79-C-0172

NL

UNCLASSIFIED

RADC-TR-81-54

1 of 2  
A KARP



RADC-TR-81-54  
Final Technical Report  
April 1981

LEVEL 1

(1)



40

AD A100461

# INTERACTION STRUCTURES FOR NARROW-BAND MILLIMETER-WAVE COMMUNICATIONS TWTs

Varian Associates, Inc.

Arthur Karp

APPROVED FOR PUBLIC RELEASE; DISTRIBUTION UNLIMITED

DTIC  
ELECTED  
JUN 23 1981  
S D

A

ROME AIR DEVELOPMENT CENTER  
Air Force Systems Command  
Griffiss Air Force Base, New York 13441

U.S. GOVERNMENT COPY

81 0 26 091

This report has been reviewed by the RADC Public Affairs Office (PA) and is releasable to the National Technical Information Service (NTIS). At NTIS it will be releasable to the general public, including foreign nations.

RADC-TR-81-54 has been reviewed and is approved for publication.

APPROVED: *Kevin O'Brien*

KEVIN O'BRIEN, Capt, USAF  
Project Engineer

APPROVED: *Frank J. Rehm*

FRANK J. REHM  
Technical Director  
Surveillance Division

FOR THE COMMANDER:

*John P. Huss*

JOHN P. HUSS  
Acting Chief, Plans Office

If your address has changed or if you wish to be removed from the RADC mailing list, or if the addressee is no longer employed by your organization, please notify RADC (OCTP) Griffiss AFB NY 13441. This will assist us in maintaining a current mailing list.

Do not return this copy. Retain or destroy.

## UNCLASSIFIED

SECURITY CLASSIFICATION OF THIS PAGE (When Data Entered)

(19) REPORT DOCUMENTATION PAGE		READ INSTRUCTIONS BEFORE COMPLETING FORM	
1. REPORT NUMBER RADC-TR-81-54	2. GOVT ACCESSION NO. AD-A100461	3. RECIPIENT'S CATALOG NUMBER	
4. TITLE (or SUBTITLE) INTERACTION STRUCTURES FOR NARROW-BAND MILLIMETER-WAVE COMMUNICATIONS TWTs.		5. TYPE OF REPORT PERIOD COVERED Final Technical Report, Jun 1979 - Aug 1980	
7. AUTHOR(s) Arthur Karp		6. PERFORMING ORG. REPORT NUMBER J.O. 19129	
9. PERFORMING ORGANIZATION NAME AND ADDRESS Varian Associates, Inc. 611 Hansen Way Palo Alto CA 94303		8. CONTRACT OR GRANT NUMBER(s) F30602-79-C-0172	
11. CONTROLLING OFFICE NAME AND ADDRESS Rome Air Development Center (OCTP) Griffiss AFB NY 13441		10. PROGRAM ELEMENT, PROJECT, TASK AREA & WORK UNIT NUMBERS 62702F 45061246	
14. MONITORING AGENCY NAME & ADDRESS (if different from Controlling Office) Same		12. REPORT DATE Apr 1981	
16. DISTRIBUTION STATEMENT (of this Report)  Approved for public release; distribution unlimited		13. NUMBER OF PAGES 122	
17. DISTRIBUTION STATEMENT (of the abstract entered in Block 20, if different from Report)  Same		15. SECURITY CLASS. (of this report) UNCLASSIFIED	
18. SUPPLEMENTARY NOTES RADC Project Engineer: Kevin O'Brien, Capt, USAF (OCTP)		19a. DECLASSIFICATION/DOWNGRADING SCHEDULE N/A	
19. KEY WORDS (Continue on reverse side if necessary and identify by block number) Traveling-Wave Tube (TWT) Slow-Wave Circuits Non-Helix TWT TWT Interaction Structures Coupled-Cavity TWT (CC TWT) Comb-Quad Structures Millimeter-Wave CC TWT Ladder Structures Narrow-Band CC TWT			
20. ABSTRACT (Continue on reverse side if necessary and identify by block number) A one-year study program was devoted to the investigation and development of new slow-wave interaction-structure technology benefiting narrow-band non-helix TWTs for millimeter-wave space-communications application. One recently introduced group of inherently narrow-band structures utilizes a one-piece copper-slab ladder enclosed in various simple ways to yield the equivalent of a chain of cavities with "staggered" or "in-line", magnetic or electric coupling between them. A major objective is			

DD FORM 1 JAN 73 1473 EDITION OF 1 NOV 65 IS OBSOLETE

UNCLASSIFIED

SECURITY CLASSIFICATION OF THIS PAGE (When Data Entered)

36910

UNCLASSIFIED

SECURITY CLASSIFICATION OF THIS PAGE(When Data Entered)

to assemble only a few pieces, regardless of the number of cavities in the chain. This objective also applies to the narrowest-band embodiments of a recently introduced novel slow-wave interaction-structure approach - "Comb-Quad" - likewise promising to alleviate fabrication difficulties, better retain dimensional precision and reduce costs relative to conventional axially stacked coupled-cavity chains at a given frequency such as 44 or 94 GHz. These new structures are mechanically and thermally robust, low in attenuation, and in particular offer electrical equivalence without sacrifice of interaction impedance.

The narrow-band design evaluations were based on analytic techniques and scale-model "cold" testing. The circuit aspects investigated included dispersion, rf fields and currents, attenuation, interaction impedance, extraneous modes and passbands, thermal effects, actual-size fabrication techniques, and the effects of several categories of geometric imperfection. Couplers to provide a match between periodic structure and external waveguide received extensive consideration. Gap coefficients were derived for the unconventional interaction-gap geometries associated with Comb-Quad circuitry. Small-signal interaction modeling supported the eventual attainment of objectives regarding gain, bandwidth and stability. The study program provides sufficient background for the construction of "hot" tubes, recommended as the logical next step toward validation of the new technology.

By  
Date  
Priority

A

UNCLASSIFIED

SECURITY CLASSIFICATION OF THIS PAGE(When Data Entered)

## TABLE OF CONTENTS

<u>Section</u>		<u>Page</u>
1.0	INTRODUCTION .....	1
	1.1 Objectives, Background and Scope .....	1
	1.2 Circuitry Studied .....	2
	1.3 Organization and Synopsis of Report .....	3
2.0	SLOW-WAVE STRUCTURES WITH A SINGLE SLAB LADDER.....	7
	2.1 General .....	7
	2.2 "Forward-Wave" Slab-Ladder Interaction Structure .....	9
	2.3 "Backward-Wave" Slab-Ladder Interaction Structure .....	11
	2.4 Further Development of T-Groove Loaded Slab-Ladder Circuit .....	14
3.0	TRI-LADDER SLOW-WAVE STRUCTURE .....	18
4.0	COMB-QUAD INTERACTION STRUCTURE .....	24
	4.1 Introduction .....	24
	4.2 Structural Basics .....	24
	4.3 Beam-Tunnel Options .....	28
	4.4 Tooth Profile Options .....	30
	4.5 Enclosure Options .....	32
	4.6 RF Fields and Currents .....	32
	4.7 Historical Precedents .....	37
5.0	COMB-QUAD PROPAGATION CHARACTERISTICS .....	40
	5.1 General .....	40
	5.2 Comb-Quad "A" and "B" .....	40
	5.3 Comb-Quad "C" and "D" .....	44
	5.4 Higher Passbands and Extraneous Modes .....	46
	5.5 Interaction Impedance .....	50
	5.6 Circuit Attenuation .....	53
	5.7 Comb-Quad B Differential-Loading Experiments ..	57
6.0	COMB-QUAD INTERACTION-GAP MODELING .....	59
	6.1 Introduction .....	59
	6.2 "Conventional" Beam-Tunnel Option .....	59
	6.3 "Virtual" Beam-Tunnel Option .....	62
	6.4 Crepeau-McIsaac Phenomena .....	70
7.0	COMB-QUAD B PERFORMANCE PROJECTIONS .....	73
	7.1 Small-Signal Interaction Modeling .....	73
	7.2 Passband Edge Stability .....	77
	7.3 Low-Frequency Backward-Wave Oscillation .....	78

TABLE OF CONTENTS (CONT'D)

7.4	Higher-Passband Concerns .....	80
7.5	Revised Small-Signal Gain Projections .....	82
8.0	COMB-QUAD B FABRICATION CONSIDERATIONS .....	84
8.1	Machining of Combs .....	84
8.2	Sensitivity to Geometric Deviations .....	85
9.0	COMB-QUAD B TRANSITIONS TO WAVEGUIDE .....	91
10.0	THERMAL CONSIDERATIONS .....	97
11.0	CONCLUSIONS AND RECOMMENDATIONS .....	102
11.1	General .....	102
11.2	Structures with a Central Slab Ladder .....	102
11.3	Comb-Quad Structures .....	103
12.0	REFERENCES .....	108

## LIST OF ILLUSTRATIONS

<u>Figure</u>		
1. Exploded View of Space-Harmonic TWT Interaction Structure Having Slab Ladder Between T-Grooved Cover Plates .....	8	
2. Space-Harmonic TWT Design Using Double-Ridge Loaded Slab Ladder (After Biggs <sup>6</sup> ).....	10	
3. Space-Harmonic TWT Design Using T-Groove Loaded Slab Ladder (After Biggs <sup>6</sup> ).....	12	
4. Brillouin Diagram for Interaction Structure of Figure 1 with Rather Thick Ladder .....	15	
5. Exploded View of Tri-Ladder CC TWT Interaction Structure .....	19	
6. Brillouin Diagram for Tri-Ladder Interaction Structure of Figure 5 .....	21	
7. Axial Stacking Concept (Applied to Coupled-Cavity Structure Using Twin Coupling Slots and 90° Re-Orientations).....	25	
8. Comb-Quad Approach to CC TWT Interaction Circuitry...	27	
9. Beam-Tunnel Options for Comb-Quad Structure (a) Conventional (CBT); (b) Intermediate; (c) "Virtual" (VBT) .....	29	
10. Tooth-Profile Options for Comb-Quad Structure, VBT Assumed (a-c) Longitudinal Sections; (d-f) Transverse Sections .....	31	
11. Transverse Sections Indicating Comb-Quad Enclosure Options .....	33	
12. Perspective Drawing and Equivalent Circuit Cell for Appreciating Comb-Quad "Cavities" and "Coupling Slots" and RF Fields and Currents .....	34	
13. Related Slow-Wave Structures Reported in the Past....	38	
14. Partially Assembled 6- or 8- Period Comb-Quad Circuit Models at C- or G- Band .....	41	
15. Brillouin Diagram Covering 4 Basic Comb-Quad $\omega-\beta$ Responses, with Regard to First Forward Space-Harmonic Wave .....	42	

LIST OF ILLUSTRATIONS (CONT'D)

16.	Basic Comb-Quad Dispersion Characters Distinguished by the Variation of Phase Velocity with Frequency in the Interval $\pi < \beta p < 2\pi$ .....	43
17.	Brillouin Diagrams for Comb-Quad B Circuit Structures Based on Third Comb Set of Figure 14; Variable X (in inches) is Defined in Figure 11(B) .....	47
18.	Brillouin Diagrams for Comb-Quad A and B Circuit Structures Based on Second Comb Set of Figure 14; Variable X (in inches) is Defined in Figure 11(B)....	48
19.	Predicted Attenuation Data for Comb-Quad B/CBT Circuit Model of Figure 17 with X = 2 Inches .....	54
20.	Typical Dependence of Gap Figure of Merit on g/p and Unit Phase Shift for Hypothetical Axisymmetric Interaction Region .....	63
21.	Interaction Region of Figure 9(c) with Mathematical Constructions Used in Deriving $E_z(z)$ Profiles for Key Electron Trajectories.....	65
22.	For $2\pi$ Static Mode: Axial E Field vs Axial Distance For One Period, in Interaction-Gap Geometry of Figure 21.....	68
23.	For $\pi$ Static Mode: Axial E Field vs Axial Distance, For One Period, In Interaction-Gap Geometry of Figure 21 .....	69
24.	Initial Comb-Quad B Small-Signal Gain Projections ...	76
25.	44-Period Copper Comb-Quad Assembly Variously Magnified.....	86
26.	19-Period Comb-Quad B/CBT Circuit Section with G-Band Waveguide for Essaying Transducer .....	93
27.	Suggested Transition Between Reduced-Height Rectangular Waveguide and Comb-Quad B/VBT Interaction Structure .....	95
28.	Schema for Thermal Analysis of a Comb-Quad Tooth ....	99

## PREFACE

Captain Kevin O'Brien was the RADC Project Engineer overseeing this contract undertaking on behalf of the Air Force Systems Command. Previously, R. Hunter Chilton had synthesized the technical objectives under which Varian's proposal for carrying out this study program was solicited.

At Varian Associates, Inc., Palo Alto Microwave Tube Division, Division R & D Operation, the design, construction and testing of the cold-test circuit models providing the experimental data referred to in Chapters 2, 3, 5, 7 and 8 were chiefly the responsibility of Gary A. Biggs, an AFTER program alumnus currently at Varian's Eimac Division, Salt Lake City. Mr. Biggs was also responsible for the extensive efforts to develop a Comb-Quad B transition to waveguide (Chapter 9). Additional support in obtaining the cold-test data associated with Figures 4 and 5 was provided by James R. Legarra.

George E. Wendell undertook the analytic task of finding field distributions for the complex three-dimensional electrode configuration of Figure 21, using the rheological problem-solving capability of Program VULCAN, which first required the augmentation implemented by Albert E. Berwick. Further processing of these results, as described in the latter half of Section 6.3, was the responsibility of Andrew L. Nordquist, who also obtained the analytical results of Section 6.2. These efforts were coordinated by Fred I. Friedlander who also participated in many helpful discussions, as did W. Revis Ayers, John A. Ruetz and others.

The small-signal interaction modeling and related impedance and attenuation calculations contributing to Chapters 2, 3, 5 and 7 were the responsibility of F. Ruth Walker, who also generated most of the graphical data presentations for this report. The thermal-problem solution summarized in Chapter 10 is due to Stephen P. Darbin, a first-year AFTER Program participant. The efforts to fabricate an initial Comb-Quad circuit section sized for 94 GHz (Figure 25) benefitted from the involvement of Wolfgang L. Vogel.

## EVALUATION

This effort in support of TPO 1A1D resulted in the identification and development of the Comb-Quad Circuit for use in millimeter-wave TWTs for space applications. This circuit, consisting of only four critical parts, should be easy to fabricate. If further developed and used, this circuit should increase the availability and decrease the cost of millimeter-wave TWTs.



KEVIN O'BRIEN, Capt, USAF  
Project Engineer

## 1.0 INTRODUCTION

### 1.1 OBJECTIVES, BACKGROUND AND SCOPE

Current objectives for Air Force satellite communications systems around 44 GHz, and eventually around 94 GHz, include a new generation of improved narrow-band non-helix CW millimeter-wave TWTs. The improvements are wanted in the areas of simplicity and economy since a conventional axially stacked coupled-cavity TWT is unduly costly and perhaps "over-qualified" (in terms of potential power/bandwidth capability) when the bandwidth needed is only on the order of 3%, and the CW output power only in the vicinity of 50 W.

The purpose of the innovations introduced and evaluated in the area of interaction-structure design and fabrication, in anticipation of, and under, the subject study program, is thus to overcome certain limitations of the millimeter-wave coupled-cavity TWT (CC TWT) art as of the late 1970s. Evaluations of new interaction-structure concepts that might qualify as technology advances would include various analytical and experimental efforts -- short of "hot tube" construction. The primary vehicles for the experimental program are "cold-test" models of the periodic structure, either a few or several periods long, scaled to a convenient frequency band (e.g., between 3 and 8 GHz). Measurements undertaken with the shorter models chiefly provide data on "cold" bandwidth and dispersion (including complete Brillouin diagram with at least two passbands), sensitivity to geometric or dimensional variations, and interaction impedance. The longer circuit models are chiefly useful in developing transitions or couplers to external waveguide. When certain conditions are met for either the shorter or longer models, circuit attenuation may be measurable directly, or through measurements of Q and group velocity.

The principal analytic activities concern the gain-vs-frequency and stability possibilities which may be projected via computer simulation of hypothetical TWTs. These calculations combine measured circuit properties with the assumed parameters of a plausible electron beam. In consideration of the eventual operating wavelengths and other factors, beam

microperveances are assumed quite low (of the order of 0.02 to 0.08, perhaps, depending on the voltage). Beam voltages in the vicinity of 20 kV are viewed as facilitating circuit design and beam focusing without being excessive in terms of the output power desired. [The factors to be considered include the tradeoffs between beam conductance ( $I_0/V_0$ ), which affects gain per unit length, and permeance ( $I_0/V_0^{3/2}$ ), which affects ease of focusing.] Nevertheless it is appreciated that the investment in "potting" and power supplies external to the tube might be reduced by favoring lower beam voltages, such as 10 kV, where possible.

At this stage, thermal properties are best predicted analytically. Other practical concerns include techniques for eventual circuit fabrication, and for the retention of the requisite geometric tolerances, along with consideration of the costs thereof. Experimentation with the preparation of actual-size circuit specimens is accordingly a worthwhile task. These interests are all facets of the beginning stages of a program working toward an advanced TWT design having a good probability of successful performance.

### 1.2 CIRCUITRY STUDIED

Prior to the award of the present contract, several promising new approaches to non-helix TWT interaction circuitry had been introduced at Varian, with ease of fabrication at millimeter wavelengths in mind. In one category of structure, a one-piece copper-slab ladder was covered over with axially uniform plates so as to provide a chain of cavities with electric or magnetic inter-cavity coupling of the "in-line" variety. The evaluations undertaken previously were resumed, and further advances were made during the conduct of the present contract. At that time, the alternative possibility of placing the central slab ladder between two slabs that were themselves ladders (of double the period of the center ladder), rather than axially uniform plates, was introduced. The coupled-cavity chain then formed in this "Tri-Ladder" structure would have the "staggered" type of magnetic coupling between cavities.

In a rather different structure category introduced prior to the award of the present contract, several distinct embodiments for the "Comb-Quad" slow-wave circuit principle had already seen partial "cold" testing, with various minor variations of each also noted. Two of the major design categories, designated Comb-Quad B and Comb-Quad D were relevant to current objectives by virtue of the modest "hot" bandwidths projected under low beam perveance. Response to other current objectives was represented by structural robustness, and increased precision and economy in fabrication, without compromise of interaction impedance. A major focus of the subject study program was consequently the further evaluation of Comb-Quad interaction circuitry in its narrower-band embodiments.

### 1.3 ORGANIZATION AND SYNOPSIS OF REPORT

The remaining chapters of this Final Report review the premises, efforts and findings of the study program in a sequence logical to their presentation. Chapter 2 is concerned with the structures based on a thick ladder with axially uniform covering and hence "in-line" inter-cavity coupling that may be either electric or magnetic. The Tri-Ladder structure, where the inter-cavity coupling is "staggered" and magnetic, is examined in Chapter 3. In these cases, the major concerns were propagation characteristics, bandwidth determinants, and interaction impedances -- especially at passband edges. Gains and bandwidths were projected only on a preliminary basis, since neither the beam parameters nor the structure geometry were necessarily optimized for the intended application.

The Comb-Quad approach to creating coupled-cavity-equivalent slow-wave circuits (with a set of four combs) is introduced in Chapter 4, with emphasis on justifying the expectations for improved precision and economy in fabrication through the avoidance of axial stacking. Attention is drawn to the inherent robustness, and R/Q values that are substantial despite the absence of ferrules. The possibility of more than one option in the matter of beam tunnels, with appealing implications for construction economics, is reviewed along with other geometry options, such as the enclosure for the combs which is a principal determinant of the cold and hot bandwidths. The spatial distributions of rf fields and currents is discussed with special

reference to the lumped-element equivalent-circuit cell. Chapter 4 concludes with references to relevant prior art.

The lead topic for Chapter 5 is the relations among enclosure geometry, dispersion profile, and "hot" bandwidth. The geometries are pointed out for which narrow "hot" bandwidths are expected. Higher passbands and extraneous modes are discussed in connection with the complete Brillouin diagram for the structure embodiments offering these narrow "hot" bandwidths in a practical tube. Matters of interaction impedance are also discussed as are the theoretical and experimental aspects of circuit attenuation and its variation across the ("cold") circuit passband. Questions of frequency-selective dielectric or dissipative loading are also included in Chapter 5. As this chapter is developed, attention becomes focused on the "B" Comb-Quad design option.

None of the interaction-region geometries that may be found in Comb-Quad structures are completely like those of conventional coupled-cavity chains, hence new sets of gap coefficients must be derived before reliable beam/wave interaction modeling can be undertaken. As discussed in Chapter 6, the most nearly conventional geometry can be treated by making relatively simple approximations, and the gap-coefficient formulations obtained also provided insights into the relation of a gap figure of merit to the gap-length-to-period ratio. At the other extreme, the least conventional interaction-region geometry (featuring a beam tunnel that can only be described as "virtual") is not even approximately axisymmetric, hence the derivation of gap coefficients for but one set of dimensions was a sizable computational effort. A qualitative finding was that this geometry, though constructionally attractive, is relatively less effective for beam-modulation purposes -- as if the tunnel diameter were effectively somewhat larger and the gap length generally somewhat longer. Unusual beam/wave interaction phenomena predicted as possible with this geometry, due to a physical feature re-occurring every two periods, is also discussed in Chapter 6.

Small-signal interaction modeling, for which previous chapters were preparatory, is taken up for the Comb-Quad B case in Chapter 7. Gain and

bandwidth are estimated for a hypothetical two-section TWT based on a representative B-type design. Also treated are the potential instabilities to which this design in particular is prone, and possible phenomena related to the second circuit passband.

Chapter 8 includes a summary of considerations given to eventual millimeter-wave fabrication of the interaction structures otherwise evaluated only via scale models and analysis. Some of the effects of geometric or dimensional deviations, in five categories, are examined -- in several cases referring to experimentally observed data. The preparation of an actual-size 42-period circuit section dimensioned for 94 GHz is also covered.

Chapter 9 reviews the extensive efforts made to develop a Comb-Quad B transition to external waveguide (for input, output and "external sever" loads). Although the design approach adopted was eminently successful in the Comb-Quad D and C cases, performance was less than completely satisfactory in the face of a B-design "hot" bandwidth very close to the passband edge. An untested coupler configuration based on a different principle is proposed as a potential alternative.

Insights into the structure's ability to accommodate heating due to beam interception and rf power dissipation were obtained through computations summarized in Chapter 10. As anticipated, the estimates of thermal capability are optimistic, even for comb teeth as small as they would be for around 44 or 94 GHz.

Chapter 11 covers the conclusions of the overall study program and the recommendations following therefrom. The interaction structures based on a thick one-piece ladder should remain in consideration, but optimization and further evaluation for that purpose are required. In the Comb-Quad case, the construction and test of a "hot" tube (whether type B, C or D) for some frequency above 20 GHz is a logical next step prior to further investment in "cold-test" or "paper" studies, including "large-signal" interaction modeling. Chapter 11 also contrasts the relative merits and drawbacks of Comb-Quad B vs Comb-Quad D designs for narrow-band CW applications. Despite

some unique advantages for the B option, and the emphasis on it under the subject contract, the D option now appears preferable.

The references cited in this report are listed as Chapter 12.

## 2.0 SLOW-WAVE STRUCTURES WITH A SINGLE SLAB LADDER

### 2.1 GENERAL

When interest first developed in using a metal ladder with half-wave rungs as the basis of a TWT interaction structure for millimeter wavelengths, the ladder rungs were visualized only as slender wires or thin tapes.<sup>1-3</sup> Flood (non-pencil) beam power densities and rf power levels were accordingly low (order of a few kW/cm<sup>2</sup> and a few tens of mW, respectively) but served the needs of the pre-solid-state era (c. 1950 - 68) at those wavelengths.

The idea of retaining the same slow-wave circuit types -- but replacing the fragile ladder with a more robust copper-slab ladder having a beam tunnel appropriate to a high-power pencil beam (the central object in Figure 1) -- appears to have been first suggested in two Varian solicited proposals to RADC (Nos. 78-11627, March 1978; and 78-30057, September 1978). One of two stimuli for these suggestions was RADC's interest in only a few percent of "hot" bandwidth (at the desired frequency and rf power levels -- 94 GHz, tens of watts); only in narrow-band applications can ladder-based slow-wave circuits be taken advantage of. The other stimulus was provided by tangible samples of the one-piece copper-slab ladders being manufactured for millimeter-wave EIKs by Varian Canada Inc. near Toronto.<sup>4</sup> Their fabrication is by electro-erosion, "burning" first the rectangular apertures between rungs, through the thickness of the slab, and then a round beam tunnel through the edge of the slab. (Only for the sake of generality does the thick ladder of Figure 1 show a square beam tunnel and the possibility of a slab comprised of two thinner slabs.)

Given the substantial ladder thickness, the box-like apertures between rungs are readily visualized as cavities, and it would not be incorrect to expect the propagation of rf power along the cavity chain to be moderated by whatever coupling was permitted between adjacent cavities. Compared with the cavities of a conventional coupled-cavity stack, those of Figure 1 lack the ferrules which provide re-entrancy and superior values of R/Q. However, at the shorter millimeter wavelengths, ferrules are nowadays being omitted

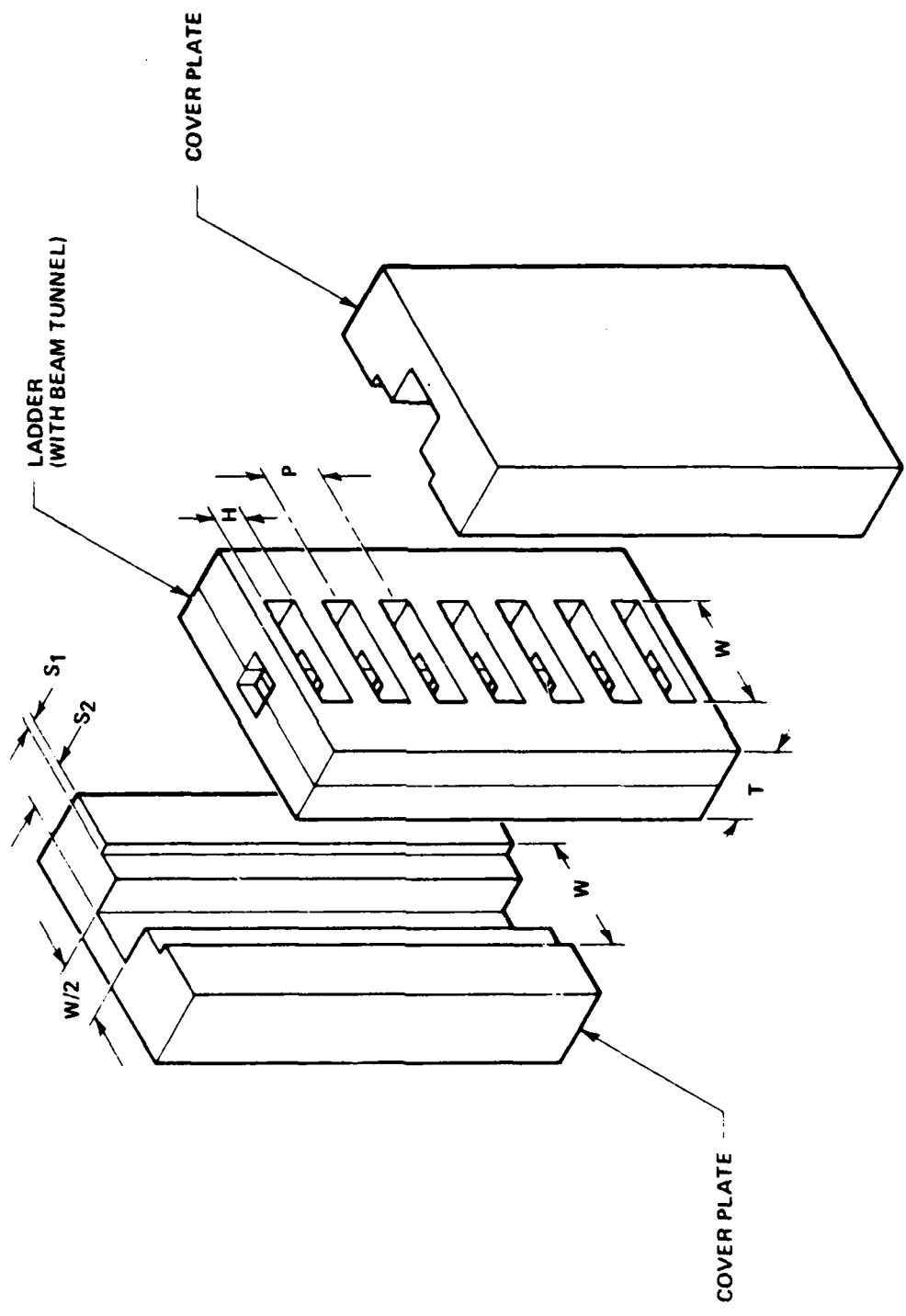


FIGURE 1. EXPLODED VIEW OF SPACE-HARMONIC TWT INTERACTION STRUCTURE HAVING SLAB LADDER BETWEEN T-GROOVED COVER PLATES.

from otherwise conventional cavities for the sake of fabrication economies,<sup>5</sup> with the decreased R/Q accepted as a design premise. In this case, the one-piece ladder approach becomes very attractive. With axial stacking eschewed, numerous metal-to-metal joints are avoided along with cumulative error in the periodicity. Optical inspection against deviations in the period (or other dimensions) can be implemented before the major expenses of tube assembly are incurred.

Techniques other than electro-erosion might be used to pierce the apertures that convert a slab into a ladder. As suggested in Figure 1, if it is not convenient to "drill" the beam tunnel (which can be either round or square) the slab can be comprised of two half-thickness slabs with a half-tunnel groove cut axially on each mating face. In any case, it is the cover plates placed against the ladder on both sides that complete a TWT slow-wave structure that is equivalent to one of several types of coupled-cavity chain. Two such examples, in which the thick ladder's cover plates were symmetrical and entirely uniform longitudinally, were investigated by Biggs<sup>6</sup> and evaluated with reference to low-perveance narrow-band TWTs having about 15 kV of beam voltage. For the interaction circuitry discussed in this chapter, there is no contact between ladder rungs and cover plates. The four longitudinal seams that are required at the sides of the ladder represent a relatively mild engineering challenge. Importantly, only three or four parts are put together regardless of the number of periods in the section.

## 2.2 "FORWARD-WAVE" SLAB-LADDER INTERACTION STRUCTURE

Figure 2 depicts a slab ladder clamped between symmetrical and axially uniform cover plates contoured so that there is no contact with the ladder rungs, but a ridge in each cover plate capacitively loads the center of each rung. In this case, the fundamental propagation ( $0 < \beta P < \pi$ ) is "forward-wave", as it is when  $T \rightarrow 0$ , and for the reasons stated in References 2, 3 and 7. Alternatively, the slow-wave structure of Figure 2 can be viewed as a coupled-cavity chain with a pair of "in-line" (i.e., not

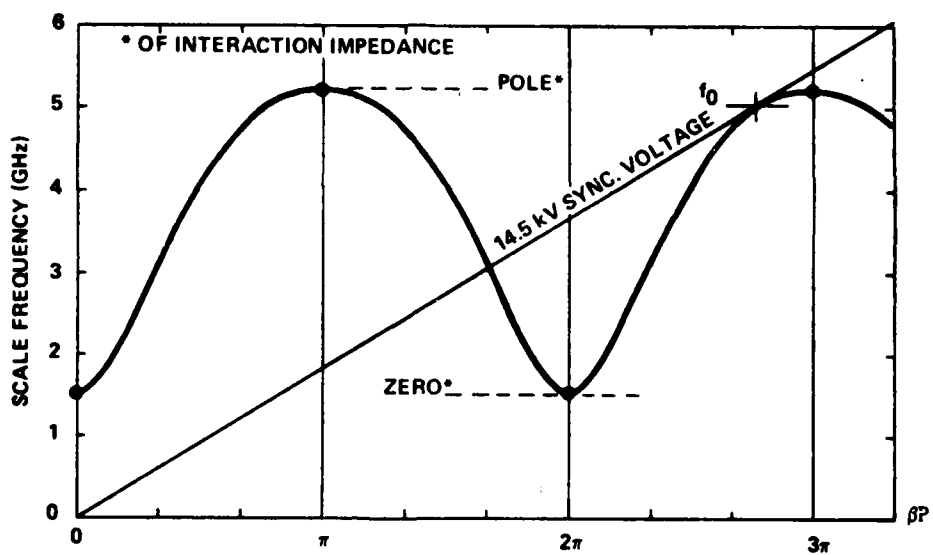
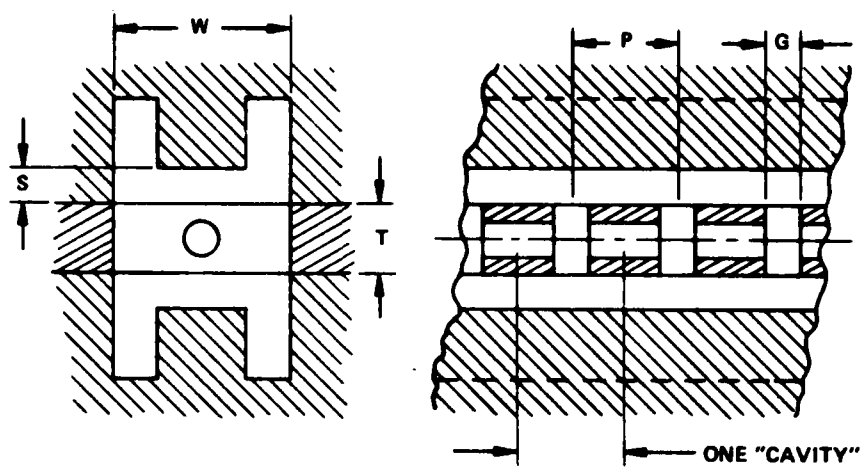


FIGURE 2. SPACE-HARMONIC TWT DESIGN USING DOUBLE-RIDGE LOADED SLAB LADDER (AFTER BIGGS<sup>6</sup>).

staggered or rotated) coupling slots between cavities. The exceptional size and shape of these slots would explain the propagation being "forward-wave" rather than "backward-wave".

The Brillouin diagram of Figure 2 was obtained by Biggs<sup>6</sup> with (in inches)  $P = 0.75$ ,  $G = 0.25$ ,  $T = 0.5$ ,  $W = 1.125$  and  $S = 0.25$ . As indicated, the electron beam must interact with the second space-harmonic wave, for which  $2\pi < \beta P < 3\pi$ . In particular, as in Millman's classic amplifier tube with a forward-wave circuit,<sup>8</sup> the line of constant phase velocity is tangent to the  $\omega-\beta$  curve, with the condition of tangency determining the potential operating center frequency and "hot" bandwidth. However, in Millman's milliwatt-output case,<sup>8</sup> where the period was small enough to call for only a few kV of beam voltage, the shape of the  $\omega-\beta$  curve placed the point of tangency for  $\beta P$  about midway between  $2\pi$  and  $3\pi$  -- whereas the higher voltage and longer period of the design of Figure 2 lead to a curve shape<sup>6</sup> placing the point of tangency for  $\beta P$  rather close to  $3\pi$ .

The circumstance of  $\beta P + 3\pi$  is not very favorable to a contemporary millimeter-wave communications amplifier design.<sup>6</sup> The Pierce impedance becomes relatively low, so that at low beam perveance, the electronic gain can barely exceed the circuit attenuation. At higher perveance, band-edge instability is likely to be a problem. Another disadvantage of an operating point so close to the passband edge is the difficulty of developing end couplers for the periodic structure. While the gain and bandwidth projections of Reference 6 do not completely rule out this design approach, it does appear to be relatively unpromising.

### 2.3 "BACKWARD-WAVE" SLAB-LADDER INTERACTION STRUCTURE

Figure 3 depicts (as does Figure 1) a slab ladder clamped between symmetrical and axially uniform cover plates contoured so no contact with the ladder rungs occurs, but a T-shaped channel is formed on each side of the ladder. As when  $T \rightarrow 0$ , the fundamental propagation ( $0 < \beta P < \pi$ ) in the lowest passband is "backward-wave" for the reasons given in Reference 7 (where this slow-wave structure, as  $T \rightarrow 0$ , is referred to as the Antikarp circuit). An alternative view of the interaction structure of Figure 3 is

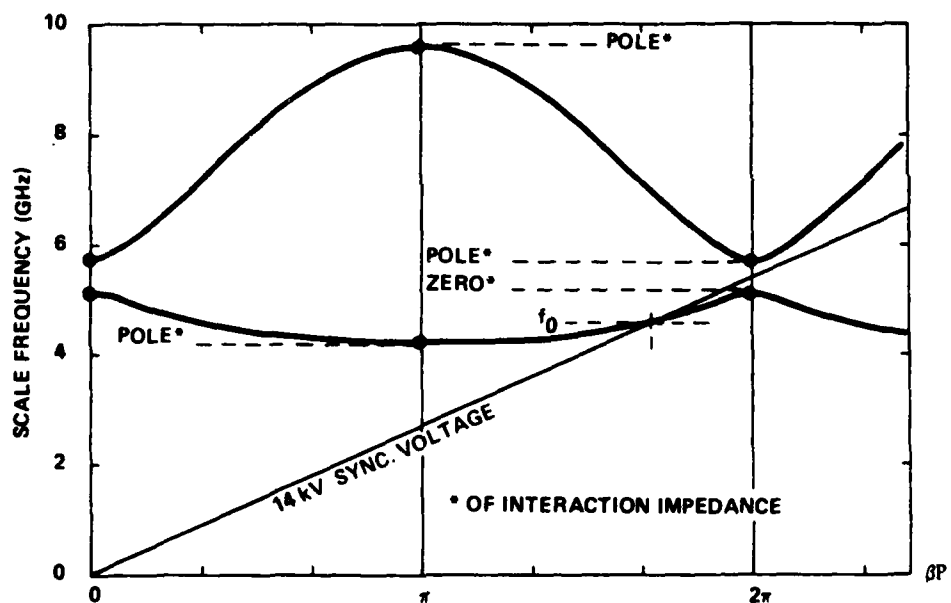
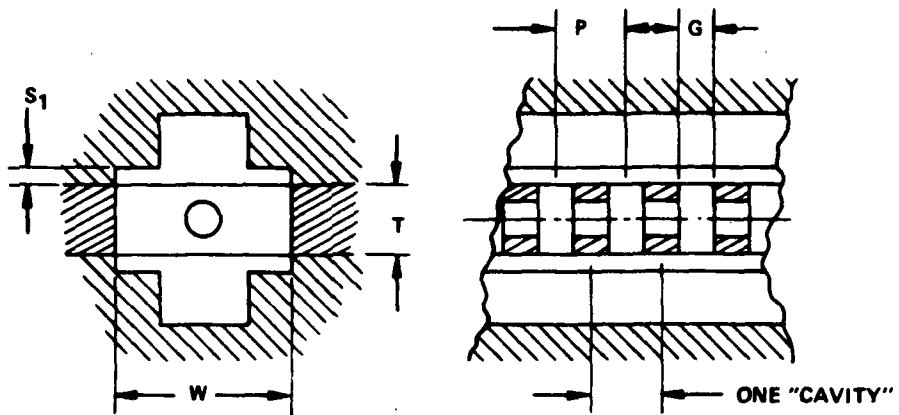


FIGURE 3. SPACE-HARMONIC TWT DESIGN USING T-GROOVE  
LOADED SLAB LADDER (AFTER BIGGS<sup>6</sup>).

as a coupled-cavity chain with twin "in-line" coupling slots whose T shape permits the net coupling between cavities to be magnetic, despite the slot length.

The Brillouin diagram of Figure 3 was obtained by Biggs<sup>6</sup> for (in inches)  $P = 0.5$ ,  $G = 0.25$ ,  $T = 0.5$ ,  $W = 1.25$  and  $S_1 = 0.125$ . As indicated, the electron beam would interact with the first space-harmonic wave, for which  $\pi < \beta P < 2\pi$ , as in most conventional coupled-cavity amplifiers. The general flatness of the  $\omega-\beta$  curve (for the lowest passband) is usual when coupling slots are "in-line" (not staggered or rotated) going from interface to interface. However, the presence of a zero rather than a pole of interaction impedance at the  $2\pi$  point (lower passband) does constitute a difference relative to conventional coupled-cavity structures, whether the coupling slots are "in-line"<sup>9</sup> or otherwise.

For the structure of Figure 3, the  $2\pi$ -point pole of interaction impedance occurs at the nearby lower edge of the upper passband, with no possibility of raising this edge through geometry changes once  $T$  is fixed. Therein lies a constraint on the potential usefulness of this design approach. If one attempts to raise the beam voltage ( $V_0$ ), to move the operating frequency ( $f_0$ ) closer to  $f_\pi$  (lower passband) and obtain a higher interaction impedance, oscillation near  $f_{2\pi}$  (upper passband) becomes possible. If one attempts to lower  $V_0$ , to move  $f_0$  closer to  $f_{2\pi}$  (lower passband), increase the "hot" bandwidth and avoid the upper-passband oscillation problem, a rapid diminution of interaction impedance at  $f_0$  is encountered. If a compensating perveance increase were contemplated,  $V_0$  would have to be increased further above the "synchronous voltage," reintroducing the likelihood of upper-passband oscillation.

Given the very narrow choice of  $V_0$ , the gain and bandwidth projections undertaken in Reference 6 are nevertheless moderately promising, even at the necessarily low beam-perveance values. At  $V_0 = 14.0$  kV, with microperveance 0.05, for example, a two-section TWT with 50 periods per section might have a gain of 40 dB and a 3 dB bandwidth of about 2.6%, neglecting circuit attenuation. Further information may be found in the reference.<sup>6</sup>

## 2.4 FURTHER DEVELOPMENT OF T-GROOVE LOADED SLAB-LADDER CIRCUIT

In the Summer of 1980 further C- or G-Band cold-test experiments were undertaken with the periodic structure of Figure 1, but with relatively large values of the ladder thickness  $T$ . At first, the period  $P$  was chosen so large that beam voltages of 40 kV or more would be required. These data are consequently not of direct interest to the current contract. However, the increased dimension  $T$  proved to be of benefit to the potential TWT performance, so a new extra thick model was developed with a reduced  $P$  appropriate to  $V_0 \approx 14$  kV. The experience of having tested both high- and low-voltage models provided the useful knowledge that the maximum cold bandwidth obtainable seems to be about inversely proportional to  $P$ .

The low-voltage structure dimensions were (in inches, per Figure 1)  $P = 0.5$  and  $H = 0.25$  (same as for Figure 3 where  $G$  and  $H$  refer to the same dimension),  $T = 1.0$  (double that in Figure 3),  $W = 1.5$  and  $S_1 = 0.125$ .  $S_2$  was made adjustable. The Brillouin diagram obtained, shown in Figure 4, has "coalesced passbands", a condition produced in this case by adjusting  $S_2$  to be 1 inch. When  $S_2$  is reduced, a stop band develops between the two passbands, with a pole of interaction impedance at  $f_{2\pi}$  (upper) and a zero at  $f_{2\pi}$  (lower); this situation is the same as in Figure 3, with the attendant limitations on potential amplifier performance.

However, when  $S_2$  is increased above the value providing "coalesced passbands," the stopband develops with the  $f_{2\pi}$  pole of interaction impedance assigned to the lower passband -- as is true for conventional coupled-cavity structures. (The lower passband also shows a pole at  $f_\pi$ .) The zero of interaction impedance at  $f_{2\pi}$  in the upper passband would indicate freedom from the upper-passband oscillation problem discussed in Section 2.3. In the "coalesced" case, the pole and zero essentially neutralize each other, so the oscillation problem is avoided there also.<sup>9</sup> Since stability should be assured either way, the "coalesced" condition would be preferred only because the cold bandwidth is thereby maximized, along with the suggested hot bandwidth. Bandwidths should also be maximized by using  $W/2$  as the width of the central trench in the cover plate,<sup>7</sup> and by making  $S_1$  as small as is practical.<sup>6,7</sup>

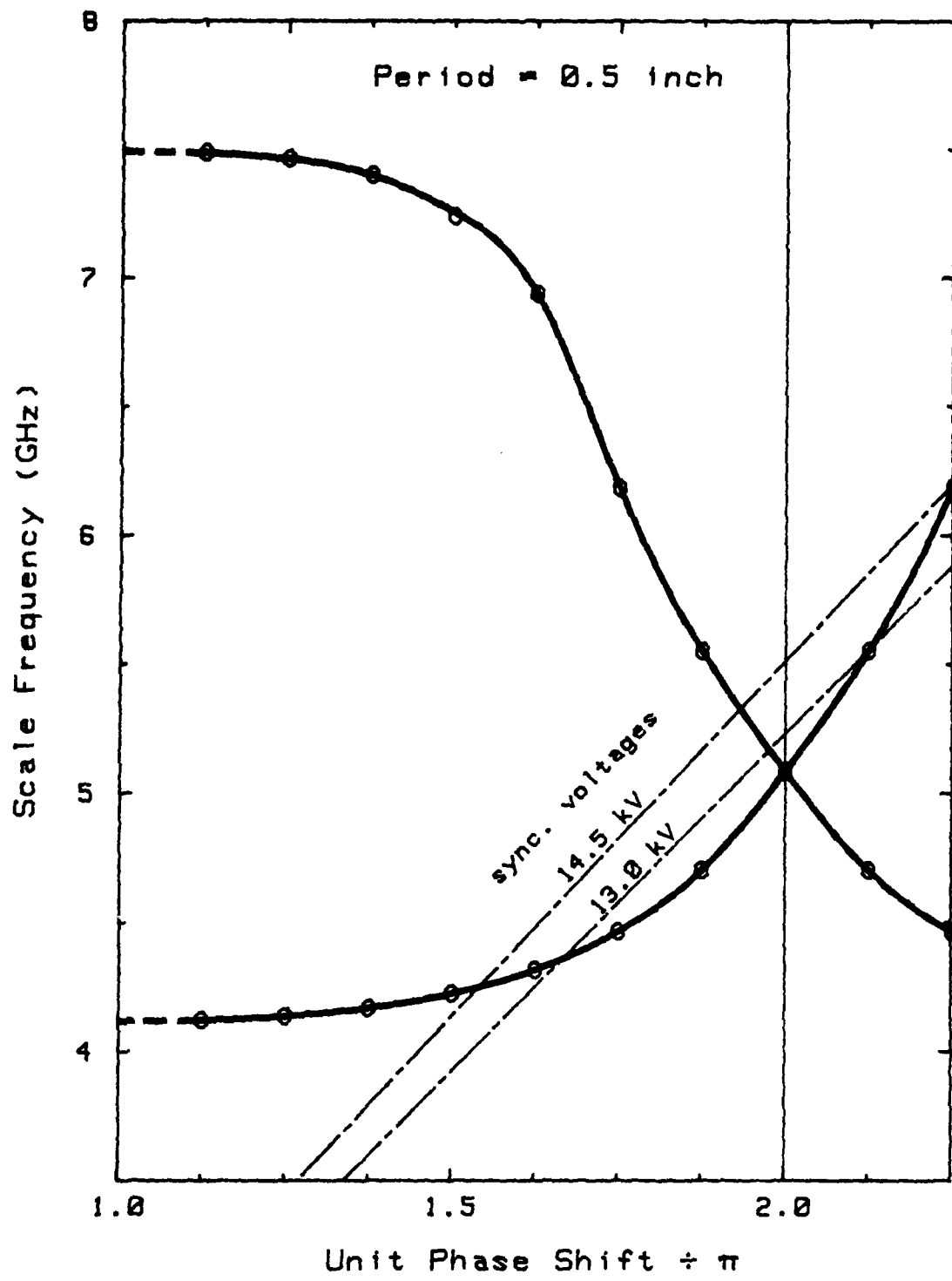


FIGURE 4. BRILLOUIN DIAGRAM FOR INTERACTION STRUCTURE OF FIGURE 1 WITH RATHER THICK LADDER.

The  $\omega$ -B curves of Figures 3 and 4 are predictable at least in part. The lowermost  $f_\pi$  is slightly above  $c/2W$ , where  $c = 3E10$  cm/sec. The TE cutoff frequency of a waveguide having the same cross-section as the T-shaped groove is about equal to the impedance-zero  $f_{2\pi}$ , while the impedance-pole  $f_{2\pi}$  (whether higher, lower, or the same) corresponds to a TM "cavity" resonance. The rf field and current distributions at these critical frequencies are easy to visualize but their description would overly lengthen this report.

Inserting a sapphire rod on the structure axis, to perturb the resonance frequencies of the cold-test circuit model, provided data for determining R/Q and the Kino interaction impedance, as tabulated below for the structure to which Figure 4 applies. The former is a measure of the ratio of the square of the axial E field,  $E_z$ , to the stored energy; the latter indicates the ratio of the square of the gap voltage to the power flow. At Varian, the relevant  $E_z$  is, for consistency, that at the edge of the beam tunnel even though the dielectric rod is introduced on the axis. The R/Q values obtained reflect this fact, as well as the unnecessarily large and square (0.41 inch across) beam tunnel adopted for this model. Since the passbands are coalesced in Figure 4, the Kino impedance is neither zero nor infinite at the  $2\pi$  point. (The third-from-last data line corresponds to this "coalescence point"; the last two lines cover the lower end of the upper passband.)

BP/ $\pi$	f (GHz)	R/Q (ohms)	Kino Impedance (ohms)
1.125	4.117	47.2	6630
1.250	4.133	45.0	3200
1.375	4.165	42.3	1680
1.500	4.221	39.5	905
1.625	4.312	33.7	442
1.750	4.462	30.6	224
1.875	4.699	23.6	95.4
2.000	5.079	21.3	47.1
1.875	5.542	17.1	23.4
1.750	6.182	13.3	11.8

Figure 4 suggests operation with a synchronous voltage between 12 and 15 kV, with  $\beta P/\pi$  ranging from 1.75 to 1.50. R/Q would thus be in the 30 to 40 ohm range. (The unlikelihood of upper-passband oscillation is reflected in the very low interaction impedances applicable to the lower end of the upper passband where backward-wave synchronism is possible, in principle.) Only preliminary modeling of a hypothetical two-section TWT using this structure has been attempted, with a very low beam perveance assumed. Due to the low gain per period in this case, a large number of periods per section was adopted, so only very narrow "hot" bandwidths were subsequently predicted.

Further study is called for to complete the evaluation of this form of interaction structure, whose chief merits are in the method of fabrication (which includes no parts in contact with the ladder rungs). Only one low-voltage cold-test model was examined, and its proportions are unlikely to be optimal with respect to gain/bandwidth. (A possible exception is in 0.5 as the widely recognized optimum for the ratio H/P or G/P when  $\beta P/\pi$  is in the vicinity of 1.5; as H/P is increased, R/Q increases but the gap coefficient  $M^2$  decreases, hence there is an optimal H/P for a given  $\beta P$ .) A somewhat higher design value of  $V_0$ , such as 20 - 25 kV, would be more in keeping with the beam-tunnel size adopted; it would also permit taller "cavities" and otherwise favor a more practical TWT.

### 3.0 TRI-LADDER SLOW-WAVE STRUCTURE

The idea expressed by Figure 5, for creating a CC TWT interaction structure with three slab ladders, evolved at Varian during the Summer of 1980. The central ladder, with its round or square beam tunnel, has all the attributes of the slab ladders to which Chapter 2 refers. However, when it is clamped between the outer pieces which enclose it, some copper/copper bonding (via brazing, diffusion, electroforming, ...) will in this case be necessary. Electrical performance advantages hopefully would offset this extra engineering concern.

The periodicity of the rungs and apertures in the two outer ladders (Figure 5) is exactly double that of the center ladder. The two outer ladders are "staggered" relative to one another, with the result that a folded waveguide or staggered-slot coupled-cavity chain is formed when all the layers are clamped together. Each "outer ladder" and adjacent "outer cover" can be either two pieces or one somewhat thicker plate with rectangular indentations on the surface facing the center ladder. In any case, only three to six pieces need to be put together regardless of the number of periods in the TWT section.

In the first cold-test model investigated,  $P$  was relatively large so the required  $V_0$  was in the range 40 to 60 kV. Although these voltages are too high with regard to present interests, the model was useful in letting the effects of varying some of the geometric parameters be demonstrated. When a low-voltage design (14 - 18 kV) was evaluated, comparison again showed that the maximum obtainable cold bandwidth is about inversely proportional to  $P$ . In both models,  $H_2$  was chosen equal to  $P$  as a matter of convenience but not necessity. As discussed previously, selecting  $H_1/P = 0.5$  should about maximize the product  $M^2 R/Q$  when  $\beta P/\pi \approx 1.5$ , where  $M^2$  is the conventional gap coefficient. As noted in Figure 5,  $W_2$  can be (and was during experimentation) varied relative to  $W_1$ ; however, selecting  $W_2 = W_1$  is not only a mechanical convenience but maximizes the cold bandwidth.

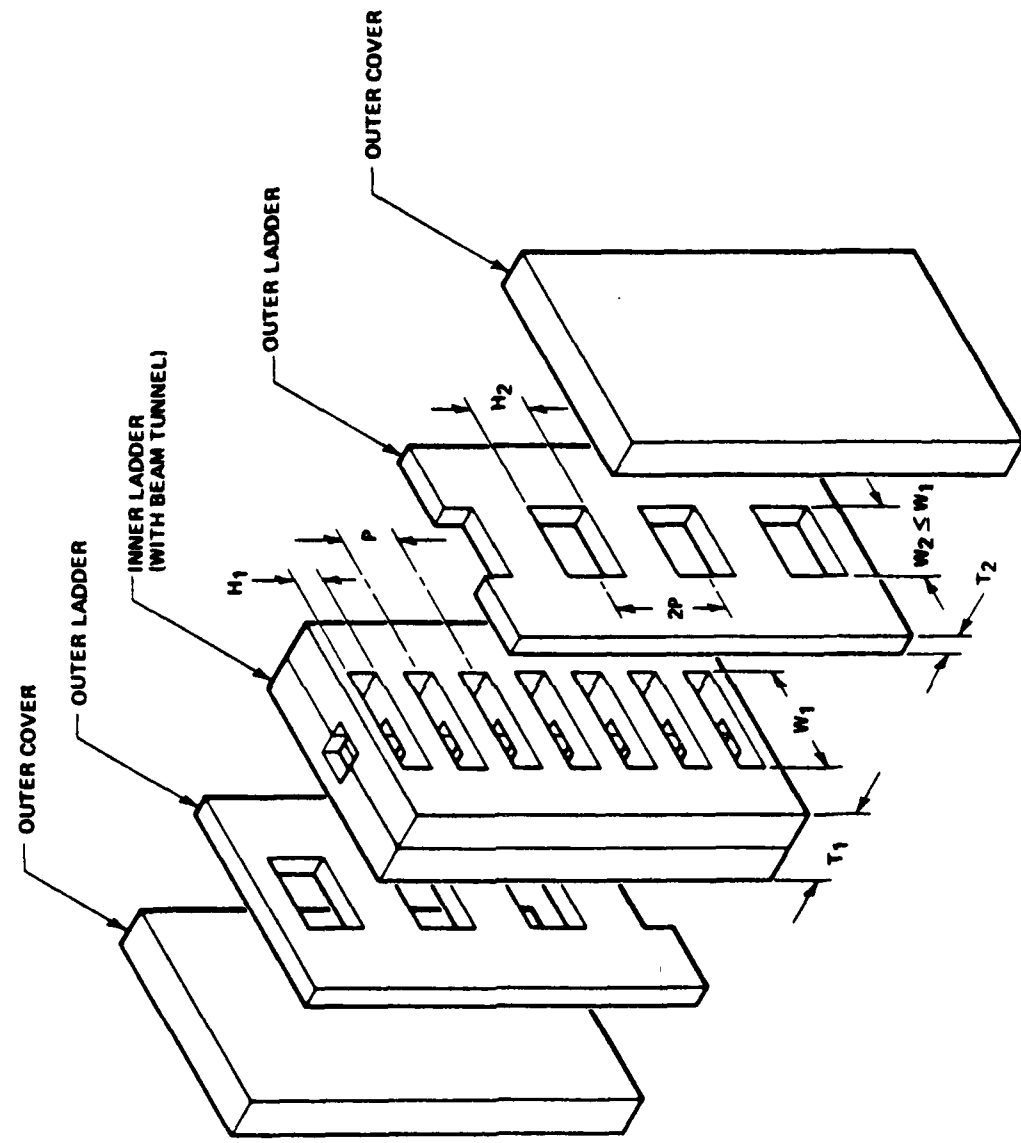


FIGURE 5. EXPLODED VIEW OF TRI-LADDER CC TWT INTERACTION STRUCTURE.

Figure 6 shows the Brillouin diagram obtained for  $P = 0.5$ ,  $H_1 = 0.25$ ,  $H_2 = 0.5$ ,  $W_2 = W_1 = 1.5$ ,  $T_1 = 1.0$  and  $T_2 = 0.375$ , all in inches. Initially,  $T_2$  was allowed to be variable, but the final value was selected to provide "coalesced" passbands. When the value of  $T_2$  is larger or smaller, a stopband appears with the interaction-impedance pole below or above the zero, in frequency, respectively. The "pole-below-zero" and "coalesced" cases are both favorable to stability, but the latter should maximize the cold and hot bandwidths. Relative to the  $\omega-\beta$  curve of Figure 4, the less extreme variation in group velocity within the lower passband of Figure 6 should favor wider hot bandwidths. This feature accounts for the considerable popularity of "staggered" coupling in CC TWTs regardless of cavity format.

With  $W_1 = W_2 = W$ , two of the critical frequencies of Figure 6 are easily predicted. The lowermost  $f_\pi$  is  $c/2W$ , or the cutoff frequency of the folded waveguide. The impedance-pole  $f_{2\pi}$  is very nearly the resonance frequency of a simple rectangular cavity measuring  $W$  by  $(T_1 + 2T_2)$  by  $H_1$ , with  $H_1$  in the direction of the uniform axial electric field.

Sapphire-rod perturbation data were processed to yield R/Q and interaction-impedance values, as tabulated below for the Tri-Ladder structure to which Figure 6 applies. These values are, for a given  $\beta_p$ , generally somewhat lower than those of the structure of Section 2.4, and also continue to reflect the absence of ferrules and an unnecessarily oversize beam tunnel. However, comparison at this level is unwarranted, since other parameters that also affect gain (such as  $V_0$  and  $\beta$ ) would be different in operation.

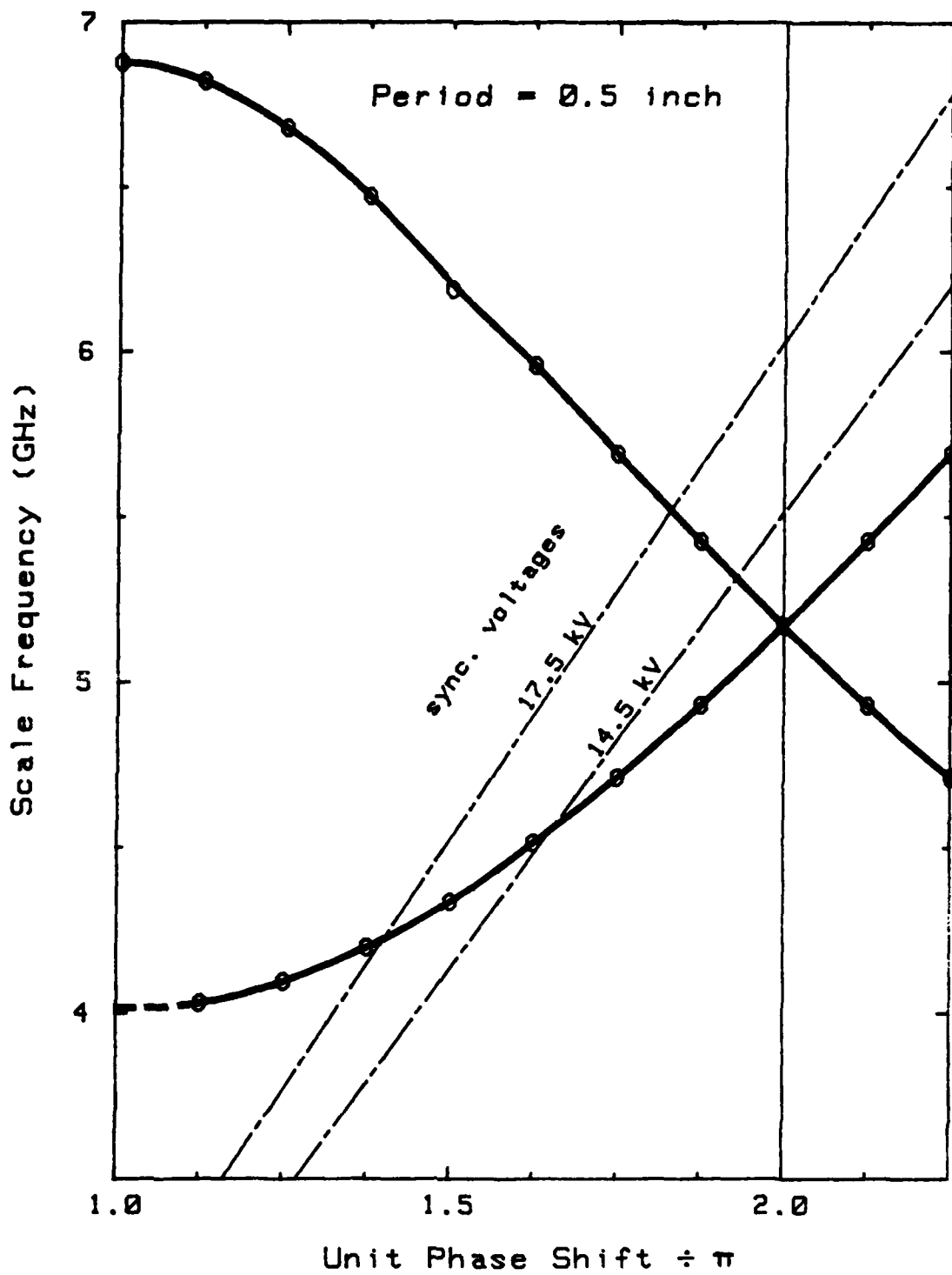


FIGURE 6. BRILLOUIN DIAGRAM FOR TRI-LADDER INTERACTION STRUCTURE OF FIGURE 5.

<u>Bp/π</u>	<u>f (GHz)</u>	<u>R/Q (ohms)</u>	<u>Kino Impedance (ohms)</u>
1.125	4.031	37.0	1075
1.250	4.096	34.6	489
1.375	4.201	31.8	301
1.500	4.336	27.3	198
1.625	4.514	25.4	150
1.750	4.714	23.0	117
1.875	4.934	20.9	95.0
2.000	5.174	17.9	75.4
1.875	5.430	14.5	58.8
1.750	5.694	12.9	52.7

Figure 6 suggests operation with a synchronous voltage of 15 to 18 kV, with  $B_p/\pi$  between 1.35 and 1.6, and R/Q in the range of 25 to 35 ohms. (As noted for the design discussed in Section 2.4, very low interaction impedances again apply to the lower end of the upper passband where backward-wave synchronism is possible in principle.) Only preliminary modeling of a hypothetical two-section TWT based on this low-voltage version of the Tri-Ladder structure has been attempted, with a very low beam perveance assumed. As was found for the model of Section 2.4, the low gain per period again suggested a large number of periods per section and consequently extra narrow "hot" bandwidths.

Further study would be needed to complete the evaluation of the Tri-Ladder approach to interaction circuitry, especially if dimensional variations could be explored with a view to optimizing gain/bandwidth. Higher design values of  $V_0$  (above 20 kV) should again favor a more practical TWT, through the relation of  $V_0$  to the cavity height, the beam-tunnel diameter, and the practicality of beam focusing at a prescribed level of beam power.

A problematic aspect of the periodic structure of Figure 5, with parallels also applying to any structure which is both "staggered" and assembled via transverse rather than axial "stacking", is the following: If the two outer ladders are not precisely alike, and if the discrepancy is

consistent along some length of structure, the resulting bi-periodicity will tend to introduce a stopband centered at the frequency for which  $\theta_p = 3\pi/2$ . The effect might not be important if the discrepancy is small and the circuit attenuation is appreciable, and it might not affect performance if the "hot" bandwidth does not include  $f_{3\pi/2}$ . (The discrepancy referred to might consist of a misalignment relative to the rungs of the center ladder, or inconsistency of  $H_2$ ,  $W_2$  or  $T_2$  between one outer ladder and the other.)

## 4.0 COMB-QUAD INTERACTION STRUCTURE

### 4.1 INTRODUCTION

The remainder of this report, as was the major effort of the subject study program, is focused on certain capabilities of a new approach to interaction circuitry [U.S. Patent No. 4 237 402, filed 26 March 1979, issued 2 December 1980] promising economic and other improvements for high-power millimeter-wave CC TWTs in several applications areas. The new concept is introduced in this chapter which also reviews the salient features and the relationship to more conventional (coupled-cavity) interaction circuitry.

### 4.2 STRUCTURAL BASICS

For purposes that will become apparent later, Figure 7 illustrates the conventional concept of creating a coupled-cavity interaction structure via axial stacking. Whether or not a "ring" and "plate" are combined into one cup-like unit, several dozen piece parts must be stacked and fused together to obtain one CC TWT section at millimeter wavelengths. During the fusing operation, any warpage invalidates the fine tolerances on axial dimensions, one purpose of which was to preserve the critical interaction gap length determined as the difference between two larger axial dimensions. Another justification for extraordinarily tight axial tolerances per part is to prevent an excessive cumulative error in the period. A concern of the operation to fuse the axially stacked parts is the numerous circumferential joints; with excessive flow of metal, the cavity volume is perturbed; with insufficient wetting, resistance is introduced into important rf cavity-current paths.

The "ferrules" (drift-tube extensions) of Figure 7 create the cavity "re-entrancy" that elevates the gain-related parameter R/Q. Measures adopted to make the structure thermally and mechanically more robust -- shorter and stouter ferrules and thicker webs -- inevitably lower R/Q. The

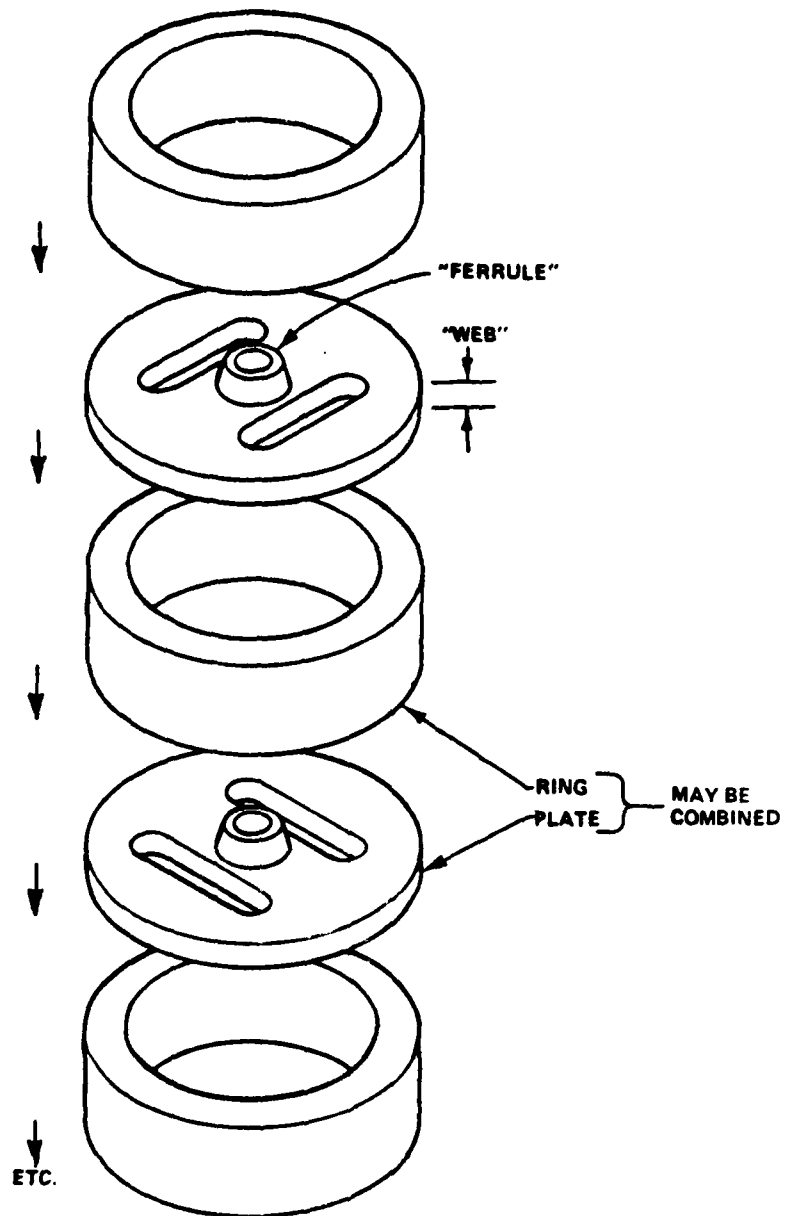


**FIGURE 7. AXIAL STACKING CONCEPT (APPLIED TO COUPLED-CAVITY STRUCTURE USING TWIN COUPLING SLOTS AND 90° RE-ORIENTATIONS).**

mechanical difficulties associated with ferrules have recently prompted their omission in otherwise conventional cavity stacks for the shorter-wavelength bands,<sup>5</sup> with the reduced R/Q accepted as a design constraint.

The coupling slots selected for illustration in Figure 7 are twinned and reoriented 90° from plate to plate, as one of the two "staggered" coupling options that are conventional at centimeter wavelengths. This coupling scheme is electrically equivalent to that of a single aperture reoriented 180° from plate to plate, the prevalent choice to date at millimeter wavelengths. In either case, the "staggering" provides the "folded waveguide" equivalence that promotes wide bandwidths. These slots must remain small, to provide only magnetic coupling, with correspondingly close tolerances to ensure uniformity along the length of the tube.

Figure 8 exemplifies the "Comb-Quad" approach to interaction circuitry that came to light at Varian in the Fall of 1978. In either case illustrated, and no matter how many periods the section is to contain, only four comb-like elements are needed to establish the periodicity and the slow-wave property of the structure. These are brought together in a way that contrasts dramatically with axial stacking. Each comb would be cut from a single piece of copper, probably by a reliable but inexpensive technique such as electroerosion or "chemical milling". All four combs might well be cut "ganged" to ensure equivalence, and thoroughly inspected for dimensional uniformity, longitudinally, before any further effort is expended on assembly. Uniformity of periods and interaction gaps would not then be something discernible only by inspection of x-ray pictures or by inference from beam interaction -- some time after a costly assembly procedure. Interestingly, the number of periods in a Comb-Quad section is twice the number of teeth in any one comb. The cutout between teeth has dimensions larger than the thickness of the comb, making each comb almost two-dimensional. These features would facilitate fabrication by chemical (photo-lithographic) or laser milling as well as by electroerosion with traveling-wire or rotating-disk "burners".

Figure 8 also indicates that four metal pieces are additionally needed to support and enclose the combs without encroaching on the tooth region.

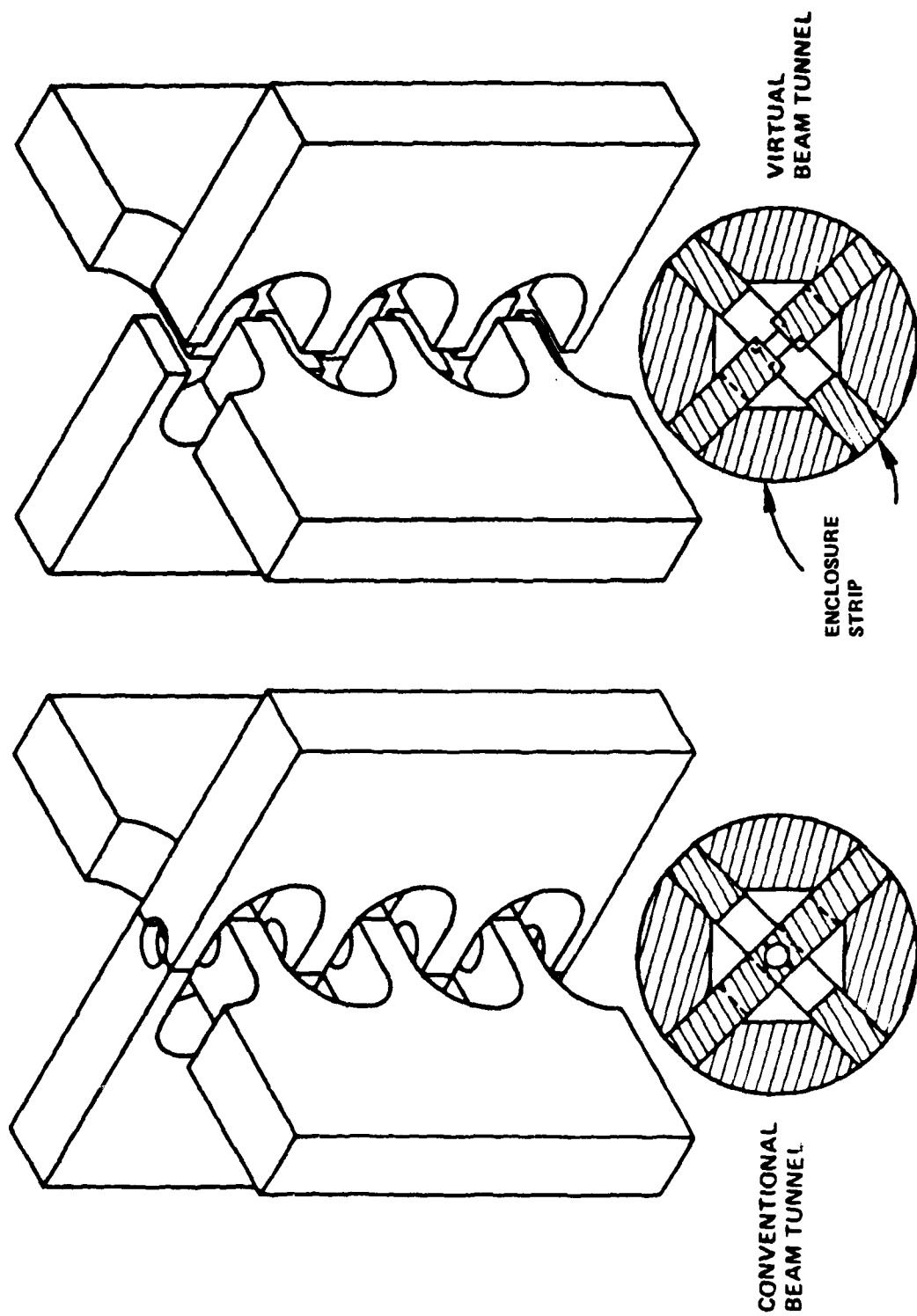


FIGURE 8. COMB-QUAD APPROACH TO CC TWT INTERACTION CIRCUITY.  
(TWO VERSIONS DIFFER WITH REGARD TO BEAM TUNNEL IMPLEMENTATION.)

These "enclosure" pieces would have a simple and axially invariant cross section, without periodic features. The final assembly would thus have eight longitudinal seams -- or perhaps only four if an enclosure strip were integral with the uniform "backbone" of a comb. As will be discussed later, these seams possess only limited potential for introducing rf attenuation into an inherently low-loss circuit. A promising assembly approach envisioned for a Comb-Quad section would begin with the four combs clamped in a fixture permitting proper alignment ("registration") of the teeth and complete subsequent inspection. The "enclosure" might then be formed by brazing or electroforming copper over a dissolvable material covering the teeth and determining the central cavity cross section.

Before this chapter is concluded, the electrical and topological equivalence of the slow-wave circuits of Figures 7 and 8 should become apparent, and less astonishing. It is nevertheless impressive that the bringing together of four combs creates, all at once, a stack of cavities with coupling slots and a beam tunnel. Moreover, these cavities effectively have the quality of re-entrancy and the consequently higher value of R/Q. This quality is fortunately obtained without compromising thermomechanical robustness and can be retained through the higher frequency ranges where the ferrules of conventional cavities must be omitted.

#### 4.3 BEAM-TUNNEL OPTIONS

The two drawings of Figure 8 illustrate two extremes with regard to implementation of a beam tunnel. At the left [see also Figure 9(a)] notched tooth tips are shown so that a conventional beam tunnel is formed when the combs are brought together to create a pair of interlaced ladders. (There is no thermal or electrical requirement for good contact where mating teeth touch.)

At the right in Figure 8, and in Figure 9(c), the teeth are somewhat shorter and a space is introduced where opposing teeth might otherwise meet. This novel approach, which suggests that the beam tunnel is now "virtual", seems exceptionally attractive mechanically and thermally. Electrically, gap/tunnel effectiveness is reduced, but not severely, as discussed

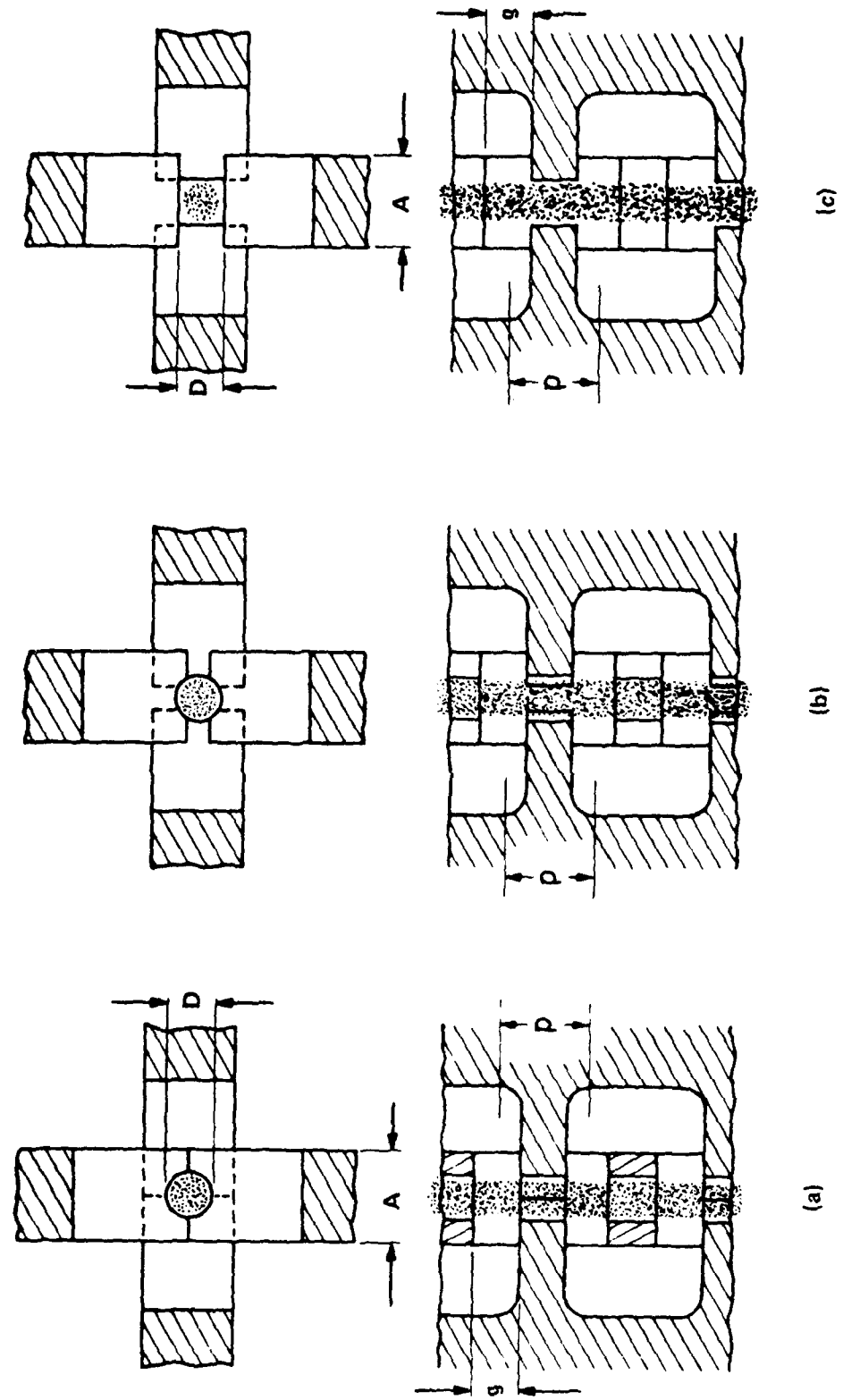


FIGURE 9. BEAM TUNNEL OPTIONS FOR COMB-QUAD STRUCTURE  
 (a) CONVENTIONAL (CBT); (b) INTERMEDIATE; (c)  
 "VIRTUAL" (VBT).

elsewhere. (The possibility of reduced or more controllable beam interception has not been evaluated.)

By way of abbreviation, the suffixes /CBT and /VBT may be added to circuit descriptors to identify the two beam-tunnel options, respectively. A third possibility is shown in Figure 9(b) -- a design intermediate between the other two and providing intermediate mechanical and electrical properties. Figure 9 also indicates how the circuit period,  $p$ , is defined for present purposes. (This preferred definition, based on the gap-to-gap distance, differs from that of References 10 and 11.)

#### 4.4 TOOTH PROFILE OPTIONS

Figure 10 depicts several choices for shaping the teeth of a comb intended for the assembly of Figure 8, assuming in this case the VBT beam-tunnel option of Figure 9(c). Three possible longitudinal profiles (a-c) are suggested, any of which might be combined with any of the suggested transverse formats (d-f). The profiles of Figure 10 are drawn to scale from cold-test models appropriate to beam voltages near 20 kV. The short, sturdy appearance of the teeth is not exaggerated, and changing  $p$  to accommodate other beam voltages would result in thicker or thinner but not longer teeth.

The combination (a, d) has been used in several Comb-Quad designs because of its simplicity. The combination (c, d) has also been implemented since this design should be more robust as well as compatible with electroerosion cutting using a traveling-wire "burner". The combination (c, e) has also provided a cold-test model suggesting maximum sturdiness and power-handling capability with little difference in the electrical properties. The transverse section (f) lends itself to comb fabrication via electroerosion using rotating-disc "burners". With four such combs, no additional parts would be required for a snug fitting "enclosure" which would then have only four longitudinal seams.

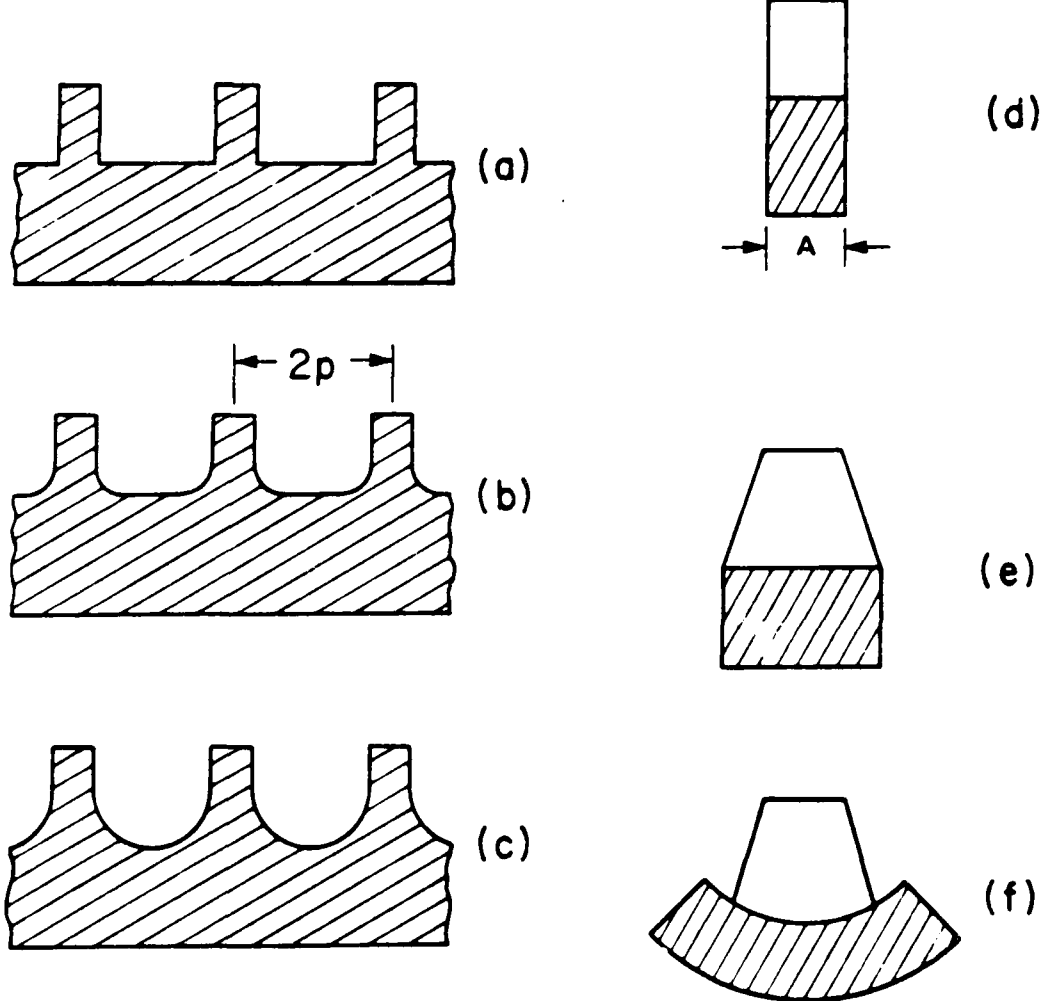


**FIGURE 10. TOOTH-PROFILE OPTIONS FOR COMB-QUAD STRUCTURE,  
VBT ASSUMED. (a - c) LONGITUDINAL SECTIONS; (d - f)  
TRANSVERSE SECTIONS.**

#### 4.5 ENCLOSURE OPTIONS

The already referred to enclosure that supports and surrounds the four combs has been found to be a major determinant of the interaction structure's electrical properties; its features are only highlighted in this introductory section. Five basic types of enclosure were distinguished during the first months of Comb-Quad investigation, as suggested by Figure 11. The resulting design possibilities were accordingly identified as "Comb-Quad A" through "Comb-Quad E". Specifically, Figure 11 illustrates, in transverse section, Comb-Quad A/CBT, Comb-Quad B/CBT, Comb-Quad C/CBT and Comb-Quad E/CBT, but as a reminder of other beam-tunnel options, both Comb-Quad D/CBT and D/VBT are illustrated. In all cases, the "enclosure" is axially invariant, with all periodicity accounted for by the combs alone.

Sketch A of Figure 11 represents four combs (or two interlaced ladders) surrounded by "free space" or a large enclosure lined with non-reflective rf-absorbing material. Even in this extreme case, a coupled-cavity-equivalent structure is obtained, as verified in "cold test". Sketches B through D suggest three successive stages of reducing the perimeter of a conducting enclosure from fairly large (B) to minimal (D). As will be discussed later, these three enclosure styles account for three basic types of  $\omega$ - $\beta$  curve, all describable, however, as coupled-cavity responses. [When suitably adjusted, Enclosure E (or its equivalent E') provides the special case of coupled-cavity  $\omega$ - $\beta$  response -- not of interest to the current contract -- in which the two lowest passbands are "coalesced".] The relationships between enclosure style and  $\omega$ - $\beta$  response are elaborated on in Chapter 5.

#### 4.6 RF FIELDS AND CURRENTS

Figure 12 shows an enlargement of the uppermost two periods of the interlaced-ladder structure at the left in Figure 8. Three imaginary planes (spaced  $p$  apart) through successive "rungs" have been added to the drawing to demarcate and aid in visualizing two successive "cavities". Twin "coupling slots" may be seen to lie in each such plane, with  $90^\circ$

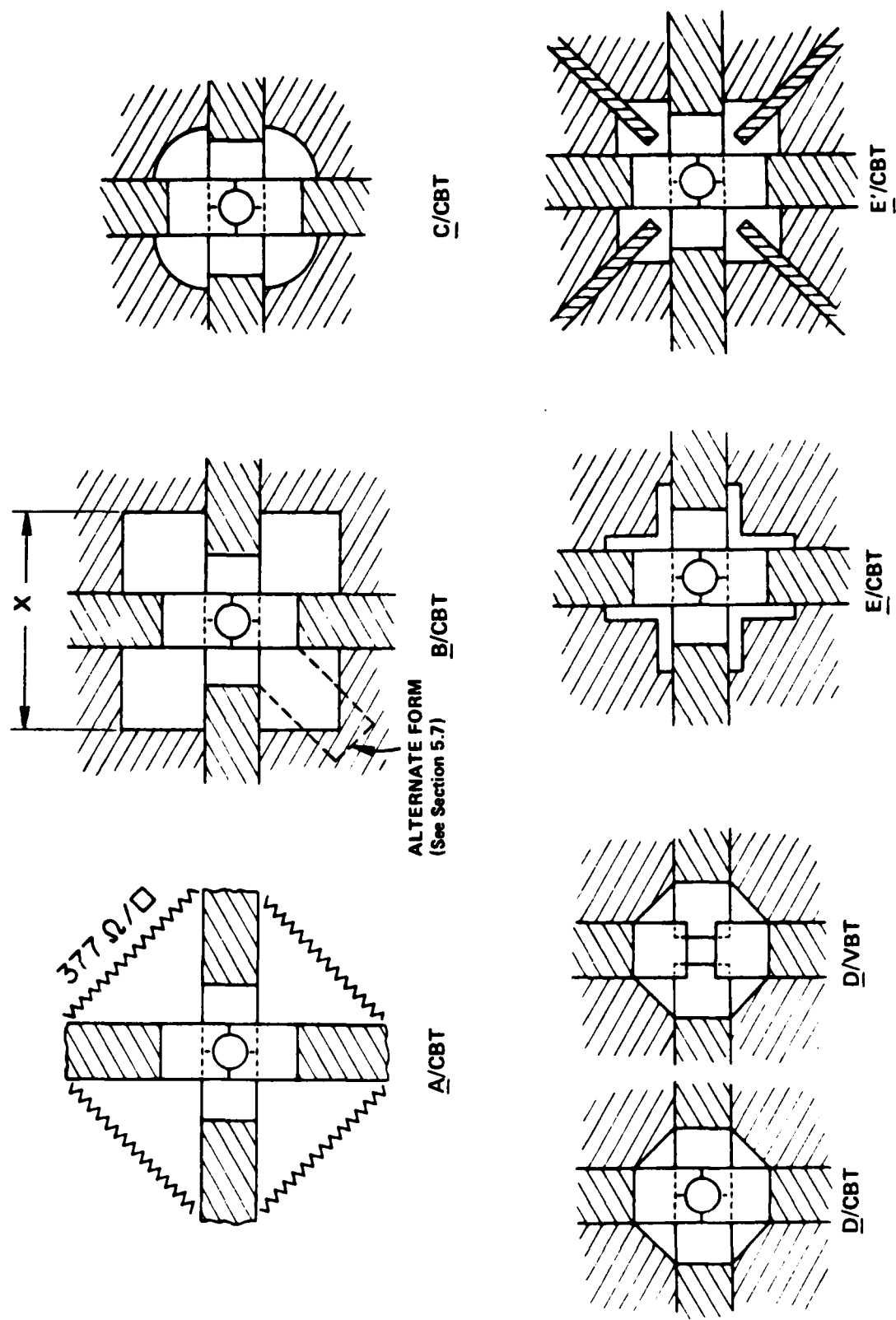


FIGURE 11. TRANSVERSE SECTIONS INDICATING COMB-QUAD ENCLOSURE OPTIONS

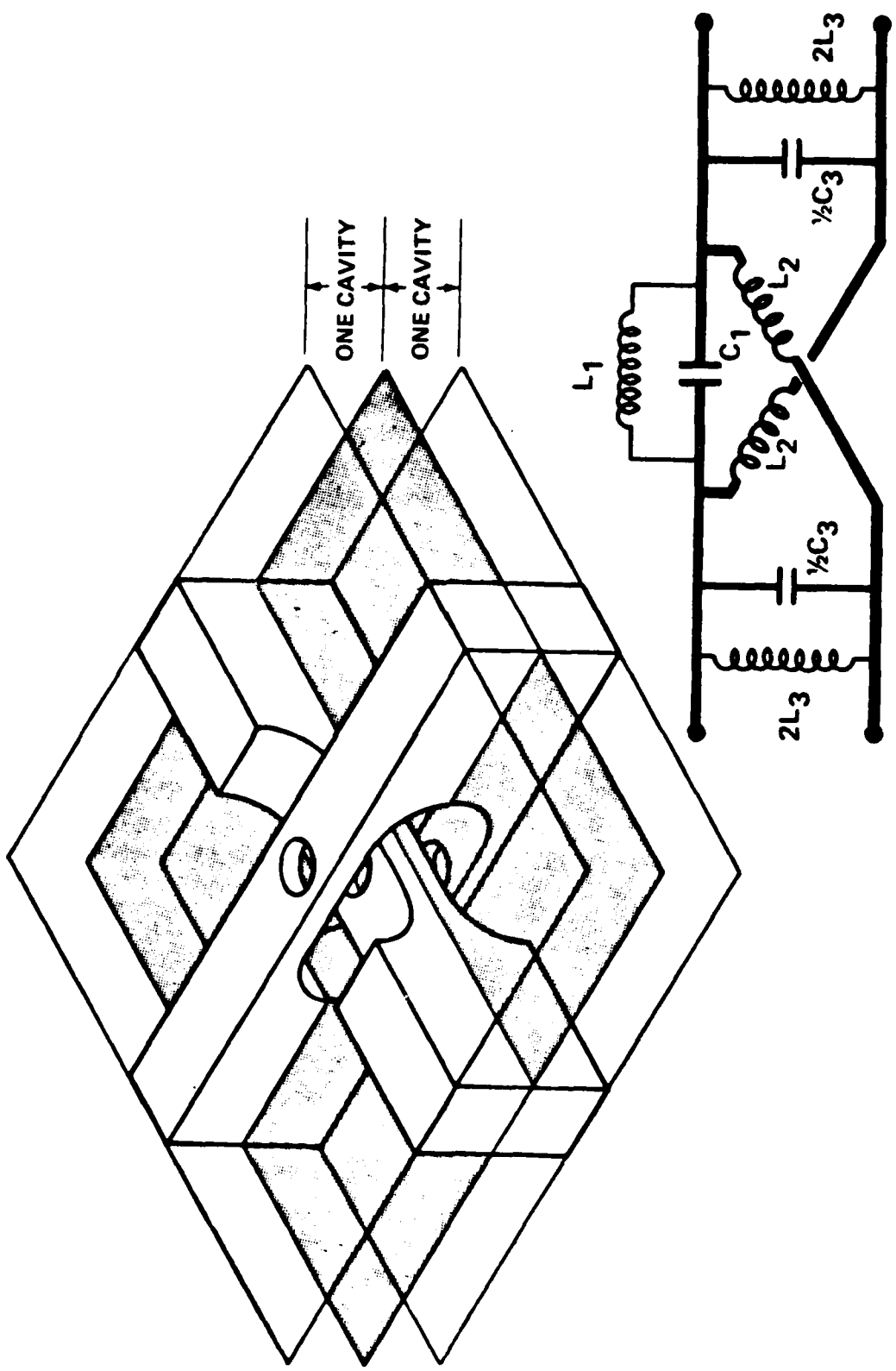


FIGURE 12. PERSPECTIVE DRAWING AND EQUIVALENT CIRCUIT CELL FOR APPRECIATING COMB-QUAD "CAVITIES" AND "COUPLING SLOTS" AND RF FIELDS AND CURRENTS.

re-orientation from level to level. Figure 12 (upper part) does not show any "enclosure" which, if visualized, may help in perceiving the cavities and coupling slots referred to. However, the orientation and distribution of rf fields at cavity resonance is such that said cavity has reality even in the absence of an enclosure (Comb-Quad A).

The coupling slots referred to are indeed large, physically, hence there is electric as well as magnetic coupling between cavities. However, the electric coupling tends to counteract all but a small amount of the magnetic. The propagation properties can then be about the same as if there were only small magnetic coupling slots.

The gap capacitance of the cavity referred to is relatively small since it is only the capacitance between two cross-oriented rungs. This situation is reflected in the relatively large observed values of R/Q, suggesting that the cavity is effectively re-entrant (or has "virtual ferrules"). An effective cavity height fully equal to the period is also suggested, whereas for conventional coupled-cavity stacks the cavity height must equal the period minus the web thickness.

Figure 12 includes one cell of a lumped-element equivalent circuit, which happens to be of the Curnow form<sup>12</sup> for staggered-slot coupled-cavity circuits. It not only facilitates interaction modeling, but in this instance very aptly aids in the visualization of the rf fields and currents of a Comb-Quad structure. A hierarchy of importance of the five lumped elements is suggested by line thickness in the drawing. In the Comb-Quad A case, the unenclosed structure is very well modeled by  $C_1$  and  $L_2$  alone, where  $C_1$  is the aforementioned capacitance between cross-oriented rungs and  $L_2$  is an inductance provided by the comb teeth. Specifically, the inductance of one tooth is  $2L_2$ , through which a predominantly radial rf current passes in flowing from one side of an interaction gap to the tooth's root. (The factor of 2 accounts for one tooth always being in parallel with its counterpart in the opposite comb.) These predominantly radial rf currents are associated with an azimuthal H field while  $C_1$  is associated with the axial E field that can modulate the electron stream.

A transverse or radial E field can exist in the interface plane associated with cavity-to-cavity coupling and is thus associated with the capacitance  $C_3$ . This capacitance is relatively small and has very little effect indeed -- except when  $L_3$  is finite and the frequency of interest is close to the  $C_3-L_3$  resonance frequency.

When there is an enclosure (of the B, C or D type of Figure 11) surfaces are introduced for the flow of axial and azimuthal rf currents. The axial rf current, which flows through  $L_1$  in the equivalent circuit, is associated with an azimuthal H field (as is the radial current through  $L_2$ ). The azimuthal rf current, which flows through  $L_3$  in the equivalent circuit, is associated with an axial H field. Since H-field lines exist as loops, one can visualize "cavity" H-field loops lying in a transverse plane within a cavity, and "slot" H-field loops lying in longitudinal planes and linking adjacent cavities.

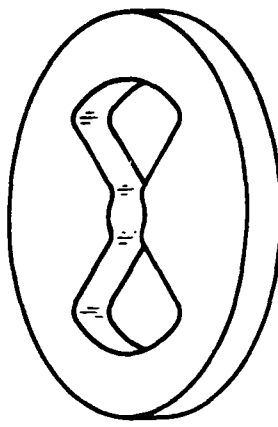
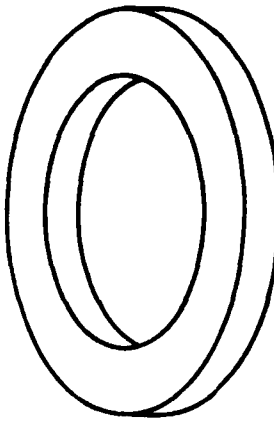
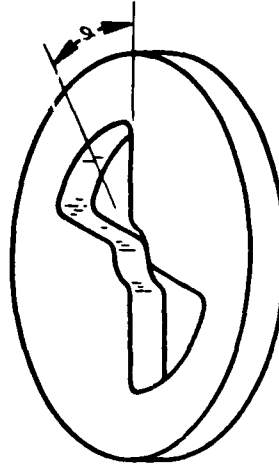
The tabulation below is an attempt to summarize the above discussion. Experimentation (with dielectric or dissipative inserts and deliberately resistive enclosure contacts) has confirmed these correspondences between fields, currents, physical elements and lumped-circuit elements. The behavior of Comb-Quad circuitry is easier to predict as a result, along with the limitations on what dielectric or differential-loss loading might possibly accomplish. For example, if the longitudinal seams referred to previously were intentionally poor in conductivity, only azimuthal rf currents would clearly be affected. The resulting loss-vs-frequency profile is correctly predicted when a resistance is introduced in series with  $L_3$  in the equivalent-circuit cell.

element	E field	H field	rf current
C <sub>1</sub> (gap)	axial		
C <sub>3</sub> (coupling slot)	radial		
L <sub>1</sub> (enclosure)		azimuthal	axial
L <sub>2</sub> (comb tooth)		azimuthal	mostly radial (some axial)
L <sub>3</sub> (enclosure delimiting coupling slot)		axial	azimuthal

#### 4.7 HISTORICAL PRECEDENTS

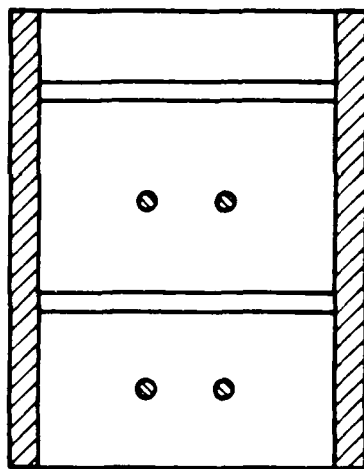
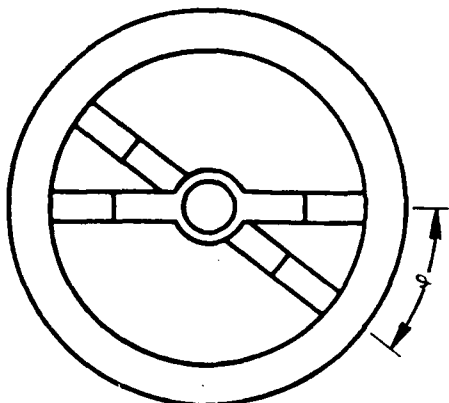
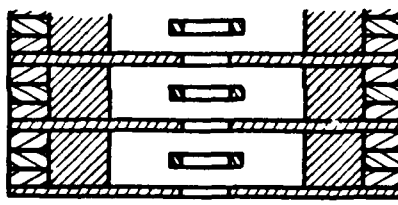
Efforts were made to learn of any previously initiated circuit studies in which Comb-Quad features may have been incorporated, and the findings of which would now be instructive. Structures based on interlaced ladders are indeed relevant; one 1962 reference thereto is that of Hiramatsu.<sup>13</sup> As sketched in Figure 13, his model should be equivalent to a Comb-Quad B design when the two ladders are orthogonal. Much importance was attached to a claimed ability to control dispersion by varying the angle  $\phi$ . However, in recent Comb-Quad studies, a deviation of  $\pm 30^\circ$  away from  $\phi = 90^\circ$  was found to have negligible effect. No doubt angle changes are significant when  $\phi$  is small, but small  $\phi$  is physically impossible in the Comb-Quad case. In any event, the illustrated assembly approach based on stacking laminae longitudinally is contrary to current objectives regarding construction.

The "Jungle Gym" structure<sup>11</sup> (Figure 13), initially proposed in 1961 for high-beam-velocity applications, should have Comb-Quad C or D propagation characteristics. In addition, the beam tunnel is unconventional and reminiscent of that of Figure 9 (c), though actually "virtual" in a different way. However, the construction approach based on slender cross wires would neither be robust nor implementable at millimeter wavelengths.



C.S.F. (c. 1958)

INTERLACED LADDERS (c. 1962)



"JUNGLE GYM" (c. 1961)

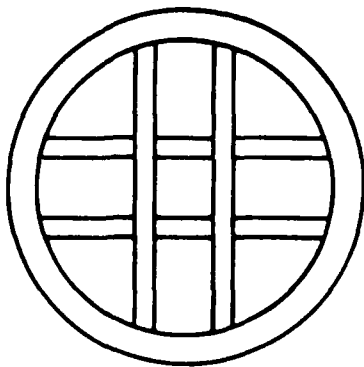


FIGURE 13. RELATED SLOW-WAVE STRUCTURES REPORTED IN THE PAST.

Reference 14 includes information, presumably not published elsewhere, on a circuit approach considered at C.S.F. around 1958, illustrated at the right in Figure 13. When stacked, and if  $\phi = 90^\circ$ , a structure equivalent to Comb-Quad C or D would be obtained, having in particular the tapered tooth format of Figure 10 (f) and the beam-tunnel approach of Figure 9 (b). However, the construction based on stacking numerous laminae is in opposition to current aims regarding fabrication. The ability to vary  $\phi$  was claimed as valuable, suggesting little actual experimentation: for  $45^\circ < \phi < 90^\circ$ , varying  $\phi$  should have produced little effect, while if  $0^\circ < \phi < 45^\circ$  the resulting beam-tunnel geometry should have resulted in poor interaction-gap properties.

## 5.0 COMB-QUAD PROPAGATION CHARACTERISTICS

### 5.1 GENERAL

All dispersion and R/Q data were obtained with the aid of the 6- or 8-period C- or G-band scaled circuit models of Figure 14, shown in various stages of disassembly. All but the second set of combs are very similar electrically, though different tooth-profile and beam-tunnel styles are evident. The "cavity" resonance frequency for the second set is close to that for the other sets, but the period is 0.375 instead of 0.5 inch, implying beam voltages roughly half as large. The first set of combs is shown enclosed to provide a C (more precisely, C/VBT) design, but the enclosure or corner pieces are removable. Any of the comb sets shown in Figure 14 can thus be "enclosed" in any of the four ways suggested by Figure 11 (A) through (D).

In Figure 15, four types of dispersion characteristics are shown in the format of frequency ( $\omega/2\pi$ ) vs phase shift per period ( $\beta p$ ). The same four curves are replotted in Figure 16 in terms of phase velocity (normalized relative to  $3 \times 10^10$  cm/sec) vs frequency, for the interval  $\pi < \beta p < 2\pi$ .

### 5.2 COMB-QUAD "A" AND "B"

Curve A (Figures 15 and 16) is obtained with enclosure A (free space) [Figure 11]. In this case, the lowest propagating passband extends downward to zero frequency, where  $\beta p = \pi$ . The group velocity is then quite fast, but it slows with increasing frequency, at first gradually and then rapidly, until it is zero, with  $\beta p = 2\pi$ , at the resonance frequency of the "cavity" referred to by Figure 12. When the relatively large enclosure B (Figure 11) is introduced, there is very little effect on the propagation except for a rise in the lower cutoff frequency,  $f_{\pi}$ , from zero to a finite value that is nevertheless well below  $f_{2\pi}$  (curve B, Figures 15 and 16).

Lines of constant phase velocity are the sloping dash-dot lines of Figure 15 or the horizontal dashed lines of Figure 16. In either figure, it can be seen that for Comb-Quad A and B designs there is only a narrow range

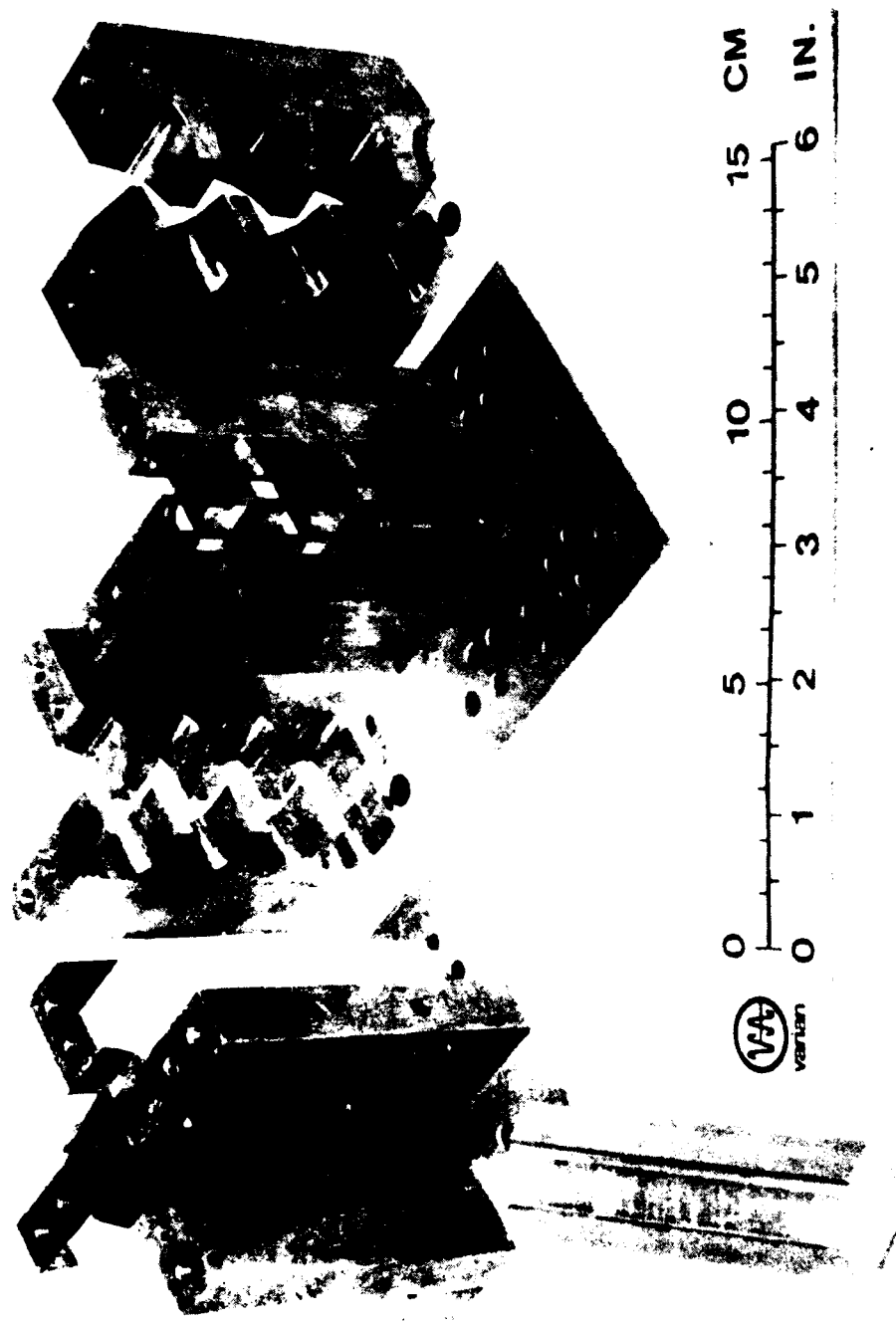
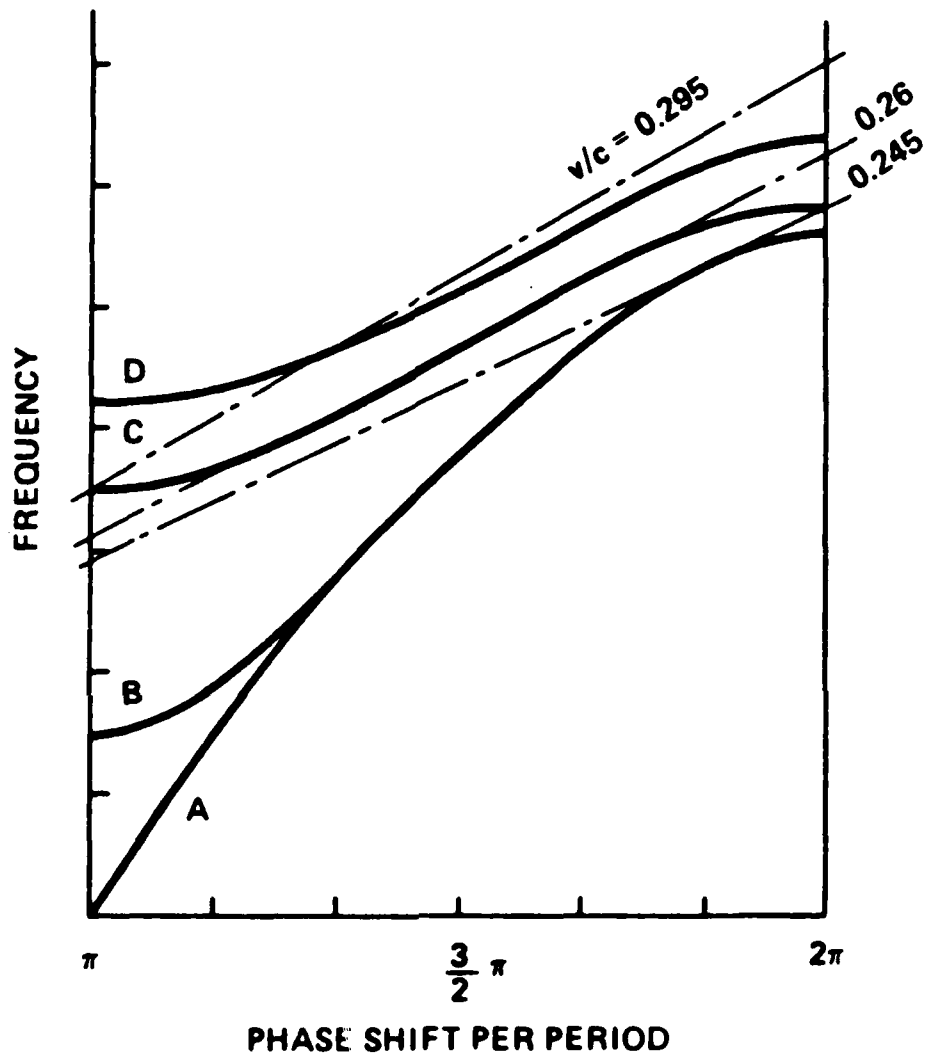
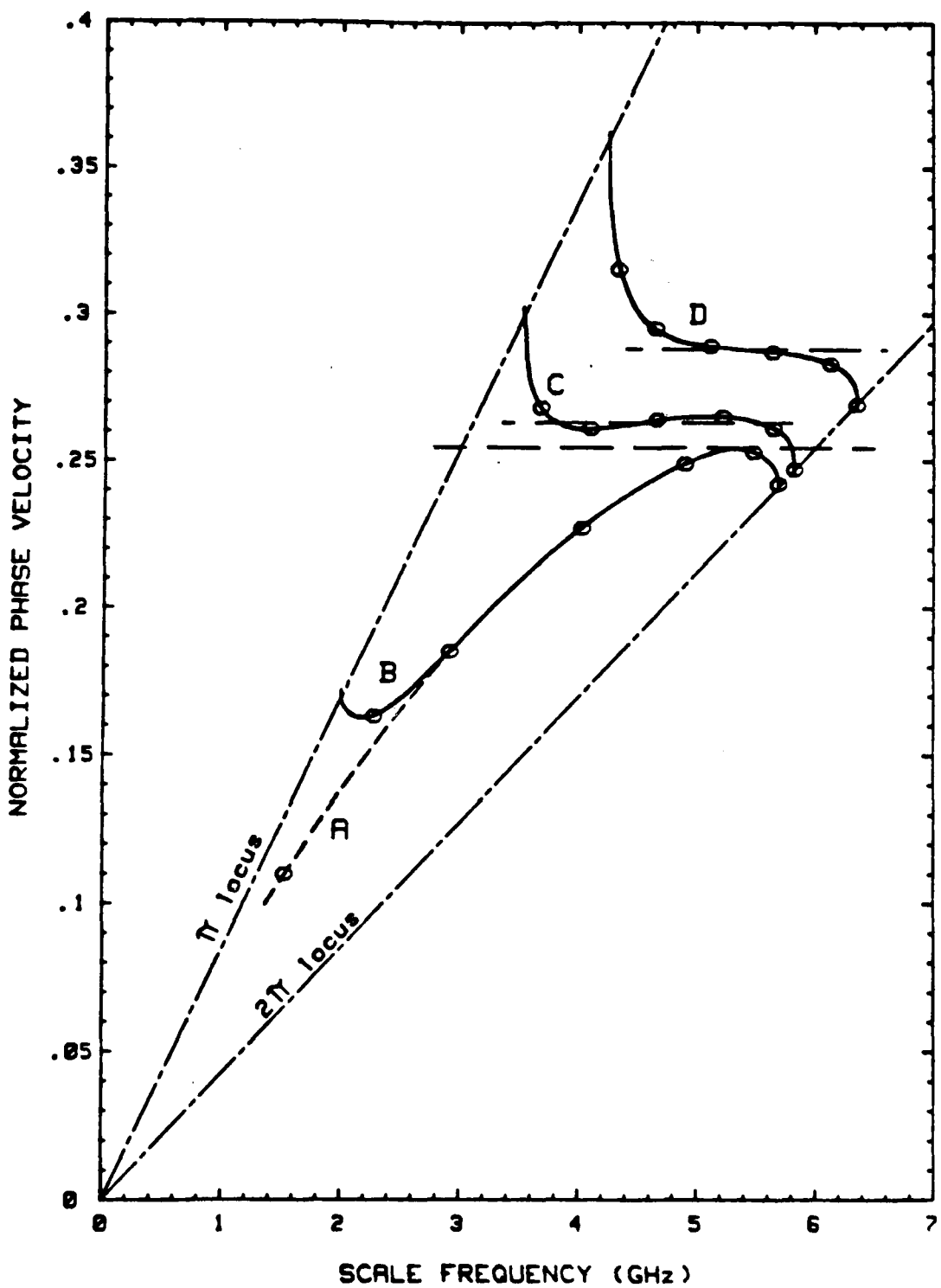


FIGURE 14: PARTIALLY ASSEMBLED 6- OR 8- PERIOD COMB-QUAD CIRCUIT  
MODELS AT C- OR G- BAND



**FIGURE 15. BRILLOUIN DIAGRAM COVERING 4 BASIC COMB-QUAD  $\omega$ - $\beta$  RESPONSES, WITH REGARD TO FIRST FORWARD SPACE-HARMONIC WAVE.**



**FIGURE 16. BASIC COMB-QUAD DISPERSION CHARACTERS DISTINGUISHED BY THE VARIATION OF PHASE VELOCITY WITH FREQUENCY IN THE INTERVAL  $\pi < \beta_p < 2\pi$ .**

of frequencies where such a line is about tangent to the dispersion curve. This potential (narrow "hot" bandwidth) mode of operation, with the "beam-velocity line" tangent to the  $\omega$ - $\beta$  curve, also applied to the design of Figure 2, except that  $\beta_P$  there was a little below  $3\pi$  whereas in the Comb-Quad analog  $\beta_P$  is a little below  $2\pi$ . [In Millman's case,<sup>8</sup>  $2\pi < \beta_P < 3\pi$  also applied, but the very fine pitch (by today's standards) led to an  $\omega$ - $\beta$  curve allowing the point of tangency to be about midway between  $2\pi$  and  $3\pi$ .]

### 5.3 COMB-QUAD "C" AND "D"

Going to the extreme of the enclosure having the smallest perimeter ( $D$  in Figure 11), the narrowest possible passband width is the result (Curves D in Figures 15 and 16). Relative to the effects of Enclosure B, the lower cutoff frequency,  $f_{\pi}$ , has been raised considerably. However,  $f_{2\pi}$  has risen relatively little since the resonance frequency of the "cavity" of Figure 12 is only slightly affected by the "enclosure".

The relatively narrow "cold" bandwidth may actually be conducive to a sizable "hot" bandwidth. This would obtain when the phase velocity is, first of all, single valued (going between  $f_{\pi}$  and  $f_{2\pi}$ ) as it is for curve D in Figures 15 and 16. Secondly, the phase velocity should remain close to a constant value over much of the passband, as again it does for curve D of Figures 15 and 16. As it happens, curve D will correspond to enclosure D only when  $p$  (and therefore also  $V_0$ ) falls within a certain range of values -- after specifying  $f_{2\pi}$  and the tooth profiles. (This circumstance in practice imposes only a lower limit on  $p$  and  $V_0$ ; when  $p$  and  $V_0$  are to be relatively large, the D type of response would be readily obtained, and adjusting the dispersion to be small, if desired, would merely require that the enclosure be enlarged toward the C-enclosure category.) However, when a curve-D response is secured, "hot" bandwidths in the neighborhood of 25% are typically predicted, even at fairly low beam perveance.

With an enclosure just slightly larger than that giving the D response, but substantially smaller than that providing the B response -- all for a given set of combs -- it is possible to obtain a dispersion curve, C in Figure 15 and 16, that hovers closely about a line of constant phase

velocity over most of the passband. In detail, the curve C is seen to cross the line three times, but between crossings as little as  $\pm 0.5\%$  deviation in phase velocity has been observed. (A "maximally flat" curve, intermediate between C and D in Figure 16, has also been observed.) The relative ease of obtaining such responses in the Comb-Quad case may be due to the peculiar nature of the coupling between cavities -- a somewhat precarious balance of antagonistic electric and magnetic couplings, the frequency dependencies of which may lead to the indicated responses and predicted hot bandwidths of 30 to 40%, even at the low beam perveances associated with millimeter-wave tubes.

Returning to the "hot" bandwidth objective of the present contract (a few percent), dispersion curves of the C type, and the consequent extended hot bandwidths, would be of no interest. Even curves of the D type suggest more hot bandwidth than is needed. However, the Comb-Quad B design, nominally ideal for the small bandwidths desired, may prove to have more liabilities than virtues. In that case, a D design would be the only remaining Comb-Quad option, preferably with  $p$  and  $V_0$  as large as permissible to obtain the smallest possible cold bandwidth. [In conventional coupled-cavity chains, as the coupling apertures are enlarged, the cold bandwidth can range from zero up to an upper limit determined by the maximum practical aperture size. The situation is reversed in the Comb-Quad case; as the enclosure perimeter is reduced, the cold bandwidth can range from something enormous down to a lower limit determined by the minimum possible enclosure perimeter.]

Although Comb-Quad D designs are potentially very useful, little attention is given to them in this report. Comb-Quad D design possibilities, with a hot bandwidth close to 20%, were the sole focus of NRL Contract N00173-79-C-0347 which was started in October 1979, but will not be completed (in terms of the Final Report) until early in 1981. The major effort there was the construction and evaluation of an exploratory "hot" test vehicle, scaled for X band but reflecting attenuation and perveance values associated with millimeter wavelengths.

Additionally, "half-octave" Comb-Quad C design possibilities were a major focus of attention under AFAL Contract F33615-79-C-1792 which was started in June 1979 and completed within FY 1980.<sup>15</sup> In that study program, Comb-Quad D circuitry was often studied along with the C, or by way of preparation -- given the similar properties but not quite so much bandwidth to contend with. The Final Report<sup>15</sup> includes data specifically relevant to circuits having the C- and D-type responses and to beam/wave interaction therein. Insofar as possible in the remainder of this report (RADC Contract F30602-79-C-0172) attention will be focused on Comb-Quad B design possibilities and problems.

#### 5.4 HIGHER PASSBANDS AND EXTRANEous MODES

The Brillouin diagrams of Figures 17 and 18 include the two lowest passbands for two families of Comb-Quad B interaction structure. Within each family, the only dimension varied was the size of the square outer enclosure [dimension X in Figure 11(B)]. By analogy with conventional coupled-cavity structures, the lowest passband would be identified with the "cavity mode" and the next higher passband with the "slot mode". However, with wrong-sign or both-sign group velocity within one  $\omega$ - $\beta$  curve segment, the "slot mode"  $\omega$ - $\beta$  curves in Figures 17 and 18 are unlike those of conventional coupled-cavity circuits -- except when the enclosure becomes rather small (curve for  $X = 1.25$  inches in Figure 17). In that case, as for Comb-Quad C and D cases,<sup>15</sup> the upper  $\omega$ - $\beta$  curve is "conventional" (negative group velocity in the interval  $\pi < \beta p < 2\pi$ ).

For the six-period model (third in Figure 14) to which Figure 17 applies, the beam-tunnel/interaction-gap geometry was "conventional" (CBT) and the period was such that the type-B amplifying regime would require  $V_0 = 18$  kV. No extraneous modes of propagation could be detected within the frequency range covered in Figure 17.

Figure 18 applies to an eight-period model (second in Figure 14) featuring the unconventional (VBT) tunnel/gap geometry. The period was incidentally  $3/4$  that of the model of Figure 17 so that the corresponding  $V_0$

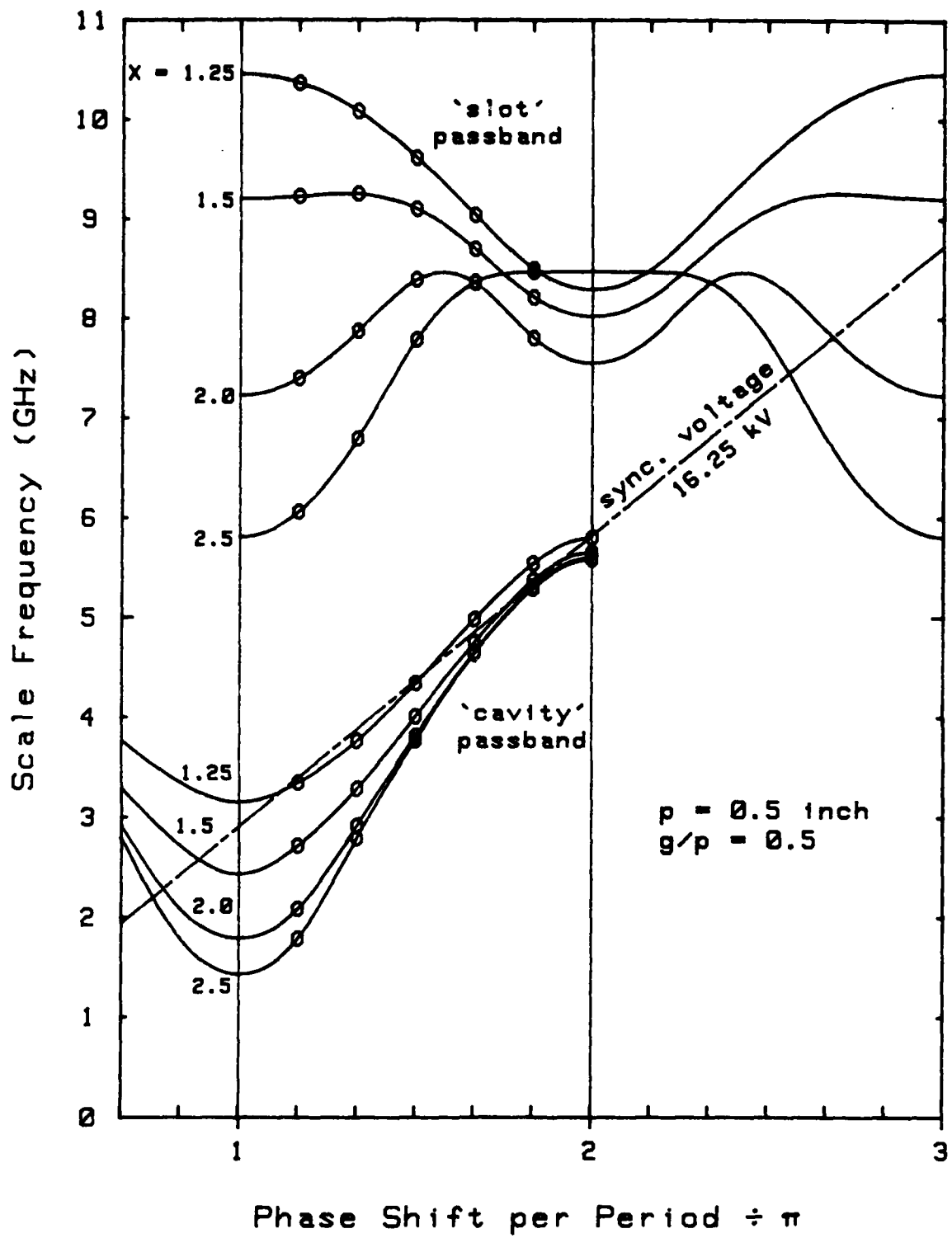


FIGURE 17. BRILLOUIN DIAGRAMS FOR COMB-QUAD B CIRCUIT STRUCTURES BASED ON THIRD COMB SET OF FIGURE 14; VARIABLE X (IN INCHES) IS DEFINED IN FIGURE 11 (B).

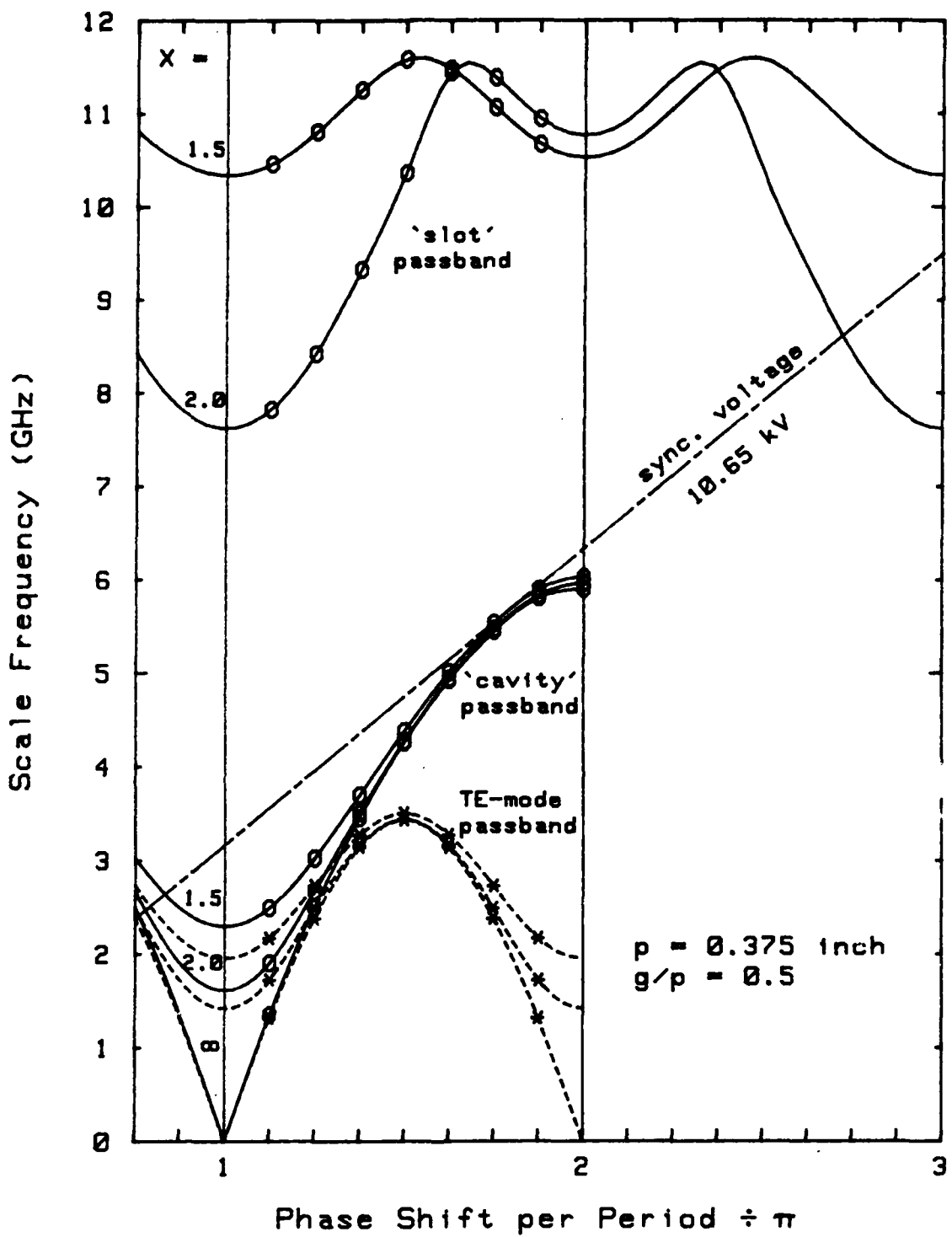


FIGURE 18. BRILLOUIN DIAGRAMS FOR COMB-QUAD A AND B CIRCUIT STRUCTURES BASED ON SECOND COMB SET OF FIGURE 14; VARIABLE X (IN INCHES) IS DEFINED IN FIGURE 11(B).

would be  $\approx 10$  kV. The curve for  $X = \infty$  in Figure 18 actually designates a Comb-Quad A structure; in this case, no higher propagation passbands were observed.

The extra feature included in Figure 18, a concomitance of the unconventional tunnel/gap geometry, is a TE mode (actually a degenerate pair of modes) that may propagate with an rf potential difference across the space between opposing tooth tips. The fields of such a mode are consistent with having a Dirichlet boundary (visualized as a conducting plane) through the tunnel axis in the plane of either ladder (whence the degeneracy if both ladders are equal).

Unlike the essentially TM Comb-Quad mode with predominantly axial ( $z$ -directed)  $E$  fields, wanted for TWT interaction, the extraneous mode's  $E$  fields are predominantly transverse, extending from a tooth tip toward the aforementioned Dirichlet plane opposite said tip. The largely transverse  $E$  fields would not, of course, interact with axially confined electrons. However, there are some  $z$ -directed fringing components which might. (The fringing  $E_z$  fields are directed from the aforementioned tooth tip toward the corners of the tips of the interleaved teeth.) All  $E_z$  fields of the extraneous mode must, of course, be zero on the beam axis and across the diameter that is the Dirichlet plane. With a modest beam filling factor, the net interaction with such  $E_z$  fields as are within the beam cross section should therefore be minimal.

Nevertheless, mapping the extraneous mode as extensively as possible would be a valuable precaution in case problems arose, requiring understanding and solution. The mapping plotted as dotted in Figure 18 (always representing space-harmonic waves) employs the same definition of the period ( $p$ ) used elsewhere (Figure 9) and refers only to  $E_z$  field components that might exist off the beam axis. The extraneous-mode passband is first mapped with the "enclosure" removed ( $X = \infty$ ). It is then very clear that the lower passband edge (zero frequency) must correspond to  $\beta p = \pi$  and the upper edge to an odd multiple of  $\pi/2$ . As the enclosure is gradually reduced in size, the change in the  $\omega-\beta$  curve is also gradual, so there is no uncertainty regarding position in the Brillouin diagram.

Since the extraneous-mode passband lies well below the anticipated signal bandwidth (between 5 and 6 GHz in Figure 18), there is no possibility of problems due to mode conversion (engendered by any kind of asymmetric imperfection). However, oscillation might occur (at some elevated level of beam current) at a frequency close to where the dash-dot "beam velocity" line (Figure 18) intersects the spurious-mode  $\omega$ - $\beta$  curve. The diagram indicates that the potential oscillation would be "backward-wave" ( $\beta_p < \pi$ ) with  $\omega$  and  $\beta$  about the same as for the intersection of the dash-dot line with the lower portion of the "cavity-mode"  $\omega$ - $\beta$  curve. That intersection indeed implies an important oscillation risk, as discussed in Section 7.3, hence the means introduced to deal with the greater of the instability risks should also deal with the lesser. The high group velocity at the aforementioned intersection point would, in any event, promote a high start-oscillation current.

Notably, the spurious-mode passband is very sensitive to the transverse capacitance between opposing comb teeth. As the geometry is changed from that of Figure 9 (a) to 9 (b), the spurious-mode passband would shift downward in frequency. Working with laboratory cold-test models, the mode in question is identified by seeing if the evidence for it vanishes when any kind of conducting path is introduced between opposing tooth tips.

### 5.5 INTERACTION IMPEDANCE

With a newly introduced interaction-structure geometry, interaction-impedance data must rely on an initial experimental R/Q determination, preferably at several frequencies within the circuit passband. Working with resonated section containing N periods of the slow-wave structure, the resonance frequency of a selected one of the N resonances is perturbed by inserting a slender quartz or sapphire rod on the axis. The percentage frequency perturbation is then processed to yield R/Q, a parameter indicative of the ratio of the square of the axial field ( $E_z$ ) to the stored energy. At Varian, R/Q is for consistency based on the  $E_z$  at the edge of the beam tunnel, even though the dielectric rod is placed on the axis.

The aforementioned processing of perturbation data includes corrections for the finite rod diameter. The processing must therefore take into account the radial and axial variation of  $E_z$  for the applicable value of  $\beta$ . When the geometry is axisymmetric, these variations are easily expressed, given the gap length ( $g$ ), the period ( $p$ ), the tunnel diameter ( $D$ ), and an index relating to the disposition of metal just outside the tunnel. At one extreme, there might be knife-edged ferrules; at the other, large flat planes the distance  $g$  apart. The profile  $E_z(z)$  at the tunnel edge would then be expressed with either of two kinds of mathematical function for these two extreme cases, or a weighted mixture of these for intermediate cases. The weighting is governed by a computer input, FSIN, ranging from 0 to 1, respectively, as the gap geometry varies from that of zero-wall-thickness ferrules to that of large flat planes (with the tunnel either gridded or having  $D \ll g$ ).

For a potential Comb-Quad B TWT design, the R/Q value of primary interest is that applying at  $\beta p = 1.8\pi$ , the point of tangency (or of maximum phase velocity -- Figures 15 - 18). (This R/Q magnitude should be fairly close to that for  $\beta p = 2\pi$ .) Moreover, these R/Q values should be substantially uninfluenced by the outer enclosure dimension  $X$ , as is the  $\omega-\beta$  curve itself in the vicinity of  $f_{2\pi}$  (Figures 17, 18).

Viewing the higher-voltage comb set to which Figure 17 applies as representative, and also including similar but not identical data obtained with the two other same-period comb sets of Figure 14,  $R/Q = 56 \text{ ohms} \pm 10\%$  can serve as an appropriate experimentally determined magnitude for  $\beta p/\pi$  around 1.8 to 2.0. Some small degree of indeterminacy reflects uncertainty in the correct value of FSIN, though unlikely to be  $< 0.7$  or  $< 0.8$  for  $g/p = D/p = 0.5$ . However, a major source of uncertainty (in processing perturbation data) resides for the present in choosing effective values for  $g/p$  and  $D/p$  when the non-axisymmetric (VBT) tunnel/gap geometry has been implemented for the structure being evaluated. This happens to apply to the lower-voltage comb set covered by Figure 18, for which  $R/Q = 47 \text{ ohms} \pm 4\%$  was initially determined (for the  $\beta p$  range of interest) naively using actual instead of effective values of  $g/p$  and  $D/p$ , in a supposedly equivalent axisymmetric approximation. [When the results of Chapter 6 later became

available, it was found that the preliminary R/Q determinations were pessimistically low, but only by a percent or so.)

Neglecting variations of R/Q with frequency, as well as the discussed uncertainty regarding 56 and 47 ohms, respectively, projected values of the cube root of the Pierce impedance,  $K^{1/3}$ , are as tabulated below for the higher- and lower-voltage circuit models.  $K^{1/3}$ , rather than K, is more indicative of TWT gain, and conveniently reduces the effects of the variously originating imprecisions in R/Q to about 1/3 of the percentage uncertainty. By convention, K is defined here as "on-axis", even though R/Q is defined at the edge of the beam tunnel.

Frequency in GHz and [Pierce impedance in ohms] <sup>1/3</sup>				
$\beta p/\pi$	<u>f</u>	<u><math>K^{1/3}</math></u>	<u>f</u>	<u><math>K^{1/3}</math></u>
	p = 0.5 inch	p = 0.375 inch		
	R/Q = 56 ohms	R/Q = 47 ohms		
1.60	4.323	1.04	4.796	1.03
1.65	4.570	1.03	5.040	1.03
1.70	4.803	1.03	5.272	1.04
1.75	5.020	1.04	5.462	1.06
1.80	5.208	1.07	5.643	1.09
1.85	5.369	1.13	5.777	1.16
1.90	5.492	1.23	5.880	1.28
1.95	5.570	1.47	5.942	1.41
2.00	5.596	$\infty$	5.962	$\infty$

The  $\beta p$  range slightly below  $\pi$  is another region where R/Q and interaction-impedance values are of interest, but only secondarily. In this  $\beta p < \pi$  region, backward-wave oscillation is potentially possible in a Comb-Quad B TWT (Figures 17 and 18), and impedance data help in the prediction of start-oscillation currents. For the model for which Figure 17 applies, with X = 2.5 inches, for example, R/Q = 105 and 76 ohms were determined for  $\beta p/\pi = 0.833$  and 0.667, respectively. Accordingly, 76 to 105 ohms should bracket the R/Q value applicable to the  $\omega, \beta$  point at which oscillation is threatened. By virtue of the pertinent values of  $\beta$ , group velocity, etc.,  $K^{1/3}$  then works out to about 2 (ohms)<sup>1/3</sup>  $\pm$  3%, and is the

parameter to reckon with in projecting the likelihood of oscillation near the lower edge of the Comb-Quad B passband (Section 7.3).

## 5.6 CIRCUIT ATTENUATION

### 5.6.1 Predictable Aspects

Circuit attenuation per period and its variation with frequency should be predictable solely from the group velocity and the effective cell Q at each frequency. This Q would be a composite or weighted average of the Q values for each inductor in the equivalent circuit (Figure 12). [Since the two capacitances are each shunted by an inductance, it is sufficient to assign finite Q values to the inductances alone.] The weightings at each frequency are established solely by the  $\omega-\beta$  data, hence R/Q magnitudes and variations are immaterial.

The predicted curves of Comb-Quad B attenuation per cell vs frequency of Figure 19 cover the circuit model to which Figure 17 applies, with  $X = 2$  inches. In this case, it was both convenient and possible to omit  $L_1$  from the equivalent circuit (Figure 12) without detracting from the latter's validity. One then need only be concerned with  $Q(L_2)$ , the Q of a comb tooth along which rf currents are predominantly radial, and with  $Q(L_3)$ , which can reflect the effects of resistance encountered by azimuthal currents in the enclosure walls. For a copper tooth at 44 GHz,  $Q(L_2) = 500$  has been estimated for the adopted comb geometry, including only a small allowance for surface roughness, "anomalous skin effect"<sup>16</sup> and temperature rise. (For 94 GHz,  $Q(L_2) \approx 350$  would be given by "classical" frequency scaling, but 250 is estimated to be more realistic in view of the significance of the other effects mentioned at 94 GHz.)

For a "baseline" attenuation profile [curve (a) in Figure 19],  $Q(L_3) = Q(L_2)$  was assumed. However, it will be apparent that for Comb-Quad B operating frequencies near the upper passband edge,  $Q(L_3)$  has little effect on the attenuation. The effect of halving  $Q(L_2)$  relative to the first value, and to  $Q(L_3)$ , is shown by curve (b). The effect of reducing  $Q(L_3)$  relative to the initial value, and relative to  $Q(L_2)$ , is

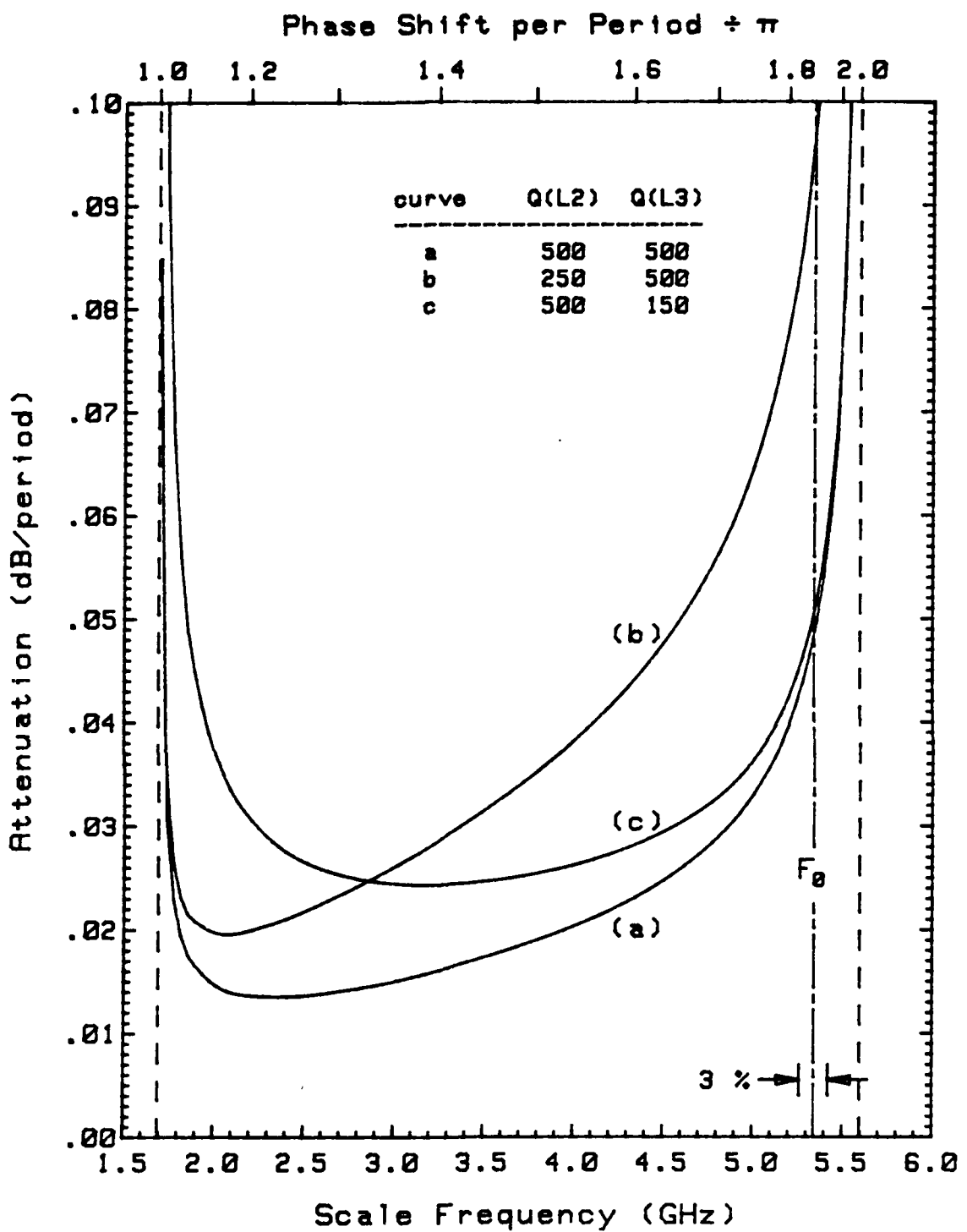


FIGURE 19. PREDICTED ATTENUATION DATA FOR COMB-QUAD B/CBT CIRCUIT MODEL OF FIGURE 17 WITH  $X = 2$  INCHES.

reflected by curve (c). These curves show that the resistance encountered by radial tooth currents is the determining factor for the uppermost portion of the passband, while the resistance encountered by azimuthal enclosure currents adds its effect almost entirely at the low-frequency end. (Due to the frequency dependence of "skin" resistivity, the concept of a Q invariant with frequency over the full range of Figure 19 is not strictly valid; however, only qualitative trends are of interest at this stage, while quantitative concerns would be limited to relatively narrow frequency intervals.)

Tying attenuation magnitude and frequency dependence to the  $\omega-\beta$  curve and two (or at most three) fixed Q values has proven a valuable technique. It can facilitate reconciliation of predicted and experimental data, indicate any possibility of differential loss loading, and suggest means for its implementation.

#### 5.6.2 Experimental Aspects

The possibilities for measuring attenuation (or composite Q) vs frequency were considered for the Comb-Quad B scaled circuit models on hand. For the resonated sections six or eight periods long (Figure 14), composite unloaded Q can be measured at six or eight well spaced frequencies. However, the relevance of the measured data would be limited since the end-plate losses would generally be significant relative to the periodic-structure losses. Toward the end of the study program, a 19-period B/CBT circuit model (with  $f_{2\pi} = 5.7$  GHz) became available (see Chapter 9). In this case, the end-plate losses might have been more nearly negligible, but the aforementioned Q measurements were not attempted because of the close spacing and consequent overlapping of the resonances expected near the band-edge frequencies of interest.

Had it been possible to obtain a waveguide-coupler design (Chapter 9) covering the Comb-Quad B frequencies of interest that approach the upper edge of the passband, two methods could have been considered for measuring the attenuation of the 19-period circuit section. To apply Steele's method, the periodic structure is connected to the automatic

network analyzer (ANA) via the waveguide port at one end while the opposite end is loaded with absorbing material. The reflection vector at each frequency of interest is then monitored while a small metal bead is pulled along the axis on a nylon filament. Thus ANA-processed data can disclose E-field magnitude and phase differences for successive gaps along the chain. However, prior experience<sup>15</sup> advises that for copper, at G-band frequencies, mid-passband Comb-Quad attenuation, even over ten or more periods, is not reliably distinguishable from measurement "noise" (although the phase measurement is completely satisfactory). For frequencies closer to the passband edge, the attenuation would be more readily measurable, but these were the frequencies for which the coupler was inadequate.

With waveguide couplers at both ends of the circuit section, direct insertion-loss measurements can be implemented. If two assemblies are evaluated, each having a different number of periods in the slow-wave section, the coupler losses might be deductible. However, the end matches must be good at the frequencies of primary interest, and this is not at present true in the Comb-Quad B case.

Evaluations of Comb-Quad D circuit sections (with  $N = 17$  or  $37$ ) undertaken at X band (Contract N00173-79-C-0347) can suggest that  $Q(L_2) = 500$  is a reasonable estimate for copper around 40 to 50 GHz. However, these data are not without uncertainty because the end-coupler correction was comparable to the general measurement error.

In the future, any of the several methods mentioned might be considered for reliable circuit-attenuation or Q measurements if a metal other than copper were used for the G- and X-band models. The skin resistance of this metal must be accurately known, however, hence magnetic materials are ruled out along with alloy or substrate-diffused platings that may not reproduce from sample to sample.<sup>15</sup>

## 5.7 COMB-QUAD B DIFFERENTIAL-LOADING EXPERIMENTS

Merely looking at the roomy, empty outer enclosure corners of the B-type circuit cross section [Figure 11 (B)] evokes the idea of loading them with lossy or non-lossy dielectric, if the result might be electrically advantageous. Some experimentation was undertaken along these lines, using suitably enclosed six-period circuit models (Figure 14) and measuring the frequency and (unloaded) Q for each of the six resonances. The Q data would be only qualitatively significant since rf contact and other losses associated with the end plates weren't necessarily negligible compared with attenuation along the length of the slow-wave structure.

One of the materials inserted in the four outer enclosure corners was graphitized paper, rolled into tubes, to introduce dissipation through interaction with E fields of any polarization, without significant dielectric loading. Observed Q values were reduced significantly throughout the passband, consistent with the following: For frequencies near  $f_{\pi}$ , E fields are predominantly transverse and dissipation occurs as expected because the paper has some conductivity in that direction. For frequencies near  $f_{2\pi}$ , the E fields that are predominantly axial must (unexpectedly) be appreciable in the enclosure corners to excite axial currents in the resistive paper. In terms of the equivalent circuit, the paper in the corners provides resistance shunting both  $C_3$  and  $C_1$ , even though the paper tubes were distant from the interaction gap. Attenuation is thus introduced across the passband as the E fields, associated with  $C_3$  and  $C_1$ , respectively, change from transverse to axial.

Another material introduced in the four outer enclosure corners was the synthetic low-loss dielectric Styrofoam, in the form of square prisms, with isotropic dielectric constant 5 or 6. The circuit model's resonance frequencies were all slightly lowered, and roughly equally at both passband ends. This suggests that both  $C_3$  and  $C_1$  were effectively increased because of the presence of both transverse and axial E fields in the region loaded, although these fields are weaker there than they are closer to the beam tunnel, and although the prevalent polarization changes with frequency.

The practical motivation for adding dielectric was the hope of obtaining a low value of  $f_{\pi}$  while maintaining a modest enclosure dimension X (to facilitate fitting the structure within a PPM stack), and not reducing  $f_{2\pi}$ . The motivation for adding dissipative material was to increase attenuation near  $f_{\pi}$  but not near  $f_{2\pi}$ . Neither example of intended differential loading proved viable for the reasons given. However, the desired result might be obtained if the dielectric and/or dissipative material were anisotropic -- so as to permit interaction with transverse but not axial E fields. A way to make isotropic materials function somewhat anisotropically is to use them in conjunction with an alternative form of the B-type enclosure [phantom lines in Figure 11(B)]. In this case, the outer enclosure corners are "cut off" for axial but not transverse E fields. Experimentally, when the Stycast prisms or graphitized-paper rolls were tucked into the "pocket" regions of the alternative B-type enclosure, a more nearly differential loading was indeed observed. (The alternative enclosure style could also provide a lower thermal resistance for heat flow outward from the comb teeth.)

Interaction with rf currents in the enclosure walls, rather than with E fields inside them, was the basis of a set of experiments demonstrating differential loss loading to the most striking degree. In this instance, attention was paid to the eight longitudinal seams between the four combs and the four L-section strips forming the (empty) B-type enclosure. Initially, a set of Q measurements was recorded with the seams closed only by the action of metal resting against metal. A second set of higher Q values was then obtained after painting over the seams with silver-loaded lacquer. The increase was rather large for the resonance nearest  $f_{\pi}$ , but progressively lessening until at  $f_{2\pi}$  the before/after difference was only slight. This useful result is entirely consistent with the notion of "contact resistance" across the seams (which could be introduced intentionally in an eventual TWT structure) interacting only with azimuthal rf currents and lowering  $Q(L_3)$  without affecting  $Q(L_2)$  or  $Q(L_1)$  since  $L_2$  and  $L_1$  are associated only with radial and axial currents. The attenuation-vs-frequency profile would then have changed as from (a) to (c) in Figure 19.

## 6.0 COMB-QUAD INTERACTION-GAP MODELING

### 6.1 INTRODUCTION

The analytic efforts reviewed in this chapter were carried out mainly under AFAL Contract F33615-79-C-1792. This chapter thus largely duplicates Chapter 4 of Reference 15 except for some editing to maximize relevance to Comb-Quad B rather than C or D TWT designs. In particular, the case  $\beta_p + 2\pi$  is of primary importance, with relevance to the potential Comb-Quad B operating band. The case  $\beta_p + \pi$  is relatively less important since the data relate only to the possibility of a backward-wave oscillation near that end of the "cold" passband.

### 6.2 "CONVENTIONAL" BEAM-TUNNEL OPTION

The coefficients characterizing an interaction gap electrically need to be reasonably correct to obtain reliable values of R/Q, to predict the gain and bandwidth obtainable with a given electron beam, and to optimize the geometry with respect to TWT performance. Unfortunately, none of the interaction-gap configurations of Figure 9 possesses the axial symmetry that permits easy derivation of accurate coefficients.

In the CBT case of Figure 9(a) -- also illustrated, in perspective, in Figures 8 (left), 12, and 14 (third from left) -- an axisymmetric equivalent geometry was introduced as a convenient approximation. Specifically, an axisymmetric conventional cavity was assumed with an overall height = p, a gap length = g (centered between equal ferrules), a tunnel diameter = D, and a ferrule diameter = A. The only dimension in Figure 9(a) that does not carry over exactly to the round equivalent is thus A. Implicit in the geometric substitution is an equating of the capacitance of gap g having hypothetical round ferrules of diameter A to the capacitance between crossed bars of width A and separation g.

With an axisymmetric geometry, the gap coefficients are computed automatically within the programs for calculating interaction gain as well as deriving R/Q from dielectric-rod perturbation data. However, it was

deemed advisable to pin down as well as possible the value of FSIN that accounts for the effects on  $E_z(z)$  of the metal surfaces just outside the beam tunnel. Accordingly, Laplace's equation was solved (numerically) for the hypothetical axisymmetric configuration, allowing A, g, and D to take on different values relative to the period p. In each case,  $E_z(z)$ , averaged over the beam cross section of diameter B, was plotted so as to permit comparison with other  $E_z(z)$  profiles generated by the routine /@GAP/. This special routine generates its profiles (given B/D, D/p and g/p) by allowing a plausible value of FSIN (such as 0.75) to dictate how the profile functions corresponding to FSIN = 0 and FSIN = 1 (see second paragraph of Section 5.5) might be mixed (e.g., 25% of the former and 75% of the latter) to replicate as closely as possible the profile given by the Laplace solution.

The table below summarizes the "best fit" FSIN values appropriate to a selection of hypothetical axisymmetric geometries. However, a further note of explanation is necessitated by the "cavity" in question being part of a cavity chain with relatively short tunnels and a zero-thickness "web" between cavities. For example, depending on whether the phase shift between cavities is  $\pi$  or  $2\pi$ , the interface plane between cavities will be either a Neumann or a Dirichlet boundary, respectively. The distribution of E fields in and around the gap and inside the tunnel will be modified accordingly, along with the effective gap capacitance. The two corresponding static modeling cases would therefore be valid only for frequencies close to the ends of the circuit passband where  $\beta p$  approximates either  $\pi$  or  $2\pi$ .

A/p	D/p	g/p	FSIN		
			2π static mode		π static mode
			B/D = 0.5	B/D = 0.7	B/D = 0.7
1	0.5	0.3	0.743	0.740	0.733
1	0.5	0.4	0.766	0.765	0.755
*1	0.5	0.5	0.783	0.782	0.764
1	0.5	0.6	0.796	0.796	0.758
1	0.3	0.5	0.873	0.876	0.873
1	0.4	0.5	0.830	0.831	---
*1	0.5	0.5	0.783	0.782	0.764
1	0.6	0.5	0.716	0.715	0.663
0.9	0.5	0.5	0.759	0.757	---

In the tabulation above, the \* marks the only geometry that has been incorporated to date into any "hardware". However, were the proportions to be changed, these data would indicate the degree to which FSIN might be affected. Beam filling factor variation between 0.5 and 0.7 is seen to affect FSIN negligibly, while the choice of static mode affects it only slightly when the physical geometry is close to that marked \*. For that case, FSIN = 0.77 should be reliable enough under quasi-axisymmetric conditions, without regard to  $\beta_p$  or filling factor.

Having accomplished the analyses that provided the information above, another use was found for some of the data acquired. These included the effective gap capacitance which is inversely proportional to R/Q. Consequently, a relative gap figure of merit,  $M^2 R/Q$ , could be calculated for each hypothetical axisymmetric geometry, where  $M^2$  is the gap coefficient that relates to the strength of space-harmonic wave/beam interaction.  $M^2$  therefore depends on  $\beta_p$  (the gap-to-gap phase shift) and also will decrease

as  $g/p$  and the gap transit angle increase. However,  $R/Q$  will increase as the gap capacitance decreases with increasing  $g/p$ . It is therefore no surprise that, as seen in Figure 20, the figure of merit is optimum for some ideal value of  $g/p$  that is, fortunately, not very sharply defined, but nevertheless decreases as  $\beta_p$  increases.

In Figure 20, the  $\beta_p$  dependence is indicated by including several curves for various values of  $\beta_p$  between  $\pi$  and  $2\pi$ . As mentioned previously, the effective gap capacitance has some dependence on  $\beta_p$ , but the best that can be done to account for this is to use " $\pi$  static-mode" and " $2\pi$  static-mode" data, respectively, for the intervals  $1.0 < \beta_p/\pi < 1.5$  and  $1.5 < \beta_p/\pi < 2.0$ . Accordingly, the two sets of curves do not form one continuous set, with the  $\beta_p/\pi = 1.5$  curve the least reliable one common to the two sets.

Figure 20 reveals that, for a narrow Comb-Quad B amplification bandwidth centered around  $\beta_p/\pi = 1.8$ , the optimum  $g/p \approx 0.25$ . However, supposing that the exigencies of fabrication dictated something larger, perhaps 0.5 (because overly tight dimensional tolerances are suggested by  $g/p < 0.5$ ), the  $\beta_p/\pi = 1.8$  curve of Figure 20 would indicate a penalty of only about 30% in  $M^2 R/Q$ , and therefore perhaps only about 10% in interaction gain.

The potential low-frequency backward-wave instability in the Comb-Quad B case corresponds to  $\beta_p/\pi = 0.7$  to 0.9, with the corresponding  $M^2 R/Q$  vs  $g/p$  curves lying above the highest curve of Figure 20. The adoption of a relatively small  $g/p$  should in this case cause  $M^2 R/Q$  to be much smaller than it might be, an effect unfavorable to the potential oscillation. Ideally, the choice of  $g/p = 0.25$  would maximize the potential for gain around  $\beta_p/\pi \approx 1.8$  and differentially discourage gain around  $\beta_p/\pi \approx 0.8$ .

### 6.3 "VIRTUAL" BEAM-TUNNEL OPTION

The data above apply, at best, to an interaction region that approaches being axisymmetric at least as well as does that of Figure 9(a). However, the VBT interaction-region geometry described by Figure 9(c) is

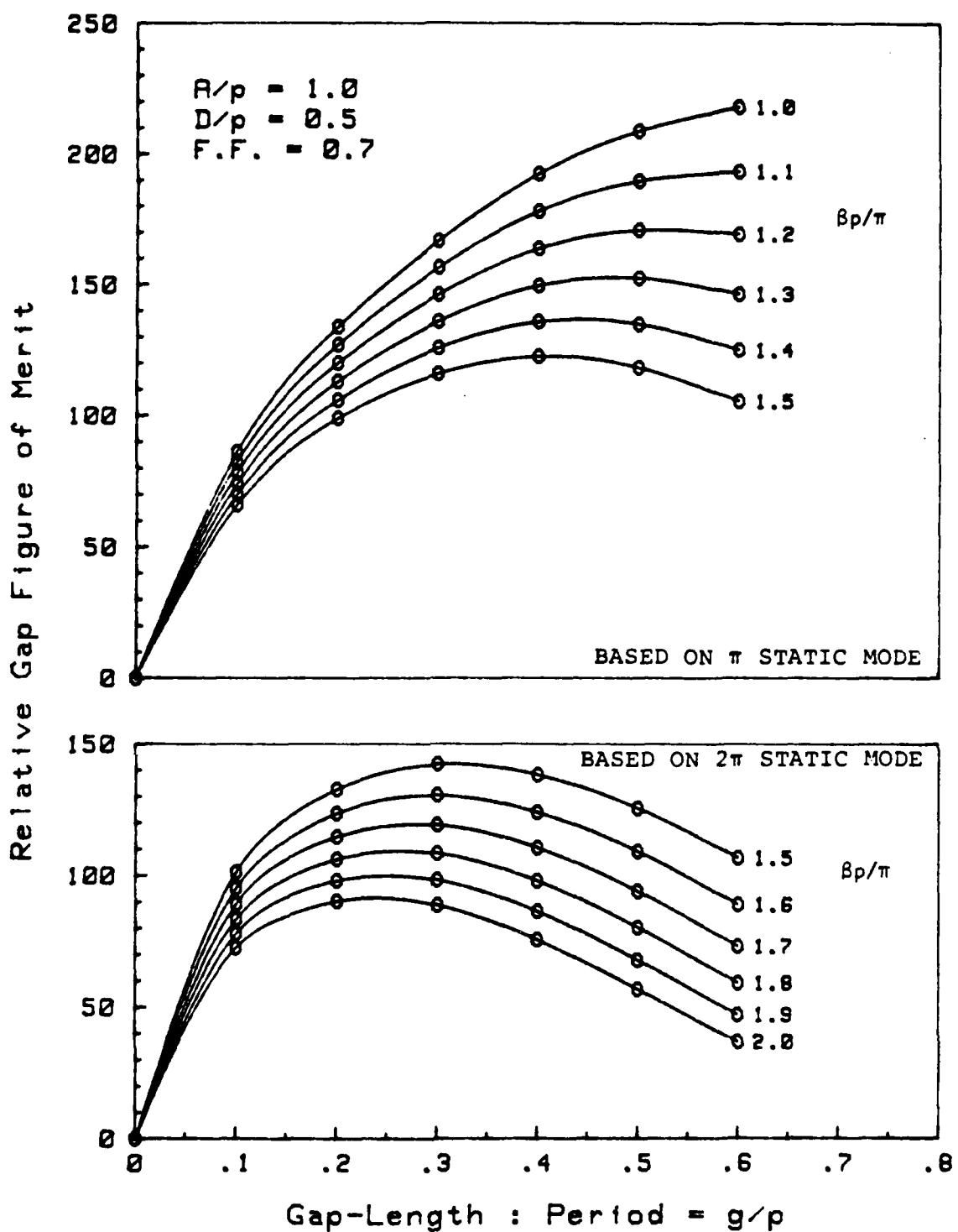


FIGURE 20. TYPICAL DEPENDENCE OF GAP FIGURE OF MERIT ON  $g/p$  AND UNIT PHASE SHIFT FOR HYPOTHETICAL AXISYMMETRIC INTERACTION REGION.

very attractive constructionally, and modeling its fields is the only way to know how it might compare with the more conventional (but more difficult to implement) tunnel/gap geometry as regards beam-modulation effectiveness. The procedures and results of such modeling are reviewed in this section. Due to the cost and time involved, only one configuration was considered -- that for which  $A/p = 1.0$ ,  $g/p = 0.5$ ,  $D/p = D/A = 0.5$  [see Figure 9(c)] and  $B/A \approx 0.7$ , where  $B$  is the effective beam diameter. True, these are the only proportions incorporated to date (for mechanical convenience) in any circuit models, but it is a loss not to know the effect of altering any of these proportions on beam-modulation effectiveness or to know how far from optimum they are electrically in the  $\beta p/\pi \approx 1.8$  case.

The interaction region in question is shown again in Figure 21. A round electron beam is included, and the points numbered 0 through 6 represent hypothetical electron trajectories (under totally confined flow). Thus  $E_{z0}(z)$  would express the variation of the axial component of  $E$  field with axial distance along the system or beam axis.  $E_{zi}(z)$ , for example, with  $i = 1, 2$  or  $3$ , would apply along three key trajectories on the effective edge of the beam, while the  $E_z(z)$  profile implies that all  $E_{zi}(z)$  have been averaged over the entire beam cross section for each value of  $z$ . The job was to derive these profiles (by solving Laplace's equation for the non-axisymmetric configuration depicted) and then use them to generate gap coefficients, or equivalent means for predicting beam/wave interaction.

To begin with, solving the wave equation was not feasible, though desirable because of dimensions generally significant relative to wavelength. The best that could be done was to consider only a small region close to the beam, assumed small enough for a static (Laplace) field solution to be valid. In Figure 17 the four planes labelled T-T were selected to bound such a region. These planes, which truncate the comb teeth at a distance ( $1.5 D$ ) from the axis judged to be reasonable, are accepted as Neumann boundaries. That is, one assumes that all  $E$  fields close to these planes are parallel to them.

The two planes L-L (a distance  $p$  apart) demarcate a unit cell along the length of the periodic structure. Once again, the phase shift between

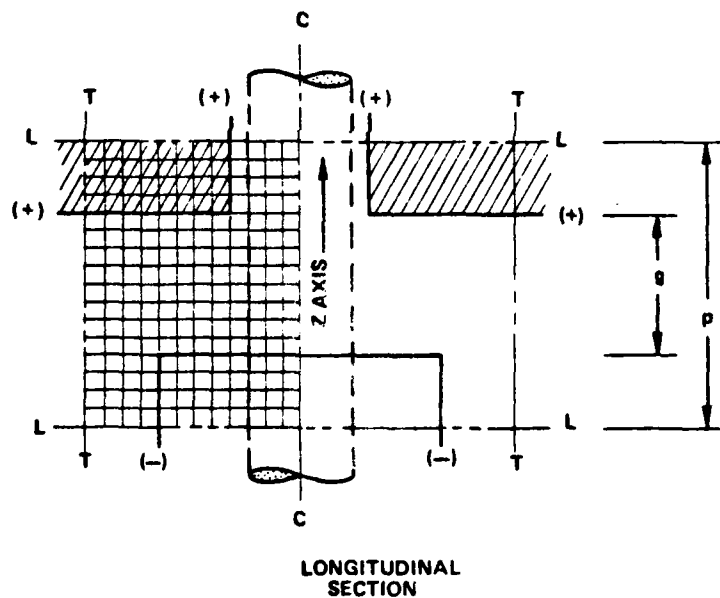
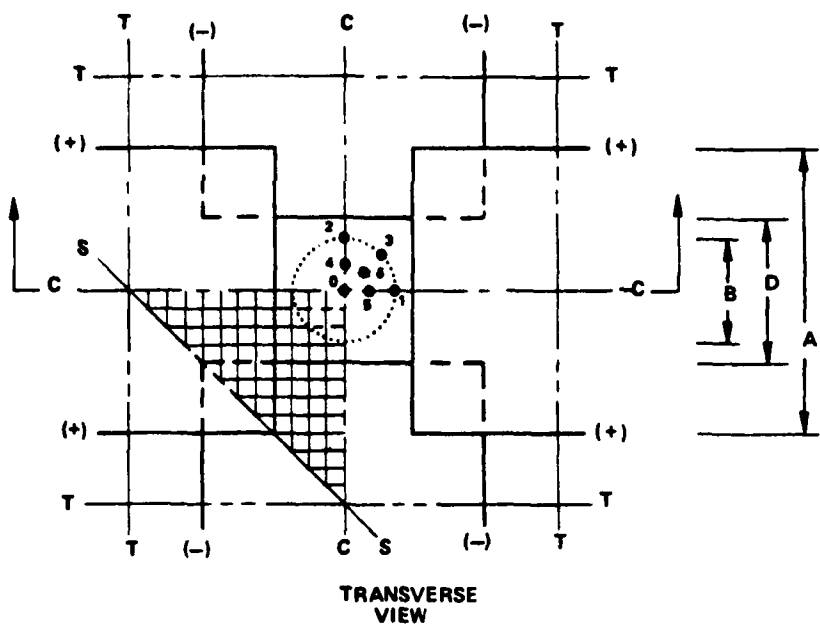


FIGURE 21. INTERACTION REGION OF FIGURE 9(c) WITH MATHEMATICAL CONSTRUCTIONS USED IN DERIVING  $E_z(z)$  PROFILES FOR KEY ELECTRON TRAJECTORIES.

adjacent cells will affect the fields in any one cell, hence the two possible static modes must also be introduced into this problem. For the  $2\pi$  static mode (no polarity reversals for  $E_z$  along z) planes L-L are Dirichlet boundaries, or equipotentials, with E fields only normal to them. However, for the  $\pi$  static mode (polarity of  $E_z$  along z reverses at L-L) planes L-L are Neumann boundaries.

While the geometry of Figure 21 is not axisymmetric, there are two planes of symmetry through the axis, labelled C-C. Thus only one quadrant of the system need be modeled. Planes C-C are, through symmetry, Neumann boundaries. Lastly, inspection of the figure reveals that because of the location selected for truncation planes T-T, diagonal plane S-S is also a plane (and a Neumann boundary) about which symmetry prevails. In consequence, the volume within which a Laplace solution needs to be sought is only 1/8 the original volume. Within this volume, the transverse distance from the axis to planes T-T was divided into 12 mesh intervals of  $D/8$  or  $p/16$  each, while the axial distance between planes L-L was divided into 16 mesh intervals of  $p/16$  each.

Despite the simplifications made, and the relative coarseness of the mesh (especially relative to the beam radius), the 1248 cube and prism mesh cells presented a formidable task in running the computer program VULCAN, used for solving, via many iterative "relaxations", any electrostatic or temperature-distribution problem that can be expressed with a rheological model. "Nodes" on the surfaces of each mesh cell, where needed, as well as at the center of a cell, add up to a very large number of nodes. Up to six "resistors" may come together at one of these nodes, leading to a vast number of interconnecting resistors, not all equal in value. To communicate to the computer all the node numbers, the resistance values, the interconnections, and the voltages applied to certain surface nodes (to account for the conductive electrodes) supplementary programs had to be developed just to input this information without recourse to thousands of manual entries. In fact, VULCAN had not previously been used to handle any problem of so large a "dimension", hence an initial block of time was spent changing the original program to make this possible.

When these efforts were completed for each static-mode case, each (reasonably well "converged") Laplace solution was delivered in the form of a file of the potentials at each node. These potentials ranged from -1000 V, arbitrarily "applied" to the boundaries marked (-) in Figure 21 to +1000 V at those marked (+). At this stage, the nodes of interest were those within and close to the electron beam, and arrayed according to a Cartesian coordinate system. By means of computer-implemented interpolation techniques, each tabulation of potentials was converted from the Cartesian-coordinate system to a cylindrical-coordinate one. Moreover, within the volume of interest, the axial gradient of potential, which is  $E_z$ , was derived as a continuous function, finally permitting plotting of the desired  $E_{z1}(z)$  or  $\bar{E}_z(z)$  profiles.

Some of these profiles are plotted in Figures 22 and 23. Following standard procedures at Varian,  $E_z$  is normalized here relative to the field between infinite parallel plates the distance  $p$  apart, with the same voltage (e.g., 2000 V) applied. Thus, for the  $2\pi$  static mode (Figure 22), the area under any  $E_z(z)$  profile is one unit because each electron trajectory starts and ends on a Dirichlet boundary. For the  $\pi$  static mode, the corresponding area is somewhat less. For profiles  $E_{z0}(z)$ ,  $E_{z3}(z)$  and  $\bar{E}_z(z)$  (Figures 22 and 23) there is symmetry about the center of the interaction gap, where  $E_z$  is a maximum. For the  $2\pi$  static mode (Figure 22),  $E_z$  does not vanish or change polarity within the "tunnel" and the profiles mentioned also have symmetry about the center of the tunnel. For the  $\pi$  static mode (Figure 23),  $E_z$  reverses polarity within the tunnel and hence must be zero at its center. The non-symmetry of the profiles for trajectories 1 and 2, which come closest to grazing the tooth tips of the circuit structure, will be discussed below.

For purposes of beam/wave interaction modeling, the profiles of interest are  $\bar{E}_z(z)$ , the dash-dot curves of Figures 22 and 23. To make good use of these hard-won plots, routine /@GAP/ was run to see if an equivalent effective axisymmetric interaction-gap configuration might not produce comparable  $E_z(z)$  profiles, given the liberty of  $g'/p$ ,  $D'/p$  and FSIN' having any value necessary, since  $g'$  and  $D'$  would be fictitious dimensions. (The prime is used here to identify geometric parameters of the fictitious

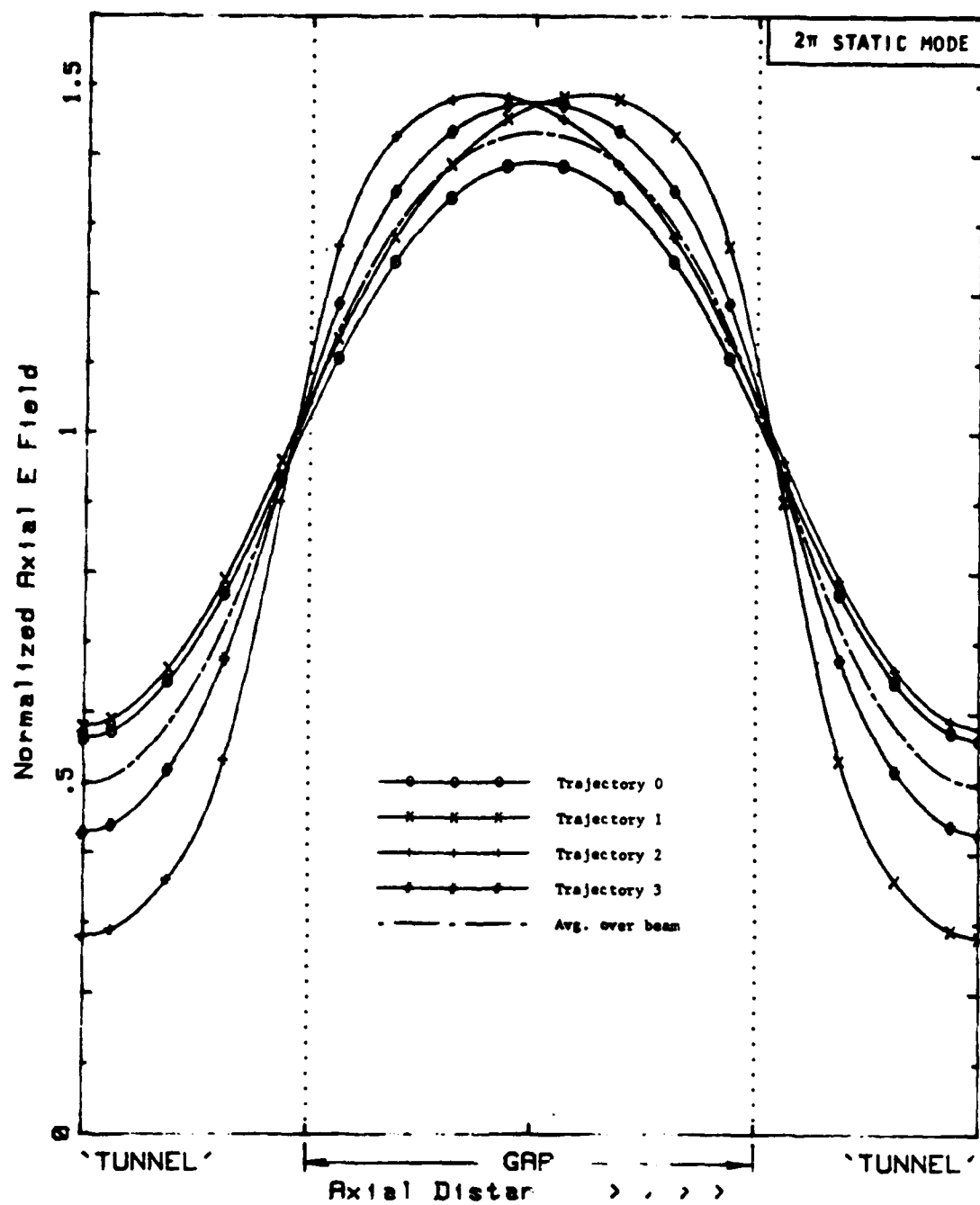


FIGURE 22. FOR  $2\pi$  STATIC MODE: AXIAL E FIELD VS AXIAL DISTANCE, FOR ONE PERIOD, IN INTERACTION-GAP GEOMETRY OF FIGURE 21.

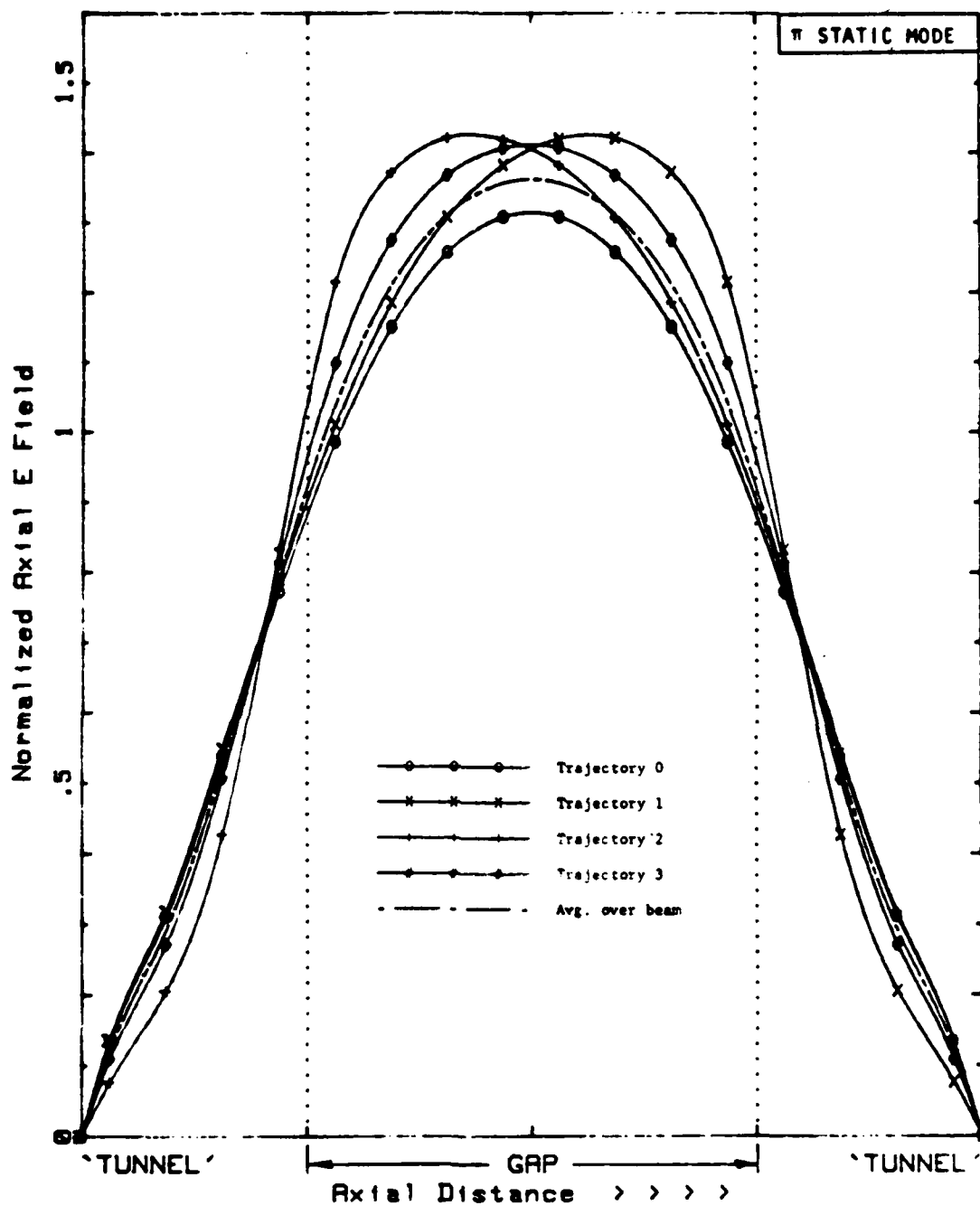


FIGURE 23. FOR  $\pi$  STATIC MODE: AXIAL E FIELD VS AXIAL DISTANCE, FOR ONE PERIOD, IN INTERACTION-GAP GEOMETRY OF FIGURE 21.

axisymmetric configuration that is most nearly equivalent to the non-axisymmetric VBT geometry with regard to beam modulation.)

Accordingly, for the  $2\pi$  static mode, and presumably also for non-static cases for which  $\beta_p \approx 2\pi$ , one finds that  $D'/p = 0.68$  (or  $D'/D = 1.36$ ) and  $g'/p = 0.56$  (or  $g'/g = 1.12$ ), with  $\text{FSIN}' = 0.79$ , give the best replication of  $E_z(z)$ . That is, at least for  $\beta_p \approx 2\pi$ , the gap geometry of Figure 9(c) provides very nearly the same beam/wave coupling as would the gap geometry of Figure 9(a) with the gap lengthened 12% and the round hole enlarged 36%. These effective enlargements both suggest relatively less modulation effectiveness, but not so much less that the VBT concept becomes less attractive per se. Conveniently, the equivalence is almost indifferent to the value of  $B/D$  and is about as good with regard to  $E_{z0}(z)$  as to  $E_z(z)$ . The equivalence can be used both for deducing  $R/Q$  from dielectric-rod perturbations and for beam-interaction modeling (with a reduced filling factor of 0.51, redefined as  $B/D'$ ). Of course, as  $\beta_p$  deviates further and further from  $2\pi$ , the validity of this equivalent axisymmetric geometry is suspect since different values of  $g'$  and  $D'$  apply for  $\beta_p \neq \pi$ .

For the  $\pi$  static mode, and presumably for non-static cases with  $\beta_p \approx \pi$ , the  $E_z(z)$  profile of Figure 23 is reasonably well replicated in a fictitious axisymmetric gap configuration featuring  $D'/p = 0.86$  (or  $D'/D = 1.72$ ) and  $g'/p = 0.48$  (or  $g'/g = 0.96$ ) with  $\text{FSIN}' = 0.85$ . That is, a hole enlargement of 72% and a gap shrinkage of 4% are what it would take to reduce the modulation effectiveness of an axisymmetric interaction region to that of the VBT region illustrated by Figures 9(c) and 21 -- but only for  $\beta_p$  in the vicinity of  $\pi$ . (Relative to  $D'$ , the revised filling factor would be 0.41 in this case.)

The use and implications of these findings for gain-vs-frequency predictions will be reviewed in Section 7.5.

#### 6.4 CREPEAU-McISAAC PHENOMENA

The  $E_z(z)$  profiles (Figures 22 and 23) for tooth-grazing trajectories 1 and 2 (Figure 21) have the greatest observable degree of lopsidedness or

lack of perfect symmetry about the center of a gap. If each such profile were plotted over several periods, each resulting waveform could be resolved into two waveform components -- a major component repeating itself with the period  $p$  (with or without polarity reversal for  $\beta p = \pi$  or  $2\pi$ , respectively) and a smaller-amplitude component having the period  $2p$ . This is consistent with the fact that the teeth grazed by a tooth-grazing electron are separated axially by  $2p$ , as a consequence of the  $90^\circ$  reorientations of tooth pairs from one layer to the next. [While the effect on  $E_z(z)$  is easily apparent for the interaction-region geometry of Figure 9(c), it nevertheless also exists for the case of Figure 9(a), though probably not to an important degree. Insofar as  $A$  is not  $\gg D$ , the  $90^\circ$  reorientations of the transverse bars will introduce a (small) bi-periodic component into the  $E_z$  fields at some points within the beam cross section.]

This situation is a perfect illustration of one of the topics of the 1964 paper<sup>10</sup> by Crepeau and McIsaac, which deals in part with TWTs whose circuit features have both a periodicity  $p$  (gaps) and a periodicity  $2p$  (orientation of crossbars). To characterize the major (Bloch wave) traveling-wave component, the authors draw  $\omega$ - $\beta$  curves with symmetry about every vertical line  $\beta p = n\pi$ , with  $n = 1, 2, 3, \dots$ . To account for the minor (Crepeau-McIsaac wave) traveling-wave component, there must be symmetry about every vertical line  $\beta p = m\pi/2$ , with  $m = 1, 2, 3, \dots$ . To implement this symmetry for a "cavity passband" curve of Figure 17 or 18, an additional curve is needed, passing through the original at  $\beta p = 3\pi/2$ , with negative slope.

Examining the augmented Brillouin diagram, the question of coupling between the Bloch and Crepeau-McIsaac waves, at the frequency for which  $\beta p = 3\pi/2$ , might be raised. Since this frequency is well below the Comb-Quad B "hot" bandwidth, the possibility of such coupling would have no import. On the other hand, if the beam current is sufficiently elevated, backward-wave oscillation is a possibility near the frequency at which the "beam-velocity line" intersects the negative-slope  $\omega$ - $\beta$  curve representing the Crepeau-McIsaac wave in the interval  $\pi < \beta p < 3\pi/2$ . Working against such an effect is the relatively low interaction impedance for the periodicity  $2p$  wave. The  $E_z$  amplitude for this wave is a maximum (at less

than 9% of that of the Bloch wave) along trajectories 1 and 2, still less everywhere else within the beam, and zero altogether along the axis and along many trajectories such as 3 and 6. After averaging over the entire beam cross section, the net amplitude of the periodicity 2p wave would be quite small relative to that of the periodicity p wave.

## 7.0 COMB-QUAD B PERFORMANCE PROJECTIONS

### 7.1 SMALL-SIGNAL INTERACTION MODELING

Ultimate indicators of the merit of a Comb-Quad B slow-wave structure would be the gain possible with a given electron beam, the variation of this gain with frequency (under fixed beam parameters), and the confidence that a reasonable degree of regulation of the beam parameters would suffice to avoid unwanted oscillation ("instability"). Currently available computer-simulation capability has proven very reliable, but only the small-signal type of interaction modeling has been attempted to date for Type B and other hypothetical Comb-Quad TWT designs.

If one were to project gain per period, or gain per isolated section of N periods, the result would depend on whether the excitation is by rf convection current or by rf voltage. Consequently, it has become a standard and convenient practice to model a hypothetical TWT with two sections of N periods each and a zero-length sever. The first and second sections are then waveguide and beam excited, respectively. The value of N has generally been chosen so that there would be about 20 dB of midband gain per section in the absence of circuit attenuation. Admittedly, an eventual TWT would not be designed so simplistically, but these simplifications do expedite the computer simulation and facilitate direct comparisons among circuit variants while providing sufficiently indicative "hot" performance projections. The major function of the modeling is to account for the interplay of effective interaction impedance and the deviation from beam/wave synchronism (Pierce's b parameter) as these vary with frequency and determine the overall gain vs frequency dependence. The variation of circuit attenuation with frequency would also contribute importantly when the variation is rapid, as it is near a passband edge.

To account for the effect of the magnetic focusing field on space-charge forces, the field is assumed to greatly exceed the Brillouin value, as in stiffly "confined" flow. The electron flow is modeled as if there were a well defined diameter, equal to 70% of that of the physical tunnel, within which the current density is uniform. With dc beam-velocity

spread neglected, the interaction modeling is thereafter "one dimensional". With a diode gun assumed, permeance rather than beam current ( $I_0$ ) is held constant.

For an initial set of projections, the  $\omega\beta$  data tabulated below were adopted. These data were measured for the tapered-tooth comb set at the far right in Figure 14, unenclosed. (The interaction structure could thus be classified as Comb-Quad A, or Comb-Quad B with  $X \rightarrow \infty$ .) As compared with other Comb-Quad B  $\omega\beta$  curves, the curve observed for these almost pyramidal teeth seems to have a slightly greater radius of curvature in the vicinity of  $\beta p/\pi = 1.8$ , and this appears favorable to the eventual gain and bandwidth predicted. However, for all subsequent interaction-modeling purposes, the structure was assumed to have the conventional tunnel/gap geometry rather than that seen in Figure 14 (far right). One would thus expect the gain predicted to be slightly optimistic relative to the case of non-tapered teeth, and more than slightly optimistic relative to the case of the unconventional (VBT) tunnel/gap geometry.

$\beta p/\pi$ ( $p = 0.5$ inch)	Scale Frequency (GHz)	Computed Attenuation [dB/cell @ $Q(L_2) = 250$ ]
2.0000	5.685	$\infty$
1.8333	5.473	0.124
1.6667	4.900	0.059
1.5000	4.034	0.035
1.3333	2.918	0.021
1.1667	1.530	0.010
1.0000	$\rightarrow 0$	---

Given the  $\omega\beta$  data above, an equivalent-circuit cell consisting only of  $C_1$  and  $L_2$  (heaviest lines in Figure 12, lower right) was found entirely adequate. In this case, it becomes sufficient to establish  $Q(L_2)$  alone to predict the attenuation-vs-frequency profile, as tabulated in the third column above. The choice of  $Q(L_2) = 250$  should be viewed as representative; for frequencies near 44 GHz this  $Q$  might be somewhat pessimistic (Section

5.6), but it could be reasonable or even optimistic for 94 GHz where surface finish and "anomalous skin effect"<sup>16</sup> can have additional impact.

For the purposes of Figure 24, other parameters include  $FSIN = 0.75$ , which is close enough to the 0.77 referred to in Section 6.2, and  $R/Q = 56.7$  ohms, a realistic value (for the narrow frequency band of interest) for the model at hand if the gap/tunnel geometry were conventional. [According to Figure 20, the actual  $g/p = 0.5$  is about twice the optimum for  $gp/\pi \approx 1.8$ ; if the circuit model had been based on  $g/p = 0.25$ , the measured  $R/Q$  would have certainly been lower, but the implicit  $M^2$  would be so much greater that some net improvement in the electronic gain (perhaps 10%) should result.] The adopted periods/section were  $N = 60$  and, for simplicity, all four section ends were assumed "cold matched" (end loading adjusted for zero reflection before beam is turned on) at all frequencies covered by Figure 24, since TWT gain is affected by the impedances loading the circuit ends. The circuit attenuation per cell was assumed invariant with temperature or position in the chain.

For the constant low microperveance of 0.03, gain-vs-frequency curves similar to those of Figure 24 were also plotted for higher and lower beam voltages,  $V_0$ , differing from 18 kV in increments of a few hundred volts. However, the most promising curve corresponded to  $V_0 = 18$  kV, or about 0.75 kV above "synchronous voltage" at 5.35 GHz (the "tangency point"). For  $V_0 > 18$  kV, the maximum gain is diminished, while for  $V_0 < 18$  kV, a double-peaked gain profile results.

The predictions of Figure 24 suggest a "hot" bandwidth of a few percent, depending on how defined (and also on the eventual effective circuit Q). Should the effective interaction impedance implicit in Figure 24 be overly optimistic, N would need to be greater to provide the same maximum total gain (at the same beam perveance). In that case, narrower "hot" bandwidths would be predicted.

The "low-voltage" Comb-Quad B design of Figure 18 is a case in point. Even when modeling the tunnel/gap geometry as if it were conventional, a substantially lower maximum gain and bandwidth were predicted under the same

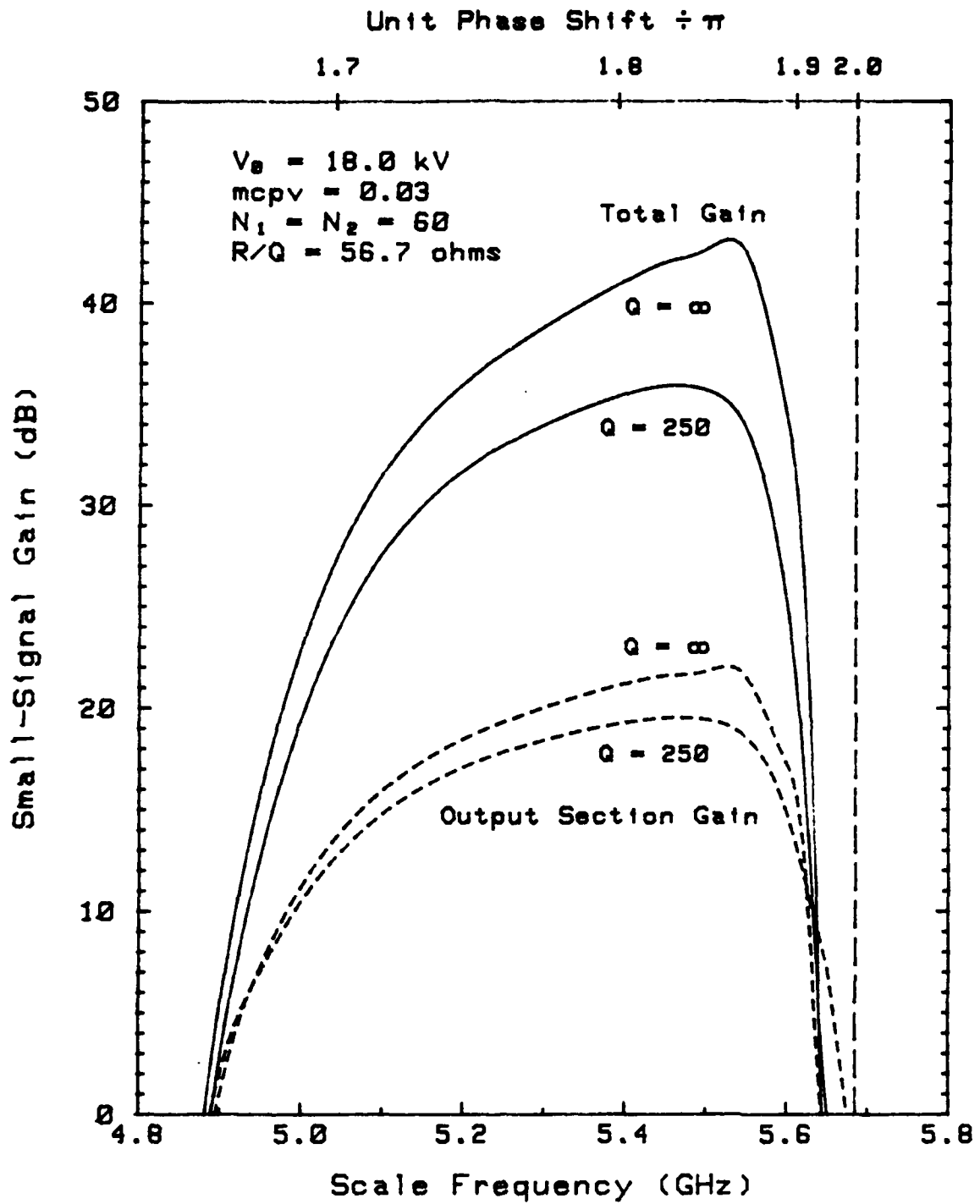


FIGURE 24. INITIAL COMB-QUAD B SMALL-SIGNAL GAIN PROJECTIONS.

$N$  and perveance as used for Figure 24. (The reduced beam conductance contributes importantly to this result.) Increasing  $N$  to raise the gain leads to even less bandwidth. Increasing the perveance instead would make PPM focusing very difficult to implement. The CC TWT design at short wavelengths rapidly becomes less and less practical as the design  $V_0$  is reduced below about 20 kV.

## 7.2 PASSBAND EDGE STABILITY

Instability at the  $2\pi$ -point band edge is a recurrent problem in many CC TWTs, though these tubes utilize much greater beam perveances (and lower frequencies) than are contemplated here. Since the potential Comb-Quad B "hot" bandwidth approaches this edge so closely (Figure 24) quantitative predictions regarding this risk are warranted.

The Varian small-signal interaction-modeling capability includes procedures for predicting the starting current ( $I_{so}$ ) and exact frequency for any potential mode of oscillation, given  $V_0$  and the other previously discussed circuit and beam parameters. These predictions were accordingly undertaken with respect to the  $2\pi$ -point passband edge, with the finding that when calculated  $I_{so}$  values are plotted as a function of  $V_0$ , a monotonically rising curve is obtained. It is thus easy to note the critical value of  $V_0$  above which  $I_{so} > I_0$ , and below which  $I_{so} < I_0$ , predicting oscillation. Three such curves were plotted, for  $Q(L_2) = 1000, 500$  and  $250$ , and it was no surprise to find that the lower the  $Q$ , the higher the curve of  $I_{so}$  vs  $V_0$ . The listings below indicate (1) how far above  $I_0$  is  $I_{so}$  if  $V_0$  remains constant at 18 kV, and (2) what drop in  $V_0$  would cause  $I_{so}$  to be only twice  $I_0$ . ( $I_{so} = 2 I_0$  suggests a reasonable margin of safety here.) In these cases,  $I_0$  is based on a microperveance of 0.03. (If an increased perveance were considered,  $N$  would be reduced accordingly, very likely tending to maintain the  $I_{so}/I_0$  ratios.)

<u>Q (<math>L_2</math>)</u>	<u><math>I_{so}/I_0</math> at <math>V_0 = 18</math> kV</u>	<u>Change in <math>V_0</math> causing <math>I_{so}/I_0</math> to drop to 2</u>
1000	3.7	- 0.45 kV
500	4.5	- 0.70 kV
250	6.2	- 1.10 kV

Since the allowable variation (regulation) of  $V_0$ , based on maintaining the desired gain profile (Figure 24), would be at most  $\pm 0.25$  kV, it is clear that this regulation would be more than adequate to prevent  $2\pi$ -point oscillation when  $Q \leq 1000$ .

It should be stated that the start-oscillation predictions referred to above utilized the same section parameters ( $N = 60$ ,  $R/Q = 56.7$  ohms, etc.) as applied for Figure 24, and took into account not only the circuit attenuation (via  $Q$ ) but the impedance presented to the slow-wave circuit by the waveguide coupler or "external sever" at each section end. For frequencies as close to the  $2\pi$  point as were those predicted in the start-oscillation calculations, the aforementioned end-load impedance would effectively be an open circuit. As calculated,  $I_{so}$  (and the corresponding oscillation frequency) curiously showed very little dependence on the end-load impedance -- whether an "open circuit" or a "cold match". Perhaps the band-edge circuit attenuation, even when  $Q$  is high, is sufficient to make the end loads immaterial in this instance. Conventionally, resonances spaced  $180^\circ/N$  apart in  $\beta_p$  are a feature of band-edge phenomena; very likely, with  $N = 60$ , the  $Q$  values considered caused these resonances to merge, given the small frequency separations between them. In executing the start-oscillation computations, no effects suggesting the presence of a series of resonances were encountered.

### 7.3 LOW-FREQUENCY BACKWARD-WAVE OSCILLATION

An inevitable feature of a Comb-Quad B TWT design is the intersection (in the Brillouin diagram) of the "beam-velocity line" with a negative sloping branch of the  $\omega-\beta$  curve, with  $\beta_p < \pi$  and the frequency,  $f_{bwo}$ , rather  $< f_{2\pi}$  at the point of intersection (Figures 17 and 18). The likelihood of

backward-wave oscillation is strong, warranting calculation of  $I_{so}$  before and after implementing any measures intended to ensure  $I_{so} > I_0$ . In the absence of such measures, two factors tending to elevate  $I_{so}$  are the relatively high group velocity that prevails when  $X$  is fairly large, and the relatively few beam wavelengths per TWT section -- at the low frequency in question ( $f_{bwo}$ ).

The computer simulation undertaken was for the structure and section parameters ( $N = 60$ , etc.) for which Figure 24 applies. In this case,  $X + \infty$ , and  $f_{bwo}$  is in the vicinity of 2.1 GHz. The R/Q used (56.7 ohms) was that measured at  $f_{2\pi}$ , and is now recognized to be too low an estimate for frequencies around  $f_{bwo}$ .

For an initial start-oscillation evaluation, a "cold match" was assumed for the load at each section end. In this case, the section is non-resonant, and the calculated  $I_{so}$  is merely a slowly increasing function of  $V_0$  (which was allowed to range from 15.5 to 19 kV). The ratio  $I_{so}/I_0$  (at micropervance 0.03) was nearly constant and not quite 2:1 under these conditions -- the exact amount depending slightly on Q. Due to the underestimation of R/Q in this case, the 2:1 apparent margin of safety could not be viewed as adequate. Moreover, the expectation of a match at the section ends around  $f_{bwo}$  is altogether unrealistic; the end loads for the circuit section would more appropriately be effective short circuits in this frequency region.

Under these circumstances, the circuit section would exhibit a series of resonances separated by  $180^\circ/N$  in  $\delta p$ , hence  $f_{bwo}$  might either be close to a resonance frequency or else midway between two of them. In one case,  $I_{so}$  would be greatly reduced and in the other case greatly augmented. Calculations show this with a curve of  $I_{so}$  vs  $V_0$  exhibiting wide undulations. Interestingly, the maximum of  $I_{so}$  ( $\approx 3.2 I_0$  for the parameters adopted) shows almost no dependence on Q. However, of practical significance is the fact that the  $I_{so}$  peak is broad in terms of  $V_0$ ; a variation of  $\pm 0.5$  kV can be tolerated before  $I_{so}$  falls significantly. Since  $f_{bwo}$  "tunes" with  $V_0$ , what has been established is the possibility of situating  $f_{bwo}$  between two circuit-section resonances (or anti-resonances,

as appropriate) and having it stay there with only a reasonable degree of regulation of  $V_0$ . In these estimates using  $N = 60$ , the resonances which are  $3^\circ$  apart in  $\beta_p$  are fortunately about 6% apart in frequency (125 MHz at 2.1 GHz) or about 12% apart in  $V_0$  (2.2 kV at 18 kV) for the  $\omega-\beta$  curve region around  $f_{bwo}$ . In practice, one would not be free to select  $V_0$  to position  $f_{bwo}$  as indicated; rather one would select  $N$  (i.e., differing from 60 by  $\pm 1$  or  $\pm 2$ , etc., so as to negligibly affect the section gain) to position the resonances relative to  $f_{bwo}$ .

A very different approach to suppressing the backward-wave oscillation at issue might rely on "smearing" the lower end of the  $\omega-\beta$  curve. As may be noted from Figures 17 and 18, variation of the enclosure dimension ( $X$ ) has a large effect on the lower end of the curve but only negligible effect on the upper. Thus  $X$  could be deliberately varied along the length of the TWT section (stepwise, gradually, randomly, or otherwise) to raise  $I_{so}$  near  $f_\pi$  without affecting amplifier gain near  $f_{2\pi}$ .

The efficacy of this approach to BWO suppression -- and perhaps of other approaches not yet considered -- should benefit from the addition of differential loss loading (Section 5.6.3). As indicated in Figure 19, a deliberate reduction in  $Q(L_3)$  only can greatly increase the circuit attenuation near  $f_\pi$  and  $f_{bwo}$  with very little effect near  $f_{2\pi}$  and  $f_0$ . In Comb-Quad interaction structures, the introduction of contact resistance between the combs and the "enclosure" strips conveniently interacts only with the azimuthal rf currents through  $L_3$ , lowering  $Q(L_3)$  but not affecting  $Q(L_2)$  or  $Q(L_1)$ .

#### 7.4 HIGHER-PASSBAND CONCERNS

The Brillouin diagrams of Figures 17 and 18 include a higher passband for each of the Comb-Quad B geometries considered. The possibility of adverse effects due to any attribute of propagation in these passbands is worth investigating.

One possibility is oscillation around the frequency at which the "beam-velocity" line intersects the  $\omega-\beta$  curve in question. (The tendency

for these curves to be atypical of coupled-cavity stacks has been noted in Section 5.4.) For the relatively larger values of the enclosure dimension X, a backward-wave oscillation with  $2\pi < \beta p < 3\pi$  might be a possibility; otherwise  $\beta p > 3\pi$  is suggested along with either positive or negative group velocity at the point of intersection.

Quantitative start-oscillation predictions were not undertaken since the Curnow equivalent circuit<sup>12</sup> is incompatible with the propagation characteristics shown. Working against too low a value of  $I_{SO}$  would be an effectively low interaction impedance -- as a consequence primarily of the long gap transit angles, especially when  $g/p = 0.5$  and  $\beta p \rightarrow 3\pi$  or  $> 3\pi$ . (According to Figures 17 and 18, the smaller X is, the larger  $\beta p$  will be at the "intersection" point.) It also seems likely that the attenuation at the suggested high frequencies would be high and readily increasable -- differentially -- on the basis of frequency, or of the azimuthal enclosure currents which should be prevalent at all frequencies within both passbands except near the amplifier-regime upper edge of the lower passband.

A very different type of adverse effect might be considered if the second harmonic (overtone) of the signal frequency could fall within the higher passband. The interaction structures of many conventional centimeter-wave CC TWTs are carefully designed so that the higher passband can include no harmonics of any planned signal frequency. Otherwise, when a signal frequency is half that of one of the N-1 resonances distributed across the higher passband, an unanticipated drop in gain may well be observed (through excitation of the resonant system by the harmonic component of the convection current).

For a Comb-Quad B TWT design, the signal bandwidth is narrow; for the case of Figure 17 it would be a few percent centered around 5.4 GHz. Thus, for  $X \geq 1.5$  inches, 10.8 GHz is simply not included in the higher passband. For the case of Figure 18, the signal band would be centered around 5.7 GHz, and it does appear that 11.4 GHz could be within the upper passband. However, at millimeter wavelengths many factors are working against second-harmonic effects becoming serious.

For one thing, the large value of N would provide closely spaced resonances in the higher passband, and these might easily become blurred together under the likely levels of circuit attenuation. Another factor would be the low Pierce C parameter characteristic of the low-perveance design; harmonic components of the rf convection current should then be rather small to begin with. Yet another favorable factor would be the low beam/circuit coupling impedances prevailing in the higher passband -- mainly as a consequence of the large gap transit angles.

### 7.5 REVISED SMALL-SIGNAL GAIN PROJECTIONS

The Comb-Quad B gain and bandwidth indicated by Figure 24 should be regarded as at least slightly optimistic, for reasons discussed previously. When improved modeling suggests a lower value for the maximum gain, an increase in N would then be recommended, one result of which (at constant perveance) is a smaller bandwidth -- in systems where beam/wave synchronism is inherently a narrow-band possibility.

The major motivation for revising the predictions of Figure 24 is to take into account the mechanically attractive but unconventional (VBT) tunnel/gap geometry of Figure 9(c). [The "intermediate" geometry of Figure 9(b) would be expected to provide a modulation effectiveness closer to that of (a) than of (c).] From the results of Section 6.3, with reference to the  $2\pi$  mode when  $g/p = 0.5$ , the effective gap length that is 12% longer than the actual, and the effective tunnel width that is 36% greater than the actual, clearly imply a reduced modulation effectiveness. Indeed, a preliminary assessment of the impact yields several dB less gain per section, at  $f_0$ , for the same N and perveance. This loss is only slightly offset by the fact that when original VBT-case dielectric-rod perturbation data are processed using  $g'$  and  $D'$  instead of  $g$  and  $D$ , the corrected R/Q expectedly comes out higher than otherwise -- but only slightly so.

Relative to Comb-Quad D performance possibilities at a given beam perveance, a Comb-Quad B design (based on the same combs) already suffers from a somewhat lower effective R/Q, hence adoption of the VBT geometry would only aggravate the B design's weakness. If possible, the tunnel/gap;

geometry of Figure 9(a) or (b) should be incorporated. Alternatively, a reduction in  $g/p$  from 0.5 to 0.25 might be considered for the VBT geometry [Figure 9(c)] if the necessarily tightened mechanical tolerances can be managed. In this case, the modulation effectiveness for the  $2\pi$  mode might be expected not to deteriorate, relative to the "conventional" geometry, to the degree it does when  $g/p = 0.5$ ; that is,  $g'/g$  and  $D'/D$  might more nearly approach unity if the analysis of Section 6.3 could be repeated for the  $g/p = 0.25$  case. Additionally, Figure 20 suggests a net improvement in  $M^2 R/Q$  for  $gp/\pi \approx 1.8$  when  $g'/p \approx 0.25$  rather than 0.5.

## 8.0 COMB-QUAD B FABRICATION CONSIDERATIONS

### 8.1 MACHINING OF COMBS

As mentioned in Chapter 4, individual combs are almost two-dimensional and the longitudinal profile can be cut on an individual basis or with four or more combs "ganged" to ensure equality. Electroerosion machining appears the most convenient, with either stationary, traveling-wire, or single or multiple rotating-disc "burners". The surface finish currently obtainable is much improved relative to that of the recent past, with a "mirror finish" reported to be achievable. However, there is at present no quantitative measure of the roughness that might be tolerated at a given high frequency in a tube where other sources of attenuation (e.g., reflections due to dimensional fluctuations) might mask that due to roughness.

Since the dimensions of the opening between teeth of an individual comb exceed the comb thickness, cutting via "chemical milling" might economically produce good results with a fine surface finish. In this case the copper is etched away, with a photo-resist pattern (or perhaps a reusable non-etchable metal template) on each side of the copper sheet. Nowadays, the angle between the cut surface and the sheet can be controlled in the etching bath to be exactly 90° or some other desired value, and the sheet thickness can be much greater than with the "photo etching" techniques of former years.

Depending on the source of information, laser milling is reported as more or less problematic if not out of the question for copper -- due to its high thermal conductivity. Its high infrared reflectivity was formerly a serious handicap, but frequency doubling of the laser beam (which then appears green) is now obtainable in response to that problem. The thermal-conductivity problem might be overcome if the copper were sufficiently thin, but quantitative criteria are not currently available. Possibly the comb contours could be established by laser milling in a material other than copper (e.g., steel) and then transferred to copper by coining. With regard to surface roughness, it is believed that any desired finish should be obtainable if the cutting process is slowed down sufficiently. Computer control would cover all aspects of laser milling, whereas for electroerosion

the computer might control the periodicity and the depth of the "burn" while the "burner" controlled the width.

Conventional machining should not be overlooked as an economical means for producing a large number of combs at the same time, according to the following procedure: A large-diameter hollow copper cylinder is threaded (spirally) so that the profile of the thread is that desired for a comb, a large number of which are obtained when the cylinder is sliced by longitudinal cuts normal to the cylindrical surface. To prevent burrs during the slicing, the threaded surface would have been filled with suitable resin, later dissolved. If the cylinder diameter is sufficiently large, the slight curvature of the tooth tips, and the slight tilt of the teeth due to the original spiral cut, will not interfere with the use of such combs in Comb-Quad structures.

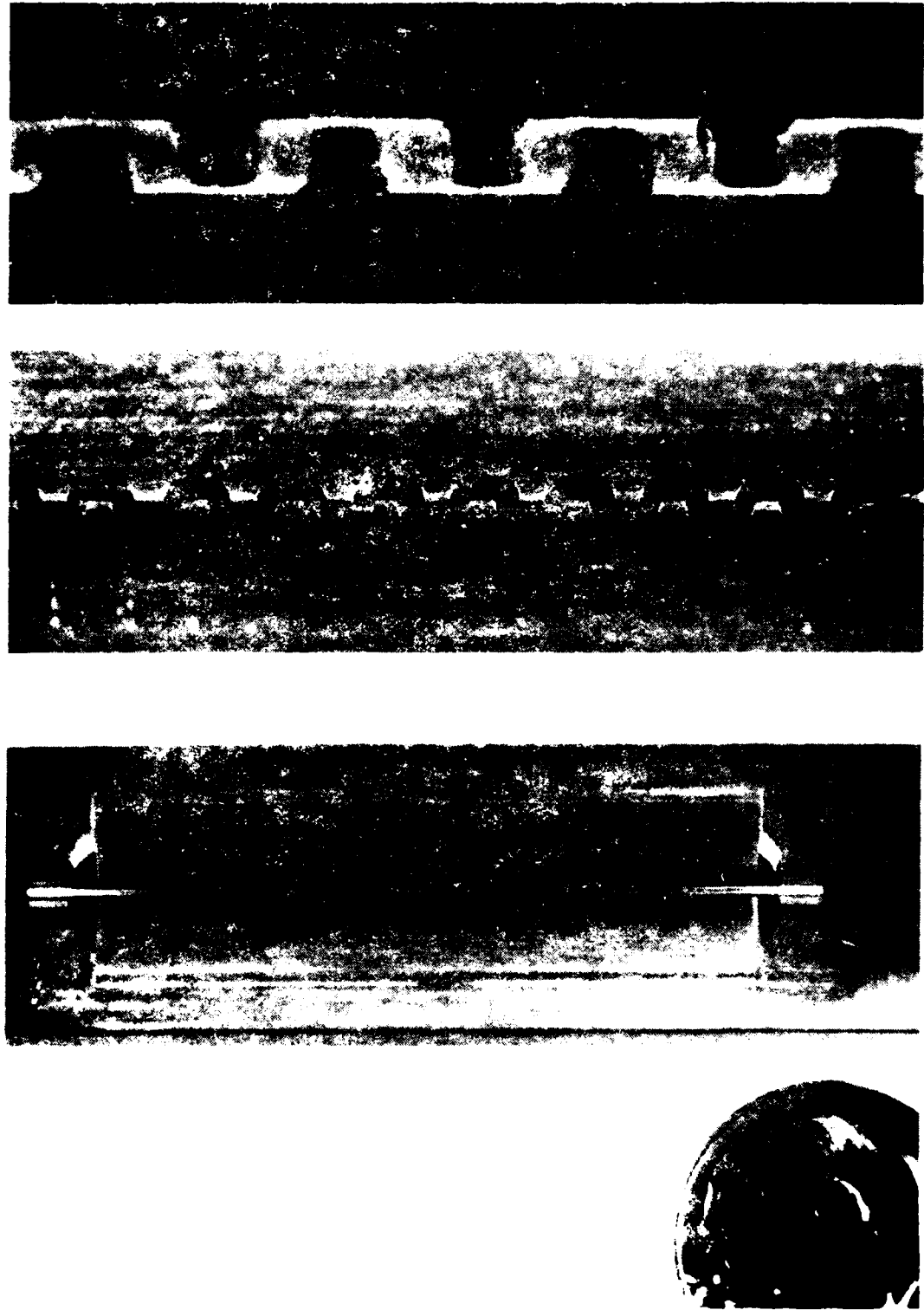
Figure 25 shows a copper Comb-Quad assembly fabricated in mid 1979 in the style of Figure 8 (right). In this case, four copper slabs (about 0.030 inch thick) were simply notched with an end mill -- 20 notches per inch longitudinally -- since the objective was merely to provide a tangible specimen as a visualization aid that was actual-size for 94 GHz. Although dimensional precision is probably lacking, the ease of preparing these parts with the quality shown was gratifying. The combs of Figure 25 are supported in the desired relation to one another with the aid of a brass fixture. The resulting period of 1/40 inch implies a potential beam voltage of roughly 20 kV. A "virtual" beam tunnel was established with a steel mandrel 0.016 inch in diameter, subsequently removed, with a slightly smaller quartz fiber inserted later for photogenic purposes.

## 8.2 SENSITIVITY TO GEOMETRIC DEVIATIONS

### 8.2.1 Periodicity of Individual Combs

A basic intention of the plan to use four combs as the sole periodicity determinant of an interaction structure was to permit thorough optical inspection (preferably under computer control) of individual combs before commencing assembly. At this stage, systematic errors in periodicity

FIGURE 25. 44-PERIOD COPPER COMB-QUAD ASSEMBLY VARIOUSLY MAGNIFIED. (DIMENSIONS IMPLY 94 GHz OPERATION AT ABOUT 20 KV. TRANSLUCENT MANDREL IS 0.015-INCH QUARTZ FIBER SLIDING IN "VIRTUAL" BEAM TUNNEL.)



AD-A100 461

VARIAN ASSOCIATES INC PALO ALTO CA  
INTERACTION STRUCTURES FOR NARROW-BAND MILLIMETER-WAVE COMMUNIC--ETC(U)  
APR 81 A KARP F30602-79-C-0172

F/6 9/1

UNCLASSIFIED

RADC-TR-81-54

NL

2 of 2  
A0461

END  
DATE FILMED  
7-8-81  
DTIC

capable of being detected optically would be cause for discarding the comb before further expenditure of assembly effort. Cumulative errors in the period should not arise. Unless smaller than the optical system in question might detect, the magnitude of random errors would be measurable and traceable to the tooth-cutting means.

Some efforts made to mathematically relate performance degradation to random dimensional fluctuations<sup>17</sup> stated that the most serious effect would be that due to an added loss per cell, averaging  $1/p$  times the mean-square reflection coefficient. When due to a variation in period, the mean-square reflection coefficient should in turn equal the mean-square period deviation times  $(\psi - 1)^2/p^2$ , where  $\psi$  is the ratio of the phase velocity to the group velocity.<sup>17</sup> (The "phase velocity" referred to here presumably is that of the fundamental Bloch wave at the frequency of interest.) Since  $\psi$  would invariably be very large near the passband edges, this statement suggests that random dimensional deviations should be differentially helpful in increasing the attenuation that promotes band-edge stability in millimeter-wave tubes. It should not be amiss to re-examine, update and continue the investigations of Reference 17 in the context of current TWT designs and objectives.

#### 8.2.2 Inequality of Combs or Comb Pairs

If one comb has any tooth dimension different from that dimension in the other three combs (or if two opposing combs are equal but different from the other two combs) the consequent bi-periodic perturbation will affect the  $\omega-\beta$  curve such that a stop band appears about the midband frequency for which  $\beta p = 3\pi/2$ . The width of the stop band increases as the inequality worsens. For a small degree of inequality, the evidence for the stop band may consist only of a rise in input VSWR which will seriously affect performance only if excessive. The presence of circuit loss increases the tolerance to comb inequality, but the consequences must be faced when this tolerance is exceeded and the stop band is well established. (As with any of the possible defects, much will depend on whether the dimensional error applies locally, or over part or all of the circuit length, or varies monotonically from one end to the other.)

Working with a representative Comb-Quad A cold-test scale model (third from left in Figure 14), the teeth of one opposing comb pair were deliberately lengthened 20% while the teeth of the other pair were shortened the same amount. The total width of the observed stopband was then about 40%. Assuming a linear dependence of stopband width on tooth-length deviation, the observed ratio of about 2 1/2 might help establish an eventual tolerance limit on tooth length inequality between one comb pair and the other.

In a potential Comb-Quad B TWT design (Figures 15, 17 or 18) the frequency for which  $\beta_p = 3\pi/2$  would be well below the (narrow) operating band, hence a bad VSWR at  $f_{3\pi/2}$  would be of no import. In this respect, Comb-Quad B designs would be relatively tolerant of comb inequality. However, if the potential stopband became definitely established, the Brillouin diagram would require redrawing to show the stopband edges and additional branches of  $\omega-\beta$  curve. With a few percent of stopband width, the "beam-voltage line" would intersect a negative-sloping branch in the interval  $\pi < \beta_p < 3\pi/2$ , signaling the possibility of oscillation at a not necessarily elevated value of beam current.

Concerning a stopband centered at  $f_{3\pi/2}$ , it is tempting to consider whether it might be deliberately introduced for some useful purpose rather than as a liability. For example, if the stopband were several tens of percent wide, the "beam-voltage line" might intersect only a positive-sloping branch of the  $\omega-\beta$  curve (above the stopband) in the interval  $3\pi/2 < \beta_p < 2\pi$ .<sup>18</sup> In fact, the relation of the beam-voltage line to this abbreviated curve segment in the  $3\pi/2$ -to- $2\pi$  interval is the same as applies in the  $\pi$ -to- $2\pi$  interval to curve D of Figure 15 -- suggesting a greater "hot" bandwidth than a Comb-Quad B design might provide without comb inequality. However, what dooms this design possibility is the observation of a zero of interaction impedance at the lower edge of the  $\omega-\beta$  curve segment in question (which is the upper edge of the aforementioned stopband). In this case, a very low interaction impedance is implied at the potential operating frequency.

### 8.2.3 Comb Mis-registration

Starting with equal combs, but given the method of assembly, it would be relatively easy for one comb to be axially misaligned with its opposing mate. Alternatively, opposing combs might be aligned, but one pair might not be correctly interleaved with the other. In either case (or any combination thereof) a bi-periodic perturbation results, accompanied by the stopband which might be very apparent or only incipient. The features of the stopband discussed in the first paragraph of Section 8.2.2 above would apply here as well; the phrase "comb mis-registration" need only be substituted for "comb inequality".

Insofar as the evidence for a stopband due to comb mis-registration was at most a very bad VSWR at  $f_{3\pi/2}$ , Comb-Quad B TWT operation would be rather tolerant of this mis-registration. In any event, it should be possible to quantify the relation of the stopband width to the degree of mis-registration, though this has not been done, experimentally or otherwise. (From the experience of working with 17- to 37-period lengths of Comb-Quad D structure at X band, it may be said that the mechanical adjustments needed to reduce stopband evidence to a modest VSWR peak were easily implemented; however, removing the VSWR peak altogether called for a higher order of finesse.)

### 8.2.4 Orthogonality of Comb Pairs

Each pair of opposing combs constitutes a ladder and the two interleaved ladders are nominally orthogonal. However, it is conceivable that in the course of assembly the final angle will differ somewhat from  $90^\circ$ . Experimental data are on hand for a Comb Quad B/CBT model (with  $f_{2\pi}$  near 5.6 GHz and  $X \approx 2.75$  inches to place  $f_\pi$  near 1 GHz) in which one ladder was deliberately rotated a sizable  $30^\circ$  away from the orthogonal position. Somewhat surprisingly, the  $\omega-\beta$  curve was affected only very little. The shift in  $f_{2\pi}$  was about - 5%, with the shift decreasing to zero at  $\beta p/\pi \approx 1.6$  and reversing to + 3% at  $\beta p/\pi = 1.3$ . Assuming the process to be linear, the effect of a deviation from orthogonality of, say,  $1^\circ$ , would be trivial indeed.

The original interest in introducing the 30° disorientation was to seek a possible change in shape for the  $\omega$ - $\beta$  curve. The result was negative in that respect, but serendipitously demonstrated the considerable tolerance of Comb-Quad performance to constructional deviation from orthogonality of the two ladders.

#### 8.2.5 Errors in Enclosure Geometry

When the "enclosure" is about minimal in size, as in the C and D cases (Figure 11), the  $\omega$ - $\beta$  curves of Comb-Quad interaction structures show rather little tolerance of enclosure-dimension deviations.<sup>15</sup> For Comb-Quad B structures, however, Figures 17 and 18 show there is very little sensitivity to the dimension X of the  $\omega$ - $\beta$  curve in the potential-amplifier range  $1.7 < \beta_p/\pi < 2.0$ . This feature is perhaps a signal virtue of the Comb-Quad B approach (when the application bandwidth is low enough to take advantage of it).

The low-frequency portion of the  $\omega$ - $\beta$  curve is . . . very sensitive to variations in X. In fact, intentionally . . . along the length of a TWT section (stepwise or otherwise) can "smear" this region of the  $\omega$ - $\beta$  curve and thus raise the steady-state electron current for the potential backward-wave instability (See . . . ).

## 9.0 COMB-QUAD B TRANSITIONS TO WAVEGUIDE

A coupling from rectangular waveguide to the interaction structure is needed at the input and output ends of the TWT, with a good "match" over the "hot" bandwidth. Since external "severs" are often preferred in high-frequency CC TWTs, these can make use of the same transition design at each end of each TWT section (with a "load" instead of a window in all but the first and last waveguides).

In the familiar trapezoidal structure of Figure 7, a TWT section would end with a pair of slots. A pair of slots and coupling is conveniently effected by connecting the slots with a loop of H field centered on the beam axis. Coupling E fields should also be provided across the narrow dimension of each slot -- with equal magnitude and the same polarity at the slot edge closest to the beam hole. The appropriate E/H ratio is greatest at frequencies near the lower edge of the "cavity-mode" passband. As the frequency increases, E/H drops rather slowly over most of this passband until it falls rapidly to zero at the upper edge. (This is consistent with zero transverse-E field at  $f_{2\pi}$  and zero azimuthal-H field at  $f_\pi$ .) The E/H vs frequency curve just described can be obtained by computing the input impedance (often called "image impedance") to a semi-infinite chain of the circuit cells of Figure 12 (lower right).

If the cavity end plate bearing the two slots is interfaced with the broad wall of a rectangular waveguide near its short-circuited end, with the waveguide axis parallel to the slots, the requisite E- and H-field orientations are automatically provided. The correct general magnitude of E/H is obtained by adjusting the waveguide height, which tends to be shallow, and necessitates a gradual taper from the original waveguide height. The necessary decrease in E/H with increasing frequency is inherent in the waveguide to begin with, but the rate can be adjusted with the guide width. This width is always less than the original width; the change can be implemented with a step, a taper, or both.

When a length of Comb-Quad B, C or D interaction structure (Figure 11) is truncated, a pair of entrance slots is invariably obtained. Though the

shape of these openings is certainly unconventional, their function is quite analogous to those of the structure of Figure 7. Successful waveguide couplers have been developed around these openings, following the principles discussed above for Comb-Quad D and C structures.<sup>15</sup> These principles could also apply to the Comb-Quad B case, but the proximity of  $\beta p$  to  $2\pi$  means that E/H should be both small and varying (toward zero) rapidly with frequency. These requirements have been found to exceed the capability of a coupler of the type described, even though the requisite bandwidth is small.

Figure 26 shows the Comb-Quad B/CBT circuit section, 19 periods long, to which a G-band waveguide coupling was sought. (The test setup shown is "single-ended"; the other circuit end is "terminated" with a long pointed "dart" of graphitized paper.) The teeth and enclosure were dimensioned so that, for  $p = 0.5$  inch,  $f_{\pi} \approx 1.5$  GHz and  $f_{2\pi} = 5.685$  GHz. The "hot" bandwidth would be expected to extend from 1.75 to 1.90 in terms of  $\beta p/\pi$ , with a center frequency of 5.4 GHz. Despite the efforts made to vary the waveguide height and width in the reduced region, and to vary the size and shape of the interface apertures, a correct E/H (and its frequency dependence) could not be produced, in the plane of these apertures, for the frequencies above the center of the projected "hot" bandwidth. In other words,  $\beta p/\pi \approx 1.80$  appears to be the upper limit to which this coupler design approach can be pushed, whereas the "hot" bandwidth of a Comb-Quad B TWT might extend through  $\beta p/\pi \approx 1.90$ .

A modification scheme investigated for possible extension of the match bandwidth closer to the  $2\pi$  point was a familiar one in conventional CC TWT experience: to make the two end cavities serve as a 90-electrical-degree transformer by raising the (local)  $f_{2\pi}$  for them such that the unit phase shift for each (in terms of the fundamental Bloch wave) would be  $45^{\circ}$ , at a frequency where the unit phase shift for unmodified cavities would be rather less. Accordingly, for the lowermost inch ( $= 2p$ ) of the slow-wave structure of Figure 26, the enclosure was moved inward sufficiently to give  $\beta p/\pi = 1.75$  at the frequency for which  $\beta p/\pi$  otherwise = 1.83. The feed waveguide was then reconfigured to provide matching fields that would be correct for the new input to the transformer section. The final result obtained did appear to be an extended match bandwidth -- but only very slightly so. One

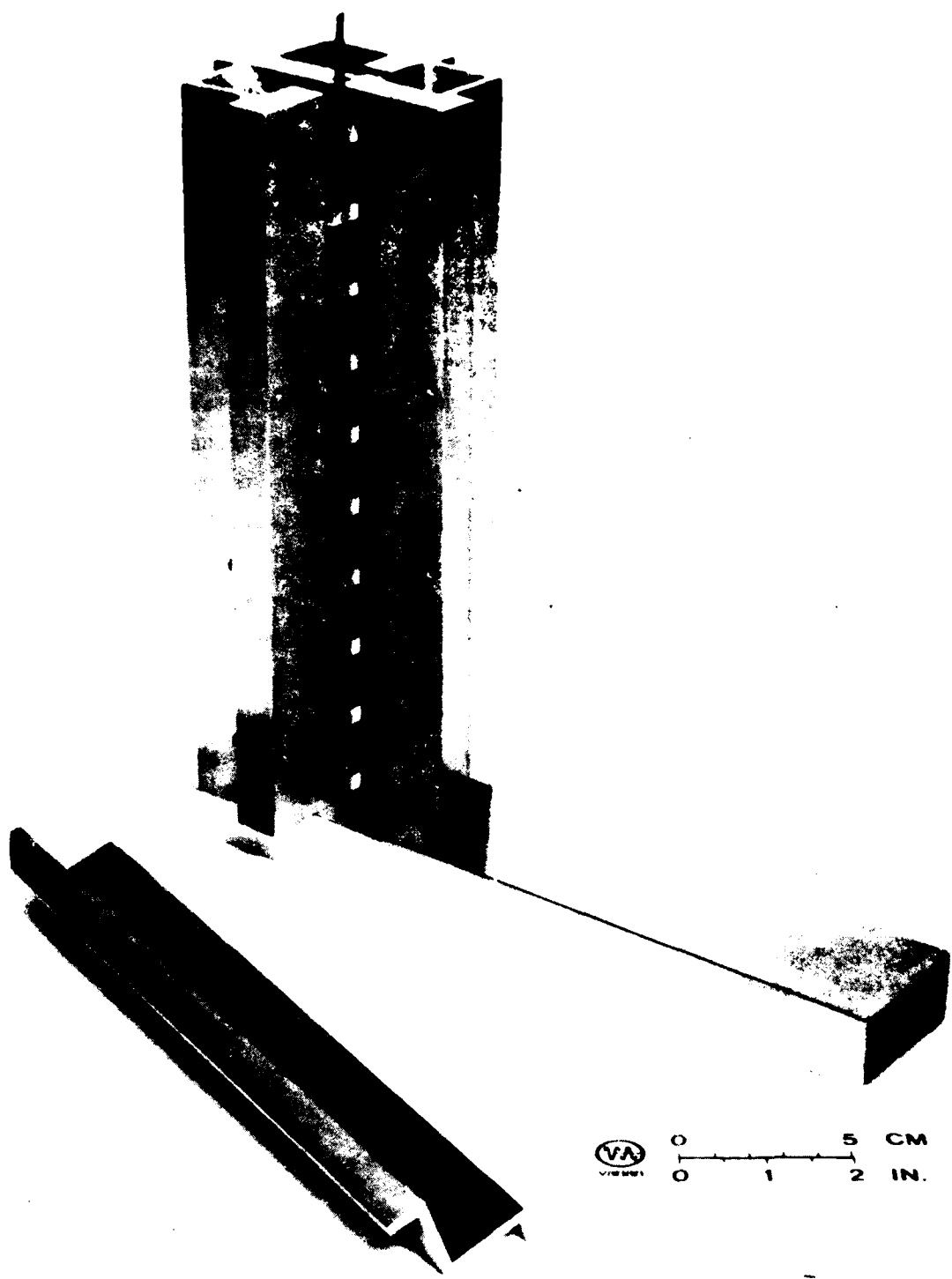


**FIGURE 26. 19-PERIOD COMB-QUAD B/CBT CIRCUIT SECTION WITH G-BAND WAVEGUIDE FOR ESSAYING TRANSDUCER. (ONE "ENCLOSURE" STRIP REMOVED TO REVEAL INTERIOR.)**

of the impediments to success here is believed to be the difficulty, in the Comb-Quad case where there is no "web" to demarcate cavities, of establishing a juncture between "cavities" of one design and "cavities" of another design.

An even more general problem, as  $\beta_p + 2\pi$ , is that due to the perturbation of the edge of the  $\omega-\beta$  curve itself by the resistive material of the terminating "dart". A way out of this difficulty would be to undertake the experimentation "double-endedly." However, one would then have to consider whether the input power "matched" in was reaching the output waveguide or getting dissipated via the circuit attenuation, which would be both high and subject to substantial variation (from scale model to actual circuit) through its dependence on the skin resistivity.

While the failings and difficulties described above might not completely rule out the eventual achievement of a Comb-Quad B match via the twin-aperture scheme, they do imply an extraordinary design effort, hypercritical adjustments, etc. A radically different approach is therefore suggested, and discussed below, though experimentation with it was not undertaken. The interface aperture in this approach is an annulus, instead of twin slots, precedent for which exists in Figure 8.12 of Reference 12.

The salient advantage of the annulus of Figure 27 lies in the accompanying very low ratio of  $E_r/H_\theta$ , where  $E_r$  and  $H_\theta$  are both transverse to the beam-tunnel axis. In the end "cavity" of the Comb-Quad stack, as  $\beta_p + 2\pi$ , of course, the dominant rf fields are  $E_z$  and  $H_\theta$ , with only a very weak  $E_r$ . In the design of Figure 27,  $E_r/H_\theta$  might representatively be only 8 ohms at the interface plane. If the characteristic impedance of the quarter-wave coaxial transformer were than 20 ohms (O.D./I.D. = 1.4), the impedance level for the conventional waveguide/co-ax transition should be a convenient 50 ohms. With the waveguide height reduced, the transition/transformer design should be easily achievable under the narrow bandwidths required. Constructional simplicity and compatibility with the electron-optical system may be noted. [With dimensions that remain reasonable at millimeter wavelengths, the coaxial line could support a higher-order mode at the frequency of interest; however, the observation of a "match" through the

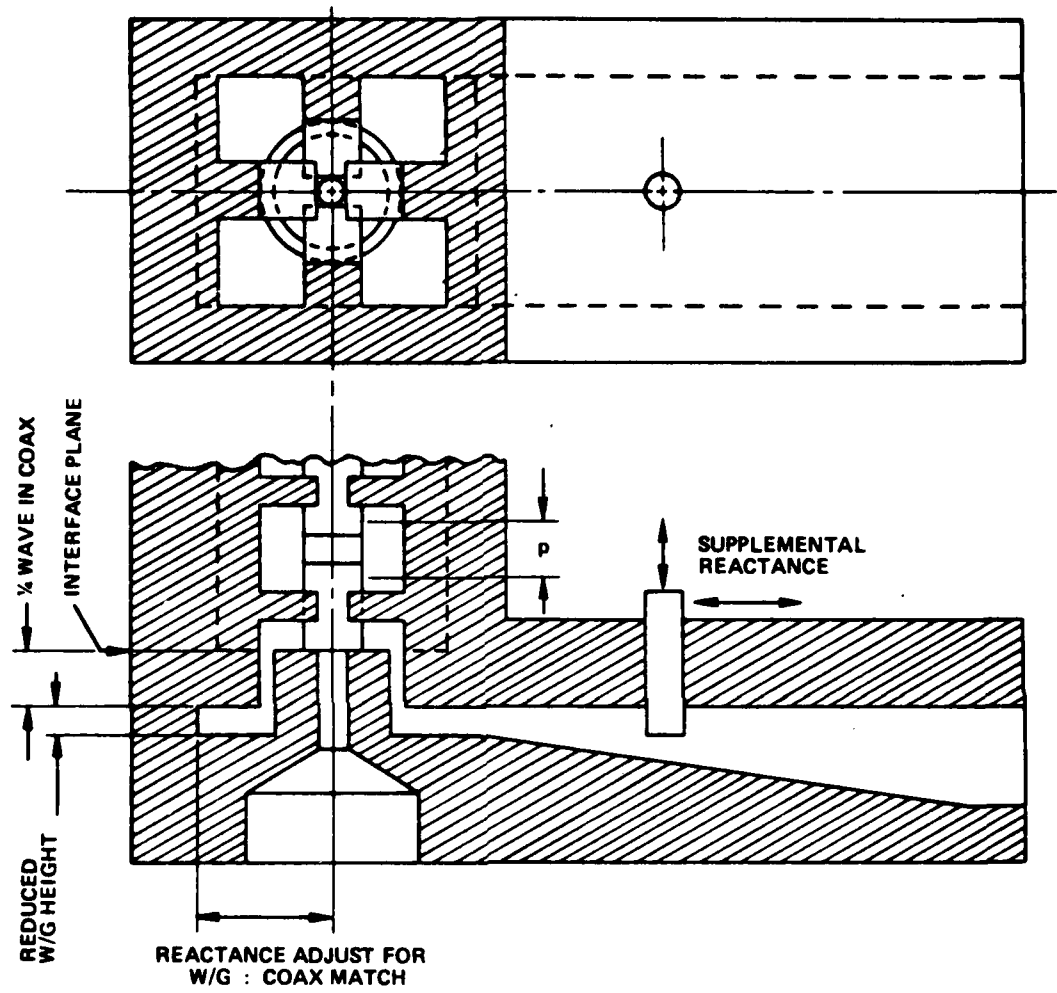


**FIGURE 27. SUGGESTED TRANSITION BETWEEN REDUCED-HEIGHT RECTANGULAR WAVEGUIDE AND COMB-QUAD B/VBT INTERACTION STRUCTURE.**

a "match" through the transition would mean that sufficient symmetry prevailed to not launch this mode, which could not in turn pass the Comb-Quad interface.]

## 10.0 THERMAL CONSIDERATIONS

This chapter largely duplicates Chapter 8 of Reference 15, except for some editing to maximize pertinence to Comb-Quad B structures, rather than C or D. The analytical results discussed below were obtained without expense to either contractor while the analyst was supported as an AFTER-program participant.

In conventional CC TWTs (with ferrules), especially those with PPM focusing, beam interception generally presents more of a thermal problem than does rf dissipation. This heat energy is deposited around the beam-tunnel wall and evacuated via the "web" (Figure 7) which one tries to keep thin to maximize the cavity height and R/Q. However, the effective transverse dimension of the evacuation path can be rather wide when the coupling slot is small, as it is in narrow-band designs. In this (narrow-band) case, the stubby teeth of a Comb-Quad structure (Figure 8) would not necessarily present a more favorable thermal situation than do conventional cavities with ferrules and thin webs.

As for conventional but ferruleless cavities,<sup>5</sup> the Comb-Quad teeth would clearly have no thermal advantage -- for the same frequency, beam voltage, period, g/p ratio, etc. However, the Comb-Quad advantage could be a higher R/Q for the same thermal capability, as discussed in Section 4.2. Something relevant to consider also is the operation at  $\beta p/\pi \approx 1.5$  of a narrow-band, conventional CC TWT, for which case g/p = 0.5 is recommended when the cavities are ferruleless.<sup>5</sup> If a Comb-Quad B design were considered as an alternative (at the same  $V_0$ ) the  $\beta p/\pi \approx 1.8$  operation, with g/p = 0.25 recommended, then suggests a substantial thermal advantage.

The actual thermal capability of a Comb-Quad B interaction structure (Figure 11) will ultimately depend on the rate of heat removal from the "enclosure" into which the thermal energy in a tooth can spread, starting from the root of the tooth. (While beam-interception power must travel to the enclosure from the tooth tip, rf-dissipation power would develop mainly near the tooth root and in the walls of the enclosure itself.) If PPM focusing is to be used, the adoption of four fin-like heat "risers", each

radiating outward from a comb, would provide the most effective overall cooling means. In this case, each polepiece and magnet ring in the PPM stack (all completely external to the rf structure in a millimeter-wave application) would consist of four curved segments, each somewhat less than 90° in arc.

In the absence of information about the geometry and cooling of the "enclosure", the absolute temperature at the root of a tooth cannot now be estimated. However, the temperature drop ( $\Delta T$ ) from the tip to the root of a tooth can be calculated in terms of the watts of total beam-interception power per tooth ( $P_{bi}$ ) and of total rf-dissipation power per tooth ( $P_{rfd}$ ). Since the thermal conductivity of copper is very nearly independent of temperature (and close to 10 watts per inch per degree C) superposition will apply and

$$\Delta T = k_1 P_{bi} + k_2 P_{rfd}$$

where  $k_1$  and  $k_2$  will depend on the size and shape of the tooth and the distribution of the energy inputs over the tooth surface.

Figure 28 describes the problem that was solved, with z directed parallel to the beam axis, and y and x directed in a transverse plane radially and azimuthally, respectively, relative to the beam. The beam-interception power was assumed inputted to the free end face of the tooth with the density distribution shown -- no variation with z and a  $\sin^2(\pi x/A)$  variation with x. This distribution is believed to be a good approximation for interception of "vagrant" electrons from the "fuzzy halo" surrounding a round beam of nominal diameter  $B = 0.35$  A, centered the distance  $D/2 = 0.25$  A from the flat surface at the tooth tip (Figure 21). Interception should be greatest at the indicated place of closest beam/tooth-tip approach, which eventually becomes the hottest spot on the tooth.

As for the input distribution of the rf dissipation power, the predominantly radial rf tooth current should vary approximately as  $\cos(\pi y/2l)$ , being zero at the tooth tip and a maximum at the root. The consequent input power density for this category should then vary as

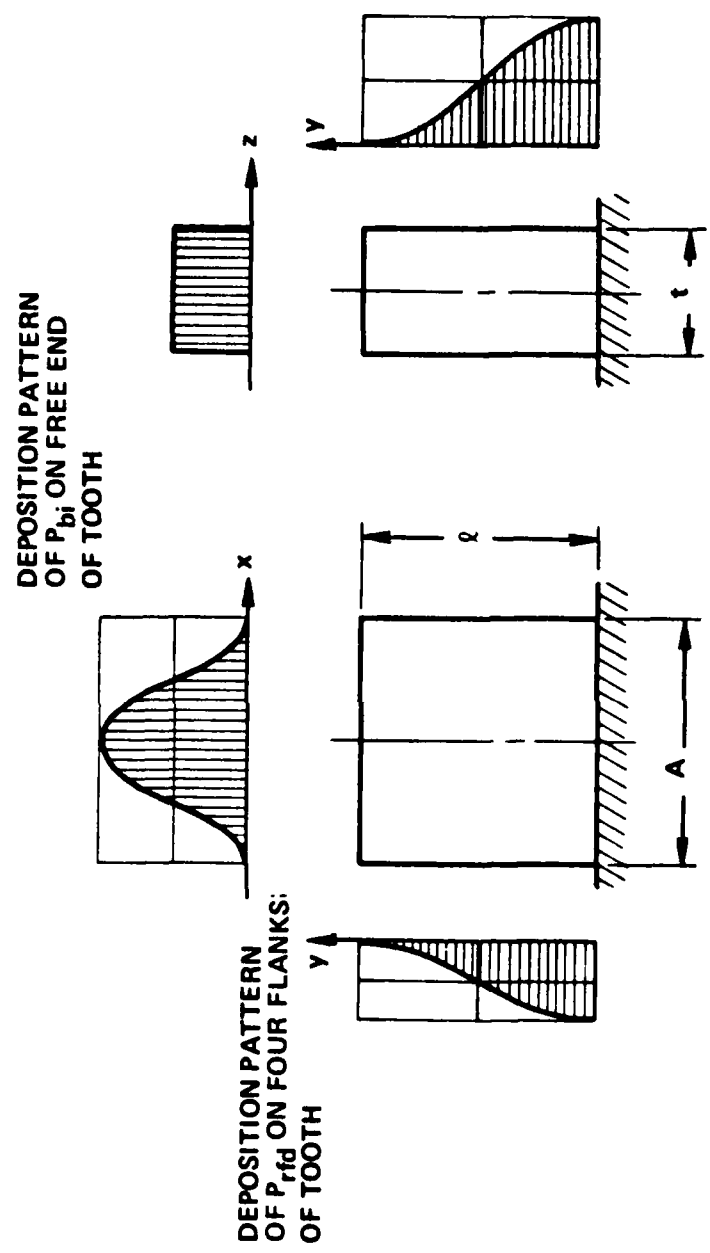


FIGURE 28. SCHEMA FOR THERMAL ANALYSIS OF A COMB-QUAD TOOTH

$\cos^2(\pi y/2\ell)$ , neglecting any variation of rf resistivity with temperature. This density is assumed not to vary with x or z on the four flanks of the tooth, as if the radial rf current density were uniform on all surfaces.

For the situation described (with radiation neglected and the temperature of the root assumed constant over its cross-section), a completely analytic solution of Poisson's equation was possible. The result (too large an expression to reproduce here) expressed the temperature rise of any point in the tooth in terms of the geometry,  $P_{bi}$ ,  $P_{rfd}$ , and the thermal conductivity. For the particular case of a copper tooth in which  $A = \ell = 0.5$  units and  $t = 0.25$  units, the numerical result for the hottest spot is (in degrees C)

$$\Delta T = 0.46 F P_{bi} + 0.40 F P_{rfd}$$

In this expression, F is the ratio of the  $2\pi$ -point frequency of the circuit structure being examined to 6.2 GHz, since  $f_{2\pi} \approx 6.2$  GHz when the unit for the values of A,  $\ell$  and t given above is the inch. That is, if the comb geometry at the far left in Figure 14 were scaled to frequencies F times higher, temperature rises would be F times greater for the same total input power levels.

In a type-B design at 44 GHz, for example, the temperature rise in question would be about  $3.4^\circ\text{C}$  per watt of  $P_{bi}$  plus  $3.0^\circ\text{C}$  per watt of  $P_{rfd}$ . If the beam voltage were 20 kV at microperveance 0.1 (an extreme upper under PPM focusing at this frequency) the total CW beam power = 5.6 kW, and with a worst-case interception of 5%, the power would be about 280 W, or 70 W per comb. saturation, most of the interception goes -- say, over the last 10 periods contribution to  $\Delta T$  = applying a thermal gradient of about  $18^\circ$  per  $\ell$  -- the output end --  $P_{bi} = 70$  W per tooth and its

upper limit at 44 or 94 GHz, a circuit attenuation of 0.05 per period (Section 5.6) implies a maximum dissipation per period

at the output end of around 1.1 to 2.3% of the output power, or half of that on a per-tooth basis. (This estimate pessimistically assumes all dissipation occurs on the tooth with none in the "enclosure" walls.) At 100 W of CW or average power output (as an example suggesting a likely upper limit for the tube types considered at either 44 or 94 GHz)  $P_{rfd} = 0.55$  to 1.15 W, contributing at most only a few degrees to  $\Delta T$ . In all, the thermal capability of the structure modeled appears to exceed that required by the tube ratings envisioned for the immediate future. For a given design frequency, the equation given above can serve as a guide to the beam and rf powers that might ultimately be accommodated -- all assuming a power limit imposed by thermal effects rather than by rf-voltage breakdown.

## 11.0 CONCLUSIONS AND RECOMMENDATIONS

### 11.1 GENERAL

The objectives of simplicity and manufacturing economy in a high-performance narrow-band non-helix linear-beam communications TWT for millimeter wavelengths (e.g., for 44 and eventually 94 GHz) have been addressed through innovation in the domain of periodic (slow-wave) interaction structures. Certain novel slow-wave circuits, introduced in anticipation of and during the execution of the subject contract, have been evaluated by cold-test and analytic means. In various ways, the structures show promise of fulfilling the goals sought while compromising other aspects of performance not at all or only in known and limited ways. Short of the heuristic experience a "hot" test vehicle can provide, and for which there is no substitute, the activities of the completed study program have accomplished much to add to the circuit options worth considering for a new generation of millimeter-wave communications TWTs.

### 11.2 STRUCTURES WITH A CENTRAL SLAB LADDER

The idea of basing an interaction structure on a copper slab perforated to create a ladder was introduced and studied<sup>6</sup> prior to the start of the subject contract, under which further advances have been made. The ladder, as fabricated according to present-day technology, would contain the beam tunnel and become a coupled-cavity-equivalent structure upon covering over its perforated faces with variously shaped plates. Promising structures were created both with and without metal-to-metal contact between the (half-wavelength) ladder rungs and the cover plates. In either case, only a few parts are put together regardless of the number of periods in the TWT section, and the penalties of axial stacking are avoided.

Among the configurations characterized, those recommended for further study (as in a "hot" test vehicle) can propagate as with either "staggered" or "in-line" magnetic coupling between "cavities". The determinants of dispersion in both cases became known through the tests made, along with the factors determining passband-edge frequencies and interaction impedances.

The interrelation of passband-edge "poles" and "zeros" of interaction impedance was also brought under control so as to promote stability in the eventual TWT.

A shortcoming of the structures introduced and investigated is the relatively low R/Q of the cavities they contain. However, the deficiency should be no worse than for a conventional but "ferruleless" coupled-cavity chain operating at the same frequency, beam voltage and gap-to-period ratio. In view of the low-R/Q tendency, the practicality of these "slab ladder" designs should increase with beam voltage (for taller "cavities") and with beam conductance (to raise the Pierce C parameter). However, a thorough (largely analytic) study is recommended to find the beam voltage and conductance ranges for which promising overall designs (including consideration of the beam focusing means) would obtain. The value of this study would be to capitalize on the advantages provided by the proposed approaches to circuit manufacture. With a one-piece slab ladder as the foundation, axial uniformity of the period (and other sensitive dimensions) would be established and maintained from the outset.

### 11.3 COMB-QUAD STRUCTURES

Having been evaluated by cold-test and analytic means, the "Comb-Quad" family of novel interaction-structure variants promises to fulfill the goals of simplicity and economy in millimeter-wave TWT designs without seriously compromising interaction impedance or stability. All variants are electrically equivalent to coupled-cavity chains with "staggered" magnetic coupling between cavities. However, the method of fabrication requires only four to eight parts per TWT section regardless of the number of periods, and avoids the problems of axial stacking germane to conventional coupled-cavity TWT sections at millimeter wavelengths. (The foremost of those problems are the numerous costly parts and the tendency of their dimensional variations to produce excessive deviations in the gap length and cumulative error in the period.)

Robustness, suggesting mechanical stability and thermal capability, is also characteristic of Comb-Quad structures, and should exceed that of a

chain of conventional coupled cavities with ferrules and the large coupling slots of a wideband design. However, relative to a narrow-band chain of conventional coupled cavities with ferrules, the Comb-Quad counterpart may not be more robust, but it can provide comparable R/Q levels without a constructional penalty akin to that which ferrules impose on a conventional cavity stack. Relative to a stack of conventional but ferruleless cavities (with the same gap-to-period ratio) no claim can be made for a Comb-Quad robustness advantage, but the R/Q will be greater. This R/Q advantage derives from an effective re-entrancy, derived in turn from a relatively low gap capacitance, in the Comb-Quad case. These benefits are a consequence of having, between adjacent "cavities", two physically large coupling apertures that nevertheless provide only a modest degree of net magnetic coupling. (These apertures incidentally provide a Comb-Quad structure section of many periods with a superior pumping speed relative to the conventional counterpart.)

The heart of any Comb-Quad interaction structure is the set of four one-piece combs, comprising two pairs in each of which the combs are opposed and aligned. The use of four one-piece combs provides the aforementioned advantages deriving from the avoidance of axial stacking. However, a penalty of the approach is the possibility of an incipient stopband at  $f_{3\pi/2}$  when the alignment or registration of comb pairs relative to one another, or the equality of the comb pairs, is imperfect. In any event, the "enclosure" surrounding and supporting the combs is a critical determinant of the manner in which beam/wave synchronism is established, and of the eventual TWT "hot" bandwidth.

For a few percent of amplification bandwidth, the applicable Comb-Quad design variants would be the "D" and the "B". In the D case, the enclosure is made as snug as possible, so the "cold" passband width is minimized. The  $\omega-\beta$  curve is cut through by the "beam-voltage line" as in a conventional CC TWT design. In the "B" case, the enclosure is large and non-critical; the cold passband is rather wide, and the "beam-voltage line" is made tangent to the  $\omega-\beta$  curve. The relative merits and drawbacks of the two options include the following:

"B" preferable to "D":

- With the B-type enclosure, its dimensional tolerances can be loose and good metal-to-metal contacts are unnecessary. The D-type enclosure features sharp internal angles whose dimensions are critical; metal-to-metal contact at these corners must be good, yet in-flow of brazing material is unacceptable.
- In the B-type design, the operating (hot) bandwidth is well apart from  $f_{3\pi/2}$ ; some comb-pair inequality or mis-registration can thus be well tolerated.
- For the B-type approach, down-side restrictions on beam voltage appear unnecessary. In fact, the lower the design voltage, the further below the  $2\pi$  point will the "tangency point" occur. For the D-type approach, it appears that unless the design voltage is at least 20 kV (or thereabouts), the requisite  $\omega-\beta$  curve shape (permitting the beam-voltage line to cut through it) is unobtainable -- for comb teeth of a simple profile.
- For a given frequency and beam voltage, the B-type design would permit a longer period (pitch) and thicker comb teeth.

"D" preferable to "B":

- The relatively larger B-type enclosure would require a PPM focusing stack to have a larger (and potentially impractical) bore.
- In the B-type approach, a low-frequency BWO possibility requires dealing with.
- For the B-type circuit structure (with operation near  $f_{2\pi}$ ) an unconventional waveguide coupler needs to be developed.

- For the B-type approach, various factors combine to yield a relatively lower net interaction impedance, the weakness of which would be aggravated by adoption of the unconventional albeit mechanically attractive (VBT) tunnel/gap geometry.

In consideration of the above, present thinking views a Comb-Quad D design approach as the better recommendation. [Possibly, the B approach might be seen as more attractive (as in Milliman's example<sup>8</sup>) in the context of a very low beam voltage ( $\leq 5$  kV) -- to move the "tangency point" well below  $f_{2\pi}$ ; a relatively high beam perveance -- to provide enough beam conductance to ensure high gain per period and sufficient output power; and a yoke-type (not PPM) permanent magnet, as then necessary. In this case, the reduced periodicity and high design frequency might combine to yield a sufficiently short tube. However, the comb teeth would be relatively delicate. A "paper design" to probe the feasibility of this Millman-type approach (but with the advantage of a lower-order space-harmonic) should be worth examining.]

Apart from these issues, the completed study program explored many facets of Comb-Quad circuitry (though with more emphasis on aspects of the B option). These included the inter-relations among rf fields and currents, equivalent-circuit elements, attenuation-vs-frequency profiles, and frequency-selective loadings. Small-signal interaction modeling was undertaken to prognose gain, bandwidth and stability; large-signal modeling is recommended additionally for any future studies. Temperature rises were related (at least approximately) to beam-interception power and rf power dissipated, but a power rating as limited by rf voltage breakdown rather than temperature rise has not yet been estimated. The development of end transitions to waveguide was generally able to rely on prior CC TWT experience, but not when the match must be good at frequencies as close to a passband edge as  $\beta p/\pi \approx 1.9$  implies.

The novel approach to creating the beam tunnel, which is a design option of any Comb-Quad structure, was examined with regard to its obvious advantages and less obvious drawbacks. The possibility of then propagating a spurious TE mode was examined, but potentially adverse effects should be

controllable inasmuch as this mode of propagation has been well characterized. The reduction in the interaction-gap modulation coefficient has been quantified by assuming a tunnel breadth and a gap length that are effectively somewhat larger than they are physically. The analytic efforts providing such data were carried out diligently and ingeniously, but the magnitude of the task permitted only one geometry ( $A/p = 1$ ;  $g/p = D/p = 0.5$ ) to be characterized. Since other proportions (e.g.,  $g/p = 0.25$ , etc.) have not been examined, there is currently little possibility of investigating the effect on gain of geometric variations, nor to seek an optimum set of proportions (for a particular value of  $\delta p$ ).

The subject of economical circuit fabrication was considered, including the aspects of surface finish and dimensional precision. A first step was taken through the preparation of a 42-period specimen dimensioned for 94 GHz application, though precision was not an objective at this stage. Qualitative and quantitative predictions were undertaken, using scale models in the latter instance, regarding the effects on propagation of several categories of dimensional deviation.

Tasks benefitting all future millimeter-wave CC TWT development, whether or not Comb-Quad based, would concern the effects of dimensional fluctuations and surface finish, quantified in newly meaningful ways. Currently, different ideas are in circulation regarding what is desirable or what is tolerable, but rigorous new analyses are needed to determine necessary and sufficient goals for precision and finish. Barring possible distortion during subsequent assembly, the one-piece combs of a Comb-Quad structure offer a unique opportunity to apply automated precision controls. Since each comb is nearly two-dimensional and contains all the periods of a TWT section, computer-controlled optical monitoring should be effective. This can be viewed as an augmentation of capability currently applied to monitoring the periodicity of helices.

## 12.0 REFERENCES

1. J.R. Pierce, Traveling-Wave Tubes, D. Van Nostrand Co., New York, 1950; Figure 5.7, p. 90.
2. A. Karp, "Traveling-Wave Tube Experiments at Millimeter Wavelengths with a New, Easily Built, Space-Harmonic Circuit," Proc. I.R.E. vol. 43, pp. 41 - 46, (1955).
3. A. Karp, "Backward-Wave Oscillator Experiments at 100 to 200 Kilomegacycles," Proc. I.R.E. vol. 45, pp. 496 - 503 (1957).
4. "Introduction to Extended Interaction Oscillators" and "Extended Interaction Oscillators - Selection Guide," Publications of Varian Canada, Inc., Georgetown, Ont. (undated).
5. M.A. Kelly, "Ferruleless Coupled-Cavity TWT," Final Report, Contract F30602-78-C-0110, Hughes Aircraft Co., Torrance, CA, June 1980.
6. G.A. Biggs, "Ladder-Based Circuit Design Concepts for Millimeter-Wave Traveling-Wave Tubes," Degree-of-Engineer Thesis, E.E. Dept., Stanford Univ., Stanford, CA, Aug. 1979.
7. J.R. Pierce, "Propagation in Linear Arrays of Parallel Wires," I.R.E. Trans. Electron Devices, vol. ED-2, pp 13 - 24, (1955).
8. S. Millman, "A Spatial Harmonic Traveling-Wave Amplifier for Six Millimeters Wavelength," Proc. I.R.E. vol. 39, pp 1035 - 1043 (1951).
9. B.G. James et al., "A New Circuit for Generating High Power at Millimeter Wavelengths," Proc. M.O.G.A. Conference, Amsterdam, Sept. 1970, pp 5-7 to 5-13.
10. P.J. Crepeau and P.R. McIsaac, "Consequences of Symmetry in Periodic Structures," Proc. IEEE, Vol. 52, pp 33-43, Jan. 1964.
11. B. Mohr, "An Investigation of the Jungle-Gym Periodic Structure," Technical Report PIB MR1-892-61, Contract AF 18(600) 1505, Polytechnic Institute of Brooklyn, 9 May 1961.
12. J.F. Gittins, "Power Travelling-Wave Tubes," American Elsevier Publishing Co., New York, 1965.
13. Y. Hiramatsu, "A Study of High-Power TWT Circuits," Technical Memorandum TMO-64, Varian Associates, Inc., Palo Alto, CA, July 1962, pp 62-67.
14. A. Karp, "Millimeter-Wave Valves," pp 73-128 in "Fortschritte der Hochfrequenztechnik," Vol. 5, M. Strutt et al., eds., Academic Press MBH, Frankfurt/Main, 1960.

15. A. Karp, "Study of Novel Wideband Coupled-Cavity Circuits for Millimeter-Wave Power TWTs," Final Report, Contract F33615-79-C-1792, Varian Associates, Inc., Palo Alto, CA, Nov. 1980.
16. F.A. Benson, "Attenuation of Rectangular Waveguides," Chapter 14 (pp 239 - 253) in Millimetre and Submillimetre Waves, F.A. Benson, Ed., Iliffe Books Ltd., London, 1969.
17. G. Convert et al., "The Generation of Submillimeter Waves," Proc. Fourth International Congress on Microwave Tubes, Scheveningen, Sept. 1962, pp. 739 - 743.
18. "A Promising New Interaction Structure for High-Frequency TWTs," Varian Associates, Inc., Document VATP 79-20686, 9 Feb. 1979; Figure 7, page 18.



## **MISSION**

**of**

### **Rome Air Development Center**

RADC plans and executes research, development, test and selected acquisition programs in support of Command, Control Communications and Intelligence (C<sup>3</sup>I) activities. Technical and engineering support within areas of technical competence is provided to ESD Program Offices (POs) and other ESD elements. The principal technical mission areas are communications, electromagnetic guidance and control, surveillance of ground and aerospace objects, intelligence data collection and handling, information system technology, ionospheric propagation, solid state sciences, microwave physics and electronic reliability, maintainability and compatibility.